NAVAL POSTGRADUATE SCHOOL
Monterey, California

THESIS

COMPUTATIONAL FLUID DYNAMICS PREDICTION OF
SUBSONIC AXISYMMETRIC AND
TWO-DIMENSIONAL HEATED FREE TURBULENT AIR JETS

by

Michael D. DeWulf

September 2000

Thesis Advisor:	Knox T. Millsaps, Jr.
Second Reader:	Garth V. Hobson
Third Reader:	Arthur Shavit

Approved for public release; distribution is unlimited.

REPORT DOCUMENTATION PAGE			Form Approved OMB No. 0704-0188

Public reporting burden for this collection of information is estimated to average 1 hour per response, including the time for reviewing instruction, searching existing data sources, gathering and maintaining the data needed, and completing and reviewing the collection of information. Send comments regarding this burden estimate or any other aspect of this collection of information, including suggestions for reducing this burden, to Washington Headquarters Services, Directorate for Information Operations and Reports, 1215 Jefferson Davis Highway, Suite 1204, Arlington, VA 22202-4302, and to the Office of Management and Budget, Paperwork Reduction Project (0704-0188) Washington DC 20503.

1. AGENCY USE ONLY *(Leave blank)*	2. REPORT DATE September 2000	3. REPORT TYPE AND DATES COVERED Master's / Mechanical Engineer Thesis	
4. **TITLE AND SUBTITLE:** Computational Fluid Dynamics Prediction of Subsonic Axisymmetric and Two-dimensional Heated Free Turbulent Air Jets		5. FUNDING NUMBERS	
6. AUTHOR(S) DeWulf, Michael D.			
7. PERFORMING ORGANIZATION NAME(S) AND ADDRESS(ES) Naval Postgraduate School Monterey CA 93943-5000		8.PERFORMING ORGANIZATION REPORT NUMBER	
9. SPONSORING/MONITORING AGENCY NAME(S) AND ADDRESS(ES) Naval Surface Warfare Center – Carderock 9500 MacArthur Blvd., West Bethesda, MD 20817-5700		10. SPONSORING/MONITORING AGENCY REPORT NUMBER	
11. SUPPLEMENTARY NOTES The views expressed here are those of the authors and do not reflect the official policy or position of the Department of Defense or the U.S. Government.			
12a. DISTRIBUTION/AVAILABILITY STATEMENT Approved for public release; distribution is unlimited.		12b. DISTRIBUTION CODE A	

13. ABSTRACT *(maximum 200 words)* A study was conducted to evaluate the accuracy of a commercial computational fluid dynamics (CFD) code (CFDRC-ACE+) for predicting incompressible air jet flows with simple geometries. Specifically, the axis-symmetric and two-dimensional heated air-jets were simulated using a standard k-ε turbulence model. These CFD predictions were directly compared to an extensive compilation of experimental data from archive literature. The round jet results indicated that the code over-predicted the velocity-spreading rate by 24% and the temperature-spreading rate by 29%. In addition, the centerline velocity and temperature decay rates were also over-predicted by 21% and 30%, respectively. The geometric and kinematic virtual origins were over-predicted, as well, by approximately 7.5 diameters for the velocity profiles and 10.5 diameters for the temperature profiles. The planar jet simulation was generally closer to experimental data ranges, with an under-prediction of the velocity-spreading rate of approximately 17% with an over-predicted temperature-spreading rate of 12%. The centerline velocity and temperature decay rates were both under-predicted at 22% and 27%, respectively. Again, the geometric and kinematic virtual origins were over-predicted by approximately 7.5 slot heights for the velocity profiles and 10.5 slot heights for the temperature profiles.

14. SUBJECT TERMS Computational Fluid Dynamics (CFD), Eductor, Ejector, Gas Turbine, Exhaust , Axisymmetric Jet, Two-Dimensional Jet, Air Jet, Free Turbulent, Jet.			15. NUMBER OF PAGES 140
			16. PRICE CODE
17. SECURITY CLASSIFICATION OF REPORT Unclassified	18. SECURITY CLASSIFICATION OF THIS PAGE Unclassified	19. SECURITY CLASSIFICATION OF ABSTRACT Unclassified	20. LIMITATION OF ABSTRACT UL

THIS PAGE INTENTIONALLY LEFT BLANK

COMPUTATION FLUID DYNAMICS PREDICTION OF SUBSONIC AXISYMMETRIC AND TWO-DIMENSIONAL HEATED FREE TURBULENT AIR JETS

Michael D. DeWulf
Lieutenant, United States Navy
B.S. Mechanical Engineering, Iowa State University, 1993

Submitted in partial fulfillment of the
Requirements for the degree of

MASTER OF SCIENCE IN MECHANICAL ENGINEERING
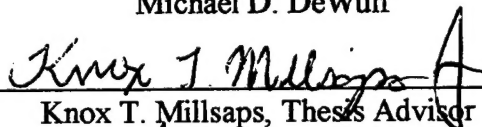### and
MECHANICAL ENGINEER
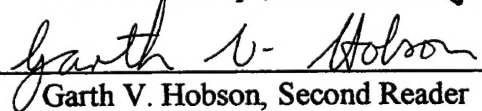
from the

NAVAL POSTGRADUATE SCHOOL
September 2000

Author: _____
Michael D. DeWulf
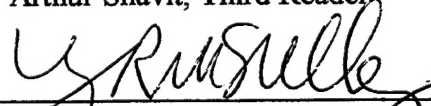
Approved by: _____
Knox T. Millsaps, Thesis Advisor

_____
Garth V. Hobson, Second Reader

_____
Arthur Shavit, Third Reader

_____
Terry R. McNelley, Chairman
Department of Mechanical Engineering

iii

THIS PAGE INTENTIONALLY LEFT BLANK

ABSTRACT

A study was conducted to evaluate the accuracy of a commercial computational fluid dynamics (CFD) code (CFDRC-ACE+) for predicting incompressible air jet flows with simple geometries. Specifically, the axis-symmetric and two-dimensional heated air-jets were simulated using a standard k-ε turbulence model. These CFD predictions were directly compared to an extensive compilation of experimental data from archive literature. The round jet results indicated that the code over-predicted the velocity-spreading rate by 24% and the temperature-spreading rate by 29%. In addition, the centerline velocity and temperature decay rates were also over-predicted by 21% and 30%, respectively. The geometric and kinematic virtual origins were over-predicted, as well, by approximately 7.5 diameters for the velocity profiles and 10.5 diameters for the temperature profiles. The planar jet simulation was generally closer to experimental data ranges, with an under-prediction of the velocity-spreading rate of approximately 17% with an over-predicted temperature-spreading rate of 12%. The centerline velocity and temperature decay rates were both under-predicted at 22% and 27%, respectively. Again, the geometric and kinematic virtual origins were over-predicted by approximately 7.5 slot heights for the velocity profiles and 10.5 slot heights for the temperature profiles.

THIS PAGE INTENTIONALLY LEFT BLANK

TABLE OF CONTENTS

LIST OF FIGURES

LIST OF TABLES

THIS PAGE INTENTIONALLY LEFT BLANK

NOMENCLATURE

Symbol	Description	Units
A, B	Sutherland's Law constants	
C	Dimensionless Virtual origin (Xo/D or Xo/H)	m
$C_{\mu,\varepsilon1,\varepsilon2}$	k-ε turbulence model constants	[1]
CFD	Computational Fluid Dynamics	
CFDRC	CFD Research Corporation	
Cp	Specific heat capacity	J/kg-K
D	Axis-symmetrical round jet diameter	m
DNS	Direct Numerical Simulation	
E	Experimental constant	[1]
FANS	Favre-Averaged Navier-Stokes	
H	Two-dimension planar jet slot height	m
ho	Stagnation enthalpy	J/kg
k	Turbulent kinetic energy	J
K	Thermal Conductivity	W/m-K
K	Multiplication constant	[1]
ℓ	Turbulent length scale	m
L	CFD code inlet size	m
LES	Large Eddy Simulation	
M	Mach number	[1]
M.W.	Molecular Weight	
R	Radial distance from the centerline of an axisymmetric round jet	m
RANS	Reynolds-Averaged Navier-Stokes	
Re #	Reynolds Number	[1]
p	Pressure	N/m^2
P	Production term	
Pr	Molecular Prandtl Number	[1]
Pr_t	Turbulent Prandtl Number	[1]
S	Source term	
T	Temperature	K
T_u	Turbulence intensity	%
u^+	Dimensionless velocity (in wall coordinates)	[1]
$\breve{u}$	Friction velocity	m/s
u, v, w	Velocity components	m/s
u', v', w'	Turbulent velocity fluctuations	m/s
U	Streamwise velocity	m/s
X, x	Streamwise jet coordinate	m
Xo	Virtual origin	m
y^+	Dimensionless distance from the wall (in wall coordinates)	[1]

<u>Symbol</u>(cont.)	<u>Description</u>	<u>Units</u>
Y, y	Transverse distance from the centerline of a two-dim. planar jet	m
ε	Turbulent kinetic energy dissipation rate	J/s
ϕ	Symbol that can represent any scalar flow variables	
δ_{ij}	Kroneker delta function	
Δ	Differential value	
γ	Turbulence intermittency factor	
Γ	Diffusivity	m^2/s
η, Eta	Dimensionless distance [R/(X-C_1D) or Y/(X-C_1D)]	
κ	von Karman constant	
μ	Dynamic viscosity	$N-s/m^2$
ν	Kinetic viscosity	m^2/s
ρ	Density	kg/m^3
$\sigma_{k,\varepsilon}$	k-ε turbulence model constants	
τ_{ij}	Viscous stress tensor	
τ_w	Wall shear stress	N/m^2

<u>Super and Subscripts</u>

1u, 1t	Associated with jet half-velocity/temperature spreading	
2u, 2t	Associated with jet centerline velocity/temperature decay	
3u, 3t	Associated with Gaussian velocity/temperature profile	
∞	Infinite surroundings	
½	Half value condition	
c, center, ¢	Centerline condition	
e	Jet exit condition	
eff	Effective	
i, j, m	Index numbers	
t	Turbulent quantity	

I. INTRODUCTION

A. MOTIVATION

The characteristics of jet development are very important in many military and industrial applications including eductors, thrust augmenting ejectors and exhaust suppression units. For example, current efforts are underway to improve present shipboard exhaust eductors without adversely effecting other parts of the ship. Former redesign of these types of systems has mainly been accomplished through extensive scale model testing of each new design proposal. The desire to reduce developmental costs of design test configurations has stimulated an increased interest in Computational Fluid Dynamics (CFD) design studies. By using CFD analysis, only the most favorable design modifications warrant further experimental testing.

B. CHALLENGE

CFD simulations help researchers to understand and visualize the complex flow patterns before costly experiments are performed. However, CFD codes are typically challenged when predicting flows that are dominated by turbulent shear mixing. The general conservation equations of continuity, momentum and energy can be solved directly by using Direct Numerical Simulation (DNS) on supercomputers. However, the extremely small grid-cell size and time steps required to resolve the smallest scales of turbulence (Kolmogorov scale) limit DNS calculations to low/moderate Reynolds number (Re) flows only.

1

In order to reduce the amount of computational resources needed, turbulence models have been developed to mimic the effects of turbulence (Reynolds stresses) that are contained within the conservation equations. This approach permits the use of smaller computers to model complex and high-speed flow configurations. However, turbulence models merely approximate the Reynolds stresses and are usually limited to a small number of simple flow regimes. Often 'turbulence model constants' must be adjusted to make the model accurately predict other types of flows.

Depending on the turbulence model used, any number of empirically derived constants may be required to properly model the flow. Overall, the process of correctly modeling the Reynolds stresses of a flow configuration is extremely difficult and problematic. Ideally, a calculation derived from the flow geometry itself would be the most desirable option when calibrating a turbulence model. However, only empirically derived constants from relatively simple experiments have been able to provide such inputs. Unfortunately, the highly complex flow patterns that typically arise in nature have precluded these experimental constants from being truly universal. Therefore, a "trial and error" methodology is often employed to adjust the turbulence model constants for reasonably accurate predictions in complex flows.

Commercial codes, designed to model many types of flows with average operator skill, often make certain concessions to provide acceptable overall predictions. Frequently, the constants are an integral part of a commercial code and can not be changed to fit the flow regime under consideration. On the other hand, 'wall functions' and other additional turbulence features

are commonly used to modify or correct the local flow conditions as necessary. Overall, the process of using turbulence models is highly challenging and the results are sometimes less than desired.

C.   OBJECTIVE

To eventually predict complex multiple-jet type flows, a single free jet must first be correctly modeled without the interference of walls or adjacent jets. Accurate simulation of the simple 'free jet' is crucial for the continued use of the CFD code and turbulence model. With this baseline of code experience and knowledge, further research can then progress towards developing and configuring more complex flow configurations.

The objective of this research is to determine the performance and sensitivity of CFD Research Corporation's numerical analysis code (CFD-ACE+) to predict simple nearly incompressible free turbulent jet flows. In particular, heated air axisymmetric (round) and two-dimensional (planar) jets were modeled and compared to tabulated experimental data. In addition, a critical review of experimental data available in the archive literature is also provided. The difficulty in predicting these simple flows has proven to be one of the more challenging problems faced by many turbulence modelers over the last five decades. The CFD-ACE+ code experience and jet behavior knowledge provided by this research was meant to create a solid foundation for further investigations.

THIS PAGE INTENTIONALLY LEFT BLANK

II. BACKGROUND ON FREE JETS

A. PREFACE

The turbulent jet has been the subject of many extensive studies, both theoretical (i.e., Abramovich 1963, Hinze 1975, Townsend 1976, Schlichting 1979, Schetz 1980, List / Rodi 1982), and experimental (i.e., Hinze / van der Hegge Zijnen 1949, Wygnanski / Fiedler 1969, Rodi 1975, Panchapakesan / Lumley 1993, Hussein *et al* 1994). Being both basic and important in many applications, 'simple geometry' jets are actually quite complex and multifaceted. From the earliest investigations, the turbulent jet has been dissected into different discrete regions for in-depth analysis. A brief description will be given here to familiarize the reader with this type of flow.

A free jet is formed when a fluid is discharged from an orifice or nozzle into quiescent, co-flowing, or counter-flowing environments. Co-flows and counter-flows are not considered in this investigation. By analyzing only subsonic flows with Mach Numbers less than 0.3, compressibility effects can be ignored. In addition, only jets with "top-hat" velocity / temperature exit profiles, negligible buoyancy effects, and stagnant surroundings are considered.
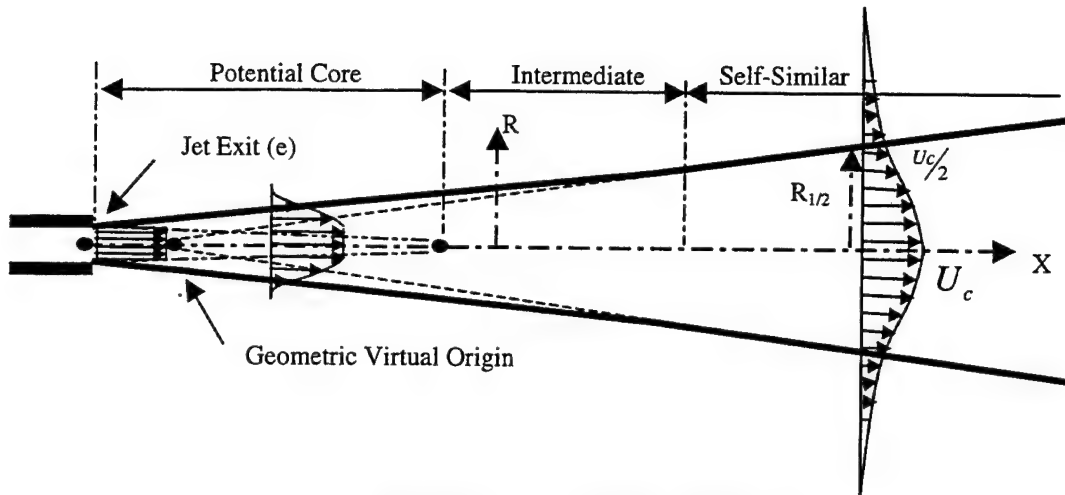
Figure 1.   **A Typical Free Jet**

As shown in Figure 1, the jet is usually divided into three main regions. Each region has its own unique characteristics that set it apart from the others. The virtual origin is conceptualized as an "ideal" jet source that produces the same self-similar jet effects without the transient regions (potential core and intermediate). The "geometric" virtual origin, as indicated in Figure 1, is obtained by extending the linear spreading profile of the jet backward to the jet's centerline. The distance from the jet center (where the velocity is Uc) to the half-velocity point (Uc/2) usually defines the jet's spreading profile length. The "kinematic" virtual origin, on the other hand, is acquired from the inverted centerline velocity decay plot (Ue/Uc). Again, a line is extended backward from the linear self-similar decay region to the X-axis to indicate the virtual origin as shown in Figure 2.

Centerline Velocity Decay
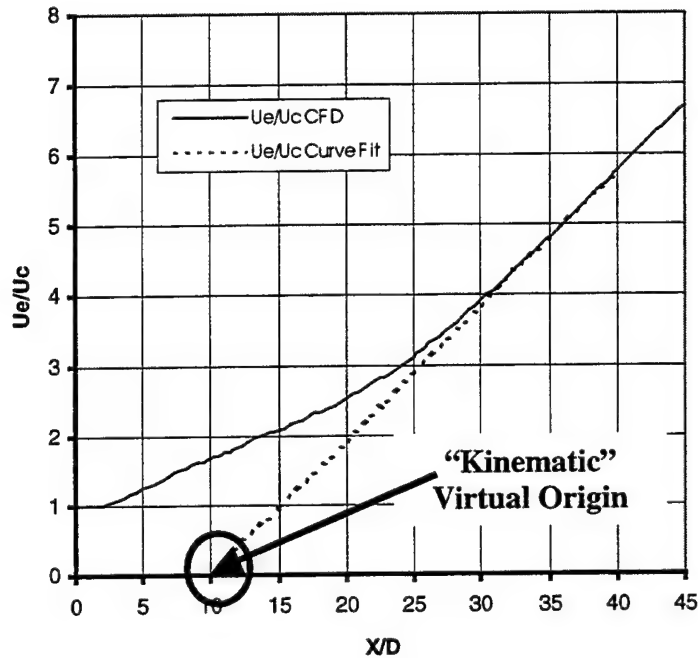
Figure 2.   Inverted Centerline Velocity Decay Plot

B.   POTENTIAL CORE REGION

The potential core region (Figure 1), closest to the orifice, is highly influenced by the outlet conditions of the orifice as well as the surrounding medium. The centerline streamwise velocity remains approximately constant in this region; it may however exhibit a slight vena contracta at higher flow rates. The significant shear distortions in the flow field rapidly generate instabilities and create turbulent energy in the shear layers and greatly effect the initial spreading rate of the jet. Thought by many early investigators to be totally incoherent fluid motions, this turbulent flow has been proven to have 'organized-structures' (coherent structure) superimposed

7

on its chaotic (or random) motion. This large-scale turbulence generated at the jet boundaries is most responsible for noise and initial mass entrainment. List/Rodi (1982) review several modes of wave/vortex growth and instabilities and their descriptions will not be repeated here.

Generally, by lowering inlet core turbulent intensity (Tu) and flattening velocity profiles (top hat), longer potential core lengths are realized in this region. Also increasing the exit velocity (effectively lowering Tu and flattening the velocity profile) can enlarge the potential core length.

C. INTERMEDIATE REGION

As entrainment develops on its periphery, the potential core disappears into the intermediate (transitional) region. The width of this transitional region spreads rapidly outward as the jet progresses down stream and the average centerline velocity decreases. This re-shaping of the mean flow tends to force the jet into self-similarity (self-preservation).

D. SELF-SIMILAR REGION

Eventually, the flow attains self-similarity in which the various terms of the momentum equation (convection, diffusion, production, etc.) maintain constant ratios so that the various processes are in dynamic equilibrium, each one changing downstream at the same rate as the others. In this region, dimensionless velocity and length scales (a function of one geometrical variable only) can completely describe the flow. The flow is also said to be independent of the

8

initial jet conditions including orifice shape and turbulence intensity. The width of this region seems to grow at a linear rate as the flow diminishes. Mean velocity profile similarity is usually reached within about 20-30 jet diameters downstream while turbulence velocity fluctuations don't obtain "true similarity" until 70 diameters or greater depending on the type of flow. Many books, such as Abramovich (1963), Launder (1975) and others, discuss similarity arguments in much greater detail.

Jets can obtain "exact" similarity only if they issue into stagnant or quiescent surroundings (as opposed to co-flow or counter-flow) and, in general, are theorized to have the following approximate streamwise characteristics under the assumptions of: steady flow, negligible body force and negligible pressure gradient (uniform static pressure).

For axisymmetric round jets, the magnitude of axial velocity at the center of the jet (Uc) varies as the inverse of the axial distance (X) from the jet exit nozzle. On the other hand, the radius at which the axial velocity of the jet profile is half of the centerline value ($R_{1/2}$) varies directly with X.

$$\text{Centerline Velocity Decay:} \quad U_c \propto X^{-1} \tag{1}$$

$$\text{Half-Velocity Radius:} \quad R_{1/2} \propto X \tag{2}$$

Planar jets exhibit slightly different characteristics due to their two-dimensional nature. The centerline velocity (Uc) and transverse half-velocity length ($Y_{1/2}$) vary in the axial direction (X) as follows.

$$\text{Centerline Velocity Decay:} \quad Uc \propto X^{-1/2} \tag{3}$$

$$\text{Half-Velocity Length:} \quad Y_{1/2} \propto X \tag{4}$$

E. TEMPERATURE PROFILE

The turbulent mixing within a jet causes a transfer of fluid particles in a direction normal to the main flow. The process is complex and involves momentum flowing away from the main stream while the surrounding fluid is being entrained toward it. In addition, there can be a transfer of heat or diffusion of the temperature field into the surroundings. As shown in Figure 3, the temperature profile is considerably broader than the velocity profile due to the higher transverse transport of thermal energy by turbulence than momentum for gas jets. The scalar values of temperature, internal energy and species concentration all behave in the same way for these types of flow.

Abramovich (1963), Hinze (1975), Schlichting (1979) and others describe heat transfer theories within the jet that are based on several simplifying assumptions. Although in general, the exact jet characteristics are not presented in the texts and the authors apply their (or other's) experimental data to obtain the required empirical constants. However, each jet tends to be unique and the limited data used by each author are only applicable for that specific jet which

10

may only be similar to one or two other experiments. Even though these limited data (usually dated) will support the author's general conclusions, many other experiments with comparable setups do not obtain the same results. Obviously not all factors (like coherent structures, etc) have been properly controlled in the experiments and incorporated into equations (1 to 4) and further investigation is certainly warranted. As will be discussed in Chapter III, factors like density ratio and facility-related disturbances can greatly effect the developing characteristics of free jets.
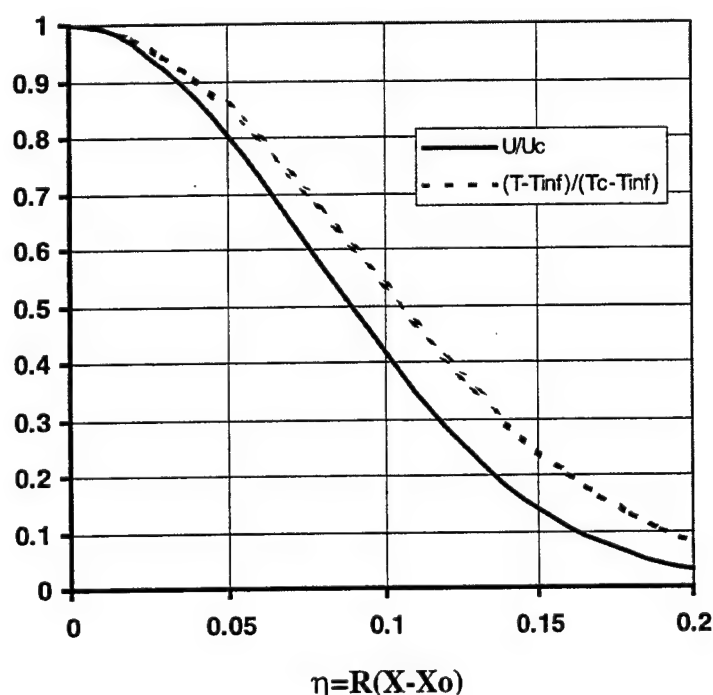
Figure 3.   **Typical Velocity and Temperature Profiles**

THIS PAGE INTENTIONALLY LEFT BLANK

III.   CRITICAL REVIEW OF EXPERIMENTAL RESULTS

A.   OVERVIEW

It is essential to have reliable experimental data against which CFD predictions can be compared. Free turbulent jets have been measured fairly extensively throughout the years and plenty of data are available.   The purpose of this chapter was to review these data, check its reliability, and select target values for a comparison with the predictions from the CFD code. As the reader will soon discover, this task is not as simple as it first may appear.

B.   MEASUREMENT TECHNIQUES

In order to make judgements on the particular quality of the measurements; we will briefly examine the merits and shortcomings of various measurement techniques used to obtain the referenced data. In most free jet flows, the static pressure varies very little across the flow. Therefore, measurement of total pressure by a Pitot tube (or similar) can be sufficient to determine the mean velocity (U). The Pitot tube, due to its slow response however, can't measure the fluctuating velocities that represent the most serious source of error. When turbulence fluctuations are high (>20% - like in the shear layer), the instantaneous yaw angles can be large enough to affect the probe reading without any reliable correction available.

The hot-wire anemometer has a sufficiently fast response to follow the turbulence fluctuations and has become the one of the more popular instruments for measuring turbulent flows. However, many sources of error are associated with the hot-wire measurement technique and not all early researchers have properly accounted for them as described by Hussein *et al* (1994) and Panchapakesan / Lumley (1993). The more common errors include improper unit calibration, turbulence interference between adjacent wires (multiple wire configurations), and failure to realize that a significant fraction of reverse flow exists in the outer shear layers of jets. These problems have introduced many uncertainties and the general reliability of the data essentially decreases with increasing turbulence level.

The relatively new laser technologies offer much promise for high accuracy data. By applying a known frequency shift to the laser beams, an offset frequency is created that is increased or decreased by the Doppler-shift phenomena. Laser–Doppler Anemometers (LDA) are one of the very few velocimeters capable of measuring flow reversals. However, concerns still arise about proper seeding material size and dispersion required to truly represent the flow. Presently, only very few jet flow configurations have been re-examined using this state-of-the-art technique and limited data are available.

C.   JET CHARACTERISTIC EQUATIONS

To efficiently compare different results, the widely accepted equations given below are used to describe round jets in the self-similar region. Most modern researchers prefer these popular equation formats. Of course, some conversions were necessary to adapt all of the data

14

into this form. The velocity profiles were typically approximated using a Gaussian format generated from the jet's spreading rate as shown below. The Gaussian profile tends to be a good approximation for the near axis regions of jets, however, the outer edges of real jets fall off slightly quicker as described by Malmstrom *et al* (1997). The following equations do not require that the virtual origins to be co-located.

1.   Axisymmetric Round Jets

Half Velocity Spreading: $\dfrac{R_{\frac{1}{2}u}}{D} = K_{1u}\left(\dfrac{X}{D} - C_{1u}\right)$ (5)

$$C_{1u} = \dfrac{X_{o,1u}}{D}$$ (6)

where: $R_{\frac{1}{2}u}$ -half-velocity radius
             D   -jet exit diameter
             X   -axial distance from the jet exit nozzle
             K_{1u} -velocity spreading rate
             C_{1u} -dimensionless velocity geometric virtual origin
             $X_{o,1u}$ -velocity geometric virtual origin

Gaussian Velocity Profile: $\dfrac{U}{Uc} = e^{\left[-K_{3u}\eta^2\right]}$ (7)

   (not all data)

where: U   -axial velocity
             U_c -centerline axial velocity

15

$$K_{3u} = \frac{\ln(2)}{K_{1u}^2} \tag{8}$$

$$\eta = \left(\frac{R}{X - C_{1u}D} \right) \tag{9}$$

Centerline Velocity Decay: $\quad \dfrac{Ue}{Uc} = K_{2u} \left(\dfrac{X}{D} - C_{2u} \right) \tag{10}$

$$C_{2u} = \frac{X_{o,2u}}{D} \tag{11}$$

where:

U_e	-jet exit axial velocity
K_{2u}	-centerline velocity decay rate
C_{2u}	-dimensionless velocity kinematic virtual origin
$X_{o,2u}$	-velocity kinematic virtual origin

Additional relationships: $\quad \dfrac{R}{R_{\frac{1}{2}u}} = \dfrac{\eta}{K_{1u}} \tag{12}$

$$\frac{R}{R_{\frac{1}{2}t}} = \frac{\eta_t}{K_{1t}} \tag{13}$$

Not all of the above variables were reported in every experiment. Sometimes the authors assumed the virtual origins were co-located and did not clearly indicate this within the article. This, in turn, constrains the reader to make certain assumptions about the jet's characteristics, which may be reflected in the data presented in Tables 1 and 2.

16

As mentioned before, the temperature differential between the surroundings and the jet, result in temperature profiles that are wider than the velocity profiles. This same reasoning can also be applied to mass concentration results. Therefore, temperature and concentration are interchangeable and characterized in the following equations

Half Temperature Difference Spreading: $\qquad \dfrac{R_{\frac{1}{2}t}}{D} = K_{1t}\left(\dfrac{X}{D} - C_{1t}\right)$ $\qquad\qquad$ (14)

$$C_{1t} = \dfrac{X_{o,1t}}{D} \qquad\qquad (15)$$

where: $\qquad$ $R_{\frac{1}{2}t}$ $\quad$ -half-differential temperature radius
$\qquad\qquad\quad$ K_{1t} $\quad$ -differential temperature spreading rate
$\qquad\qquad\quad$ C_{1t} $\quad$ -dimensionless temperature geometric virtual origin
$\qquad\qquad\quad$ $X_{o,1t}$ $\quad$ -temperature geometric virtual origin

Temperature Difference Profile: $\qquad \dfrac{\Delta T}{\Delta Tc} = \dfrac{T - T_{\infty}}{Tc - T_{\infty}} = e^{\left[-K_{3t}\eta_t{}^2\right]}$ $\qquad$ (16)

$\qquad$ (not all data)

$$K_{3t} = \dfrac{\ln(2)}{K_{1t}^2} \qquad\qquad (17)$$

$$\eta_t = \left(\dfrac{R}{X - C_{1t}D}\right) \qquad\qquad (18)$$

where: $\qquad$ T $\qquad$ -temperature
$\qquad\qquad\quad$ T_c $\qquad$ -centerline temperature
$\qquad\qquad\quad$ T_{∞} $\qquad$ -surrounding environment temperature

Centerline Temperature Diff. Decay:

$$\frac{\Delta Te}{\Delta Tc} = \frac{Te - T_{\infty}}{Tc - T_{\infty}} = K_{2t}\left(\frac{X}{D} - C_{2t}\right) \qquad (19)$$

$$C_{2t} = \frac{X_{o,2t}}{D} \qquad (20)$$

where:
U_e — jet exit temperature
K_{2t} — centerline differential temperature decay rate
C_{2t} — dimensionless temperature kinematic virtual origin
$X_{o,2t}$ — temperature kinematic virtual origin

The half-velocity (temperature) length, $R_{1/2u}$ ($R_{1/2t}$), represents the radial distance from the jet's axial centerline to the position where the velocity (temperature) is one-half the maximum centerline value. The values of the dimensionless virtual origins (C_{1u}, C_{2u}, C_{1t}, C_{2t}) and multiplication constants (K_{1u}, K_{2u}, K_{1t}, K_{2t}), in addition to several other relevant facts from several selected experiments, are listed in Table 1. As shown, the multiplication constants (K's) are fairly consistent (<10% variation) between experiments. However as noted by several researchers, the virtual origins are found to vary widely (-0.6 < C's < 4). Unfortunately, no consistent underlying reason has yet been correlated to explain the wide variations in the virtual origin values. In addition, not all virtual origins have been quoted in the research which makes comparisons between experiments difficult.

2. Two-dimensional Planar Jets

The similarity analysis for the planar jet is, as expected, very similar to the axisymmetric round jet. However, the characteristic equations take into account Cartesian (instead of cylindrical) coordinates and the use of appropriate substitutions.

The overall resultant equation forms are:

Half Velocity Spreading:
$$\frac{Y_{\frac{1}{2}u}}{H} = K_{1u}\left(\frac{X}{H} - C_{1u}\right) \qquad (21)$$

$$C_{1u} = \frac{X_{o,1u}}{H} \qquad (22)$$

where: $Y_{\frac{1}{2}u}$ -half-velocity transverse length
   H -jet height

Gaussian Velocity Profile:
$$\frac{U}{Uc} = e^{\left[-K_{3u}\eta^2\right]} \qquad (23)$$

(not all data)

$$K_{3u} = \frac{\ln(2)}{K_{1u}^2} \qquad (24)$$

$$\eta = \left(\frac{Y}{X - C_{1u}H}\right) \qquad (25)$$

Centerline Velocity Decay:
$$\left(\frac{Ue}{Uc}\right)^2 = K_{2u}\left(\frac{X}{H} - C_{2u}\right) \qquad (26)$$

$$C_{2u} = \frac{X_{o,2u}}{H} \qquad (27)$$

Additional relationships:
$$\frac{Y}{Y_{\frac{1}{2}u}} = \frac{\eta}{K_{1u}} \qquad (28)$$

$$\frac{Y}{Y_{\frac{1}{2}t}} = \frac{\eta_t}{K_{1t}} \qquad (29)$$

19

Half Temperature Diff. Spreading:

$$\frac{Y_{\frac{1}{2}t}}{H} = K_{1t}\left(\frac{X}{H} - C_{1t}\right) \tag{30}$$

$$C_{1t} = \frac{X_{o,1t}}{H} \tag{31}$$

where: $Y_{\frac{1}{2}t}$ -half-differential temperature transverse length

Temperature Difference Profile:

$$\frac{\Delta T}{\Delta Tc} = \frac{T - T_\infty}{Tc - T_\infty} = e^{\left[-K_{3t}\eta_t^2\right]} \tag{32}$$

(not all data)

$$K_{3t} = \frac{\ln(2)}{K_{1t}^2} \tag{33}$$

$$\eta_t = \left(\frac{Y}{X - C_{1t}H}\right) \tag{34}$$

Centerline Temp. Diff. Decay

$$\left(\frac{\Delta Te}{\Delta Tc}\right)^2 = \left(\frac{Te - T_\infty}{Tc - T_\infty}\right)^2 = K_{2t}\left(\frac{X}{H} - C_{2t}\right) \tag{35}$$

$$C_{2u} = \frac{X_{o,2u}}{H} \tag{36}$$

The values of the dimensionless virtual origins (C_{1u}, C_{2u}, C_{1t}, C_{2t}) and multiplication constants (K_{1u}, K_{2u}, K_{1t}, K_{2t}) for planar jets are listed in Table 2. Again, the multiplication constants (K's) are fairly consistent (<25% variation) between experiments, while the virtual origins vary widely (-6H < C's < 4H).

D.   VARIATION OF EXPERIMENTAL RESULTS

Most experiments have validated the similarity analysis, as described in Chapter II, Section D. However, works by Kotsovinas (1976) and Jenkins / Goldschmidt (1973) have continued to shed doubts on the linear behavior of planar jets in the far similarity region. Depending on the downstream range investigated, the planar jet centerline decay data appears to be slightly non-linear (greater) when using the standard similarity equations (26 & 35) far from the jet exit (X/H > 200). Therefore, the regression range used by researchers to obtain virtual origins and multiplication constants are important.

1.   Incomplete Data

Accurate universal jet predictions are very hard to acquire. Several factors can influence the development of each jet, as well as describe their general shape. Almost no text or experimental report has incorporated all of the required factors to completely characterize jet flow. Each is based on very limited data and a general overall behavior is assumed for all comparable jets. Although this is partially true, due to the similarity relationships, one can not apply these results to all jets (even when flow conditions seem to be the same).

The most commonly recognized difference among experiments is the location of the virtual origins. Many researchers have not clearly recognized that in some situations the geometric (C_{1u}, C_{1t}) and kinematic (C_{2u}, C_{2t}) virtual origins do not necessarily coincide as would be expected by the similarity arguments [See Goldschmidt / Bradshaw (1981) and Flora /

Goldschmidt (1969)]. This is further complicated when some authors fail to report all of the virtual origins. This consensus usually arises from the assessment that only the multiplication constants (K's) are required to adequately describe jet characteristics. However, one can not completely describe the longitudinal position of the centerline decay and lateral spread profiles without knowing the reference points (virtual origins) upon which they're based.

The virtual origin, therefore, is an important parameter, although it may be quite challenging to predict. Papadopoulos / Pitts (1999) have developed successful centerline prediction equations for iso-thermal jets using the initial momentum flux and local centerline turbulence intensity. However, further research on heated jets has not been performed.

2. Jet Variations

To assume that the results of one experiment will completely match another is erroneous. Slight variations in the measured multiplication constants and virtual origin values (See Table 1 and 2) can have significant effects on jet predictions using the similarity equations (Equations 5-36).

In addition, free jets have been found to contain large-scale coherent disturbances within the shear layers on top of the seemingly random turbulent motions [See Thomas / Prakash (1991), Moum *et al* (1983), Hussain (1983), Gutmark / Ho (1983) and Crow / Champagne (1971)] which are initial condition dependent. These disturbances can be excited relatively easily and can drastically effect the entire motion of the jet (non-quasi-steady). Hussein *et al*

22

(1994) and George (1989) further described how a more general analysis of the similarity theory reveals that a self-preserving state can, indeed, be uniquely determined by the initial conditions. Hence, a family of farfield similarity solutions could exist for each type of jet, depending on its initial conditions.

The density (and/or temperature) differential effect on jet development has been investigated by Drobniak *et al* (1998), Sautet / Stepowski (1995), and Russ / Strykowski (1993). Further articles by Kyle / Sreenivasan (1993) and Monkewitz *et al* (1990) describe how "hot jet to surrounding environment" density ratios less than approximately $\rho_{jet}/\rho_\infty < 0.6$ can cause a self-excited large-scale coherent mode that produces a marked jump in the spreading rate. This mode is caused by the formation of a very regular sequence of intense vortex ring structures within the jet. The behavior of the mode has been found to be independent of background disturbances within typical experimental Reynolds Number ranges (10^2 to 10^5). The resulting "strong pairing process" of the mode leads to abnormally large centerline velocity fluctuations and early potential core breakup. Current commercial CFD codes, solving RANS equations, cannot model these excited modes which have become major obstacles when accurately predicting free jet flows.

Some additional experimental variables that haven't always been controlled or reported include the following. Fan vibrations felt at the nozzle and surrounding area disturbances are known to cause significant changes in the jets, especially at low flow rates as described by Gutmark / Ho (1983). Modern researchers have tried to prevent such interactions to varying

23

degrees of success, but their reassessment of earlier experiments are still quite limited. Small or semi-confined test sections and inadequate equipment have also tainted some earlier experiments as described by Malmstrom *et al* (1997), Hussein *et al* (1994), and Panchapakesan (1993). The overall room size and re-circulation patterns seem to deform and shift the immerging jet enough to effect the results between different experimental facilities. Extreme care has been taken by modern researchers to minimize these effects.

Table 1. Axisymmetrical Round Jet Experimental Data

Investigator	Jet Dia (m) [D]	Inst.	Test Range [X/D]	Re_D	ρ/ρ∞ Ratio	Jet Vel. Prof.	Jet Tu [%]	Vel Spread Rate [K_{1u}]	Geom. Virt. Orig. [C_{1u}]	C/L Vel. Decay [K_{2u}]	Kin. Virt. Orig. [C_{2u}]	Vel Prof [K_{3u}]	Temp Spread Rate [K_{1t}]	Spread Virt. Orig. [C_{1t}]	C/L Temp Decay [K_{2t}]	C/L Virt. Orig. [C_{2t}]	Temp Prof [K_{3t}]
ISOTHERMAL CONDITIONS																	
Hussein, Capp & George (1994)	0.0254	LDA	10-120	9.6×10^4	1	Top Hat	0.58	0.094	4	0.172	4	†	N/A	N/A	N/A	N/A	N/A
Panchapakesan & Lumley (1993)	0.0061	FHW	30-160	1.1×10^4	1	Top Hat	0.01	0.096	0	0.165	0	75.2	N/A	N/A	N/A	N/A	N/A
Wygnanski & Fielder (1969)	0.0264	Hot Wire	5-100	$\sim 10^5$	1	Top Hat	0.1	0.086	3	0.175	3	–	N/A	N/A	N/A	N/A	N/A
Corrsin & Kistler (1954)	0.0127	Pitot	20-50	7.3×10^4	1	Top Hat	–	0.0945	3	–	–	–	–	–	–	–	–
TEMPERATURE OR CONCENTRATION DIFFERENCES																	
Grandmais, Rathgeb. & Becker (1982)	0.071	Laser Tech.	10-80	27×10^4	Conc. Effect	–	–	–	–	–	–	–	0.105	1.675	0.185	1.675	61.6
List & Rodi (1982) Data Review	–	–	–	–	–	Top Hat	–	0.089	–	0.161	–	87.3	0.105	–	0.194	–	62.9
Chen & Rodi (1980) Data Review	–	–	–	–	–	Top Hat	–	0.086	–	0.161	–	94	0.11	–	0.2	–	57
Hinze (1975) Data Review	–	–	–	–	–	Top Hat	–	0.08	0.5	0.169	0.5	108	0.098	–	–	–	72
Hinze & van der Hegge Zijnen (1949)	0.025	Pitot T/C	0-40	6.7×10^4	0.9	Top Hat	–	0.080	-0.6	0.157	-0.6	‡‡	0.095	0.8	0.190	0.8	‡‡

Notes: †: $\left(1+12.12\eta^2+2815\eta^4\right)e^{\left[-111\eta^2\right]}$ ‡: $\left(1+63.78\eta^2\right)^{-2}$ ‡‡: $\left(\dfrac{U}{U_c}\right)^{0.729}$

T/C: thermocouple   FHW: Flying hot wire

Table 2. Two-dimensional Planar Jet Experimental Data

Investigator	Jet Dia (m) [H]	Inst.	Test Range [X/H]	Re_H	ρ_o/ρ_∞ Ratio	Jet Vel. Prof.	Jet Tu (%)	Vel Spread Rate [K_nu]	Geom. Virt. Orig. [C_nu]	C/L Vel. Decay [K_zu]	Kin. Virt. Orig. {C_zu}	Vel Prof [K_nu]	Temp Spread Rate [K_td]	Spread Virt. Orig. [C_td]	C/L Temp Decay [K_zt]	C/L Virt. Orig. [C_zt]	Temp Prof [K_st]
ISOTHERMAL CONDITIONS																	
Thomas & Pradkash (1991)	0.0127	Hot Wire	0-24	0.8×10^4	1	Top Hat	0.24	0.11	0.14	0.22	-1.2	-	N/A	N/A	N/A	N/A	N/A
Goldschmidt & Bradshaw (1981)	0.0098	Hot Wire	10-80	2.7×10^4	1	Top Hat	0.63 0.72 0.84 1.29 2.58	0.112 0.108 0.117 0.119 0.123	0.72 0.75 2.1 1.2 -0.2	0.154 0.156 0.146 0.155 0.145	0.8 1.8 1.3 1.5 -0.8	-	N/A	N/A	N/A	N/A	N/A
Hussain & Clark (1977)	0.0318	Hot Wire	0-40	8.1×10^4	1	Top Hat	0.3	0.119	1.90	0.113	-2.11	-	N/A	N/A	N/A	N/A	N/A
Gutmark & Wygnanski(1976)	0.0127	Hot Wire	0-120	3×10^4	1	Top Hat	0.2	0.1	-2	0.188	3.0	†	N/A	N/A	N/A	N/A	N/A
Flora & Goldschmidt (1969)	0.0127	Pitot	0-90	2.6×10^4	1	Top Hat	1.06 1.21 1.28	0.130 0.113 0.127	-15.0 -6 -5.00	0.227 0.144 0.222	2.00 -1 0	-	N/A	N/A	N/A	N/A	N/A
Miller & Comings (1957)	0.0127	Hot Wire	0-40	1.8×10^4	1	Top Hat	-	0.097	-1.57	.167	-1.47	74	N/A	N/A	N/A	N/A	N/A
van de Hegge Zijnen (1957)	0.005 0.010	Pitot	0-40	1.3×10^4	1	Top Hat	- -	0.096 0.099	- -	0.163 0.205	-0.6 -1.7	75 70.7	N/A	N/A	N/A	N/A	N/A
TEMPERATURE OR CONCENTRATION DIFFERENCES																	
List & Rodi (1982) Data Review	-	-	-	-	-	Top Hat	-	0.1	-	0.189	-	-	-	-	0.277	-	-
Chen & Rodi (1980) Data Review	-	-	-	-	-	Top Hat	-	0.11	-	0.174	-	62	0.14	-	0.25	-	35
Davies, Keffer & Baines (1975)	0.051	Hot Cold Wire	10-25	4×10^4	0.95	Top Hat	0.5	0.109	-1.17	-	-	-	0.125	-1.17	-	-	-
Jenkins & Goldschmidt (1973)	0.013	Wire and Pitot	10-55	1.4×10^4	0.96 0.94 0.90	Top Hat	-	0.088 0.091 0.096	-4.5 -3.0 -2.5	0.16	4	-	0.123 0.128 0.137	-4.8 -3.6 -3.2	0.0132 ††	-7.5 ††	-
van der Hegge Zijnen(1957)	0.005	Pitot and T/C	2-40	1.3×10^4	0.84	Top Hat	-	0.096	-0.6	0.163	-0.6	75	0.1415	-0.6	0.25	-0.6	†††

Notes: †: AGARD Table

††: $\sqrt{\dfrac{\Delta Te}{\Delta Tc}} = K_{zt}\left(\dfrac{X}{H} - C_u\right) \neq \dfrac{\Delta Te}{\Delta Tc}$

†††: $\dfrac{\Delta T}{\Delta T_c} = \left\{1 + 30\eta_i^2 + 2200\eta_i^4 - 30000\eta_i^6\right\} e^{\left[-75\eta_i^2\right]}$

E. OVERALL TRENDS

Several overall trends in experimental data have been noticed throughout the years with varying degrees of consistency. Although a particular reported trend might have an exception in one experiment, the overwhelming inclinations (as described by many additional researchers) will be described here.

1. Exit Velocity Effects

Several earlier experiments report a diameter-based Reynolds Number (Re_d #) dependence of jet flows with exit Re_d #'s less than approximately 5×10^4. By varying the jet exit velocity, Re_d # dependence was seen as a change in the spreading rate and centerline decay. A more comprehensive study by Malmstrom *et al* (1997) which involved varying the exit velocity, as well as the jet diameter, concluded that the variance was based on jet exit velocity, not the Re_d #. As jet exit velocity was increased beyond 6 m/s, the velocity centerline decay multiplication factor (K_{2u}) decreased to an asymptotic 0.17 value (for round jets) which agrees well with Table 1. Below 6 m/s, as jet exit velocity is decreased, the centerline decay and spreading rate increase.

2. Turbulence Intensity Effects

The dominant factor that seems to effect experimental virtual origin location is turbulence intensity at the jet exit profile. Both the centerline turbulence intensity and boundary layer thickness can drastically shift the origins in seemingly random directions. Several researchers

have attempted to qualify these effects with limited success in narrowly defined jet configurations. Changes in the turbulence intensity have also sometimes masked the effects of velocity dependence on jet development. As the jet exit velocity increases, the core turbulence intensity generally drops (unless artificially held constant) as the boundary layers become thinner. Therefore, as exit turbulence intensity decreases, the jet spreads less and the centerline decay decreases. However, Goldschmidt / Bradshaw (1981), Kleis / Floss (1974), and Flora / Goldschmidt (1969) have shown that the above Tu effects still hold true when the exit velocity is held constant.

F.   TARGET VALUES

In order to compare the CFD results to experiments, target values must be chosen. A band (or range) of experimental data was select over a specific experiment because every jet tends to be unique as described in Section (D). After analyzing Tables 1 and 2, evaluating the references, and studying more recent investigations, the following parameters were chosen to compare and model typical jet flow for this research.

1.   Centerline Decay and Spreading Values

As shown in Tables 1 and 2, the spreading rates and centerline decay values are fairly constant, but do exhibit a slight variation (~10% for the round jet and ~25% for the planar jet). Based on measurement technique, data scatter, test range, researcher credibility, the following values will be used to compare CFD results.

Table 3. CFD Simulation Target Values

Flow Type	Vel Spread Rate $\{K_{1u}\}$	Geom. Virt. Orig. $\{C_{1u}\}$	C/L Vel. Decay $\{K_{2u}\}$	Kin. Virt. Orig. $\{C_{2u}\}$	Temp Spread Rate $\{K_{1t}\}$	Spread Virt. Orig. $\{C_{1t}\}$	C/L Temp Decay $\{K_{2t}\}$	Decay Virt. Orig. $\{C_{2t}\}$
Round Jet	0.085-0.095	-1.0 to 4.0	0.160-0.172	-1.0 to 4.0	0.098-0.110	0.0 to 2.0	0.185-0.194	0.0 to 2.0
Var.	11.7%	5D	7.5%	5D	12.2%	2D	4.9%	2D
Planar Jet	0.096-0.120	-6.0 to 2.0	0.155-0.220	-2.0 to 4.0	0.125-0.140	-5.0 to 0.0	0.250-0.280	-5.0 to 0.0
Var.	25%	8H	41.9%	6H	12%	5H	12%	5H

Target virtual origin ranges were selected to include the extreme reported variations. As mentioned, current steady-state Favre-Averaged Navier-Stokes (FANS) CFD codes can not model many important external factors (i.e., nozzle vibration, room disturbances, etc.) that can significantly effect the virtual origin position. Therefore, the virtual origin target range is used only for vague simulation result comparisons.

2. Turbulent Prandtl Number

The turbulent Prandtl Number (Pr_t) quantifies the transport rate of momentum to that of heat and was used as an input to the CFD code k-ε turbulence / energy model. Free jet flows, which are not effected by walls, display different Pr_t variations normal to the primary flow direction than typical internal flows (i.e. equilibrium pipe flow). The turbulent Prandtl Number varies across the round jet's profile and was quantified by Reynolds (1976) as shown in Table 4 and Figure 4.

Table 4.   Turbulent Prandtl Numbers for Jets

Flow Type	Local Pr_t			Recommended Global Pr_t
	$\gamma=1$	$\gamma=0.5$	$\gamma\to0$	
Round Jet	0.73	1.2	1.7	0.7
Planar Jet	0.5	0.9	1.3	0.5
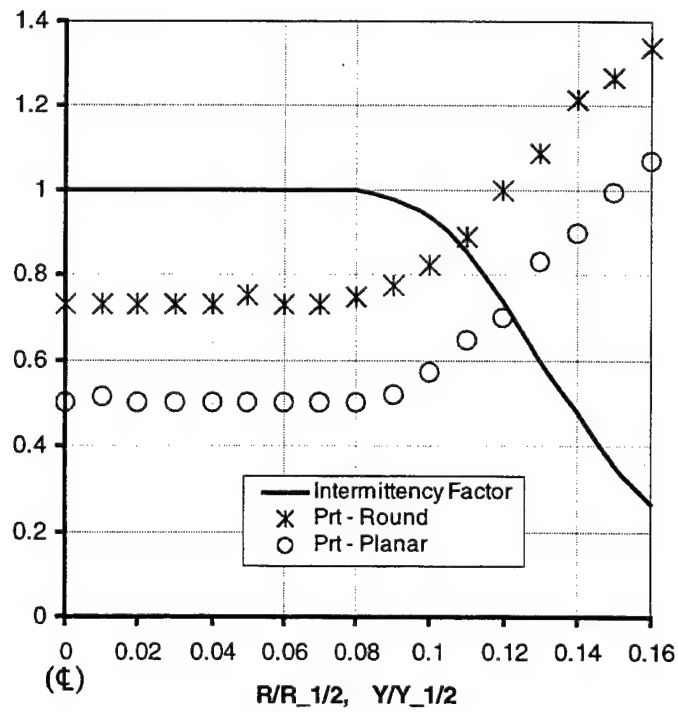
Figure 4.   Typical Prt and γ Variations across a round and planar jets [Based on Reynolds (1976)]

30

The Turbulence intermittency factor (γ) in the jet profile varies from unity near the jet centerline ($\mathcal{C}$) and inner part of its shear layer to 0.5 and below in the outer edges of the shear layer. The most striking feature of the results is the difference between the Pr_t in the body ($\gamma=1$) and the outer edges of the highly turbulent shear layer. A Pr_t greater than unity indicates that momentum is being transferred more readily than heat in these highly intermittent regions via relatively large-scale turbulent structures.

These variations, although significant across the whole jet, are fairly small across the largest inner portion of the jet and can be approximated using a single global value for the entire jet. In general, the body values for round jets are larger than for planar jets. Chen / Rodi (1980) and Reynolds (1976) recommend the well accepted global Pr_t's listed in Table 4 when the density differences are small and the molecular Prandtl Number (Pr) is close to unity ($Pr_{t,air} \approx$ 0.7). These global approximations, of coarse, result in small CFD temperature over-prediction errors in the outer edges of the jets.

THIS PAGE INTENTIONALLY LEFT BLANK

IV.   CFD SIMULATION

A.   CODE AND COMPUTER

The CFD Research Corporation (CFDRC) developed the computational fluid dynamics package used in this research to analyze the different jet configurations. The CFD-ACE+ program (version 6.2) was run on an IBM/PC-based Gateway (Model GP6-450) 450 MHz clock-speed computer. The Random Access Memory was upgraded to 384MB to handle grid files with up to 300,000 three-dimensional unstructured cells. A brief description of the CFDRC code and its operation is provided in Appendix A.

B.   THE PROCESS

To gain experience with the code, isothermal jets were initially modeled using small domains with a coarse grid to minimize solution run times. This process allowed the flow conditions to be fully understood before the complexity of heat transfer was added. After the code was mastered at each step, an additional feature or component was activated. Grid refinement was also developed in the high gradient areas. Only the final heated jet models are discussed within this report. In the anticipation of further research with more complex flows using this code, only 3-dimensional unstructured tetrahedral cells were used in the generation of all grid domains.

C. HEATED AXISYMMETRICAL JET MODEL

The heated axisymmetrical round jet was modeled to investigate the ability of the code to predict these types of flows. Although this code can not model all factors effecting jet development (i.e., coherent structural modes, etc.), an overall performance evaluation of the code compared to experimental data was desired.

1. Grid Domain

A one-quarter section axisymmetrical grid was used to accurately model the developing jet and its surroundings while minimizing the total grid size. Smaller sections (i.e. 1/6, 1/8, etc.) were not used to prevent possible symmetric edge interference problems. Typical grid dimensions and overall configuration are shown in Figure 5. The total grid length was selected to be 40 jet exit diameters with a grid radius of slightly less than 8 jet exit diameters in order to capture the flow features without boundary interference. The overall grid domain was divided into two separate sub-domains. The inner sub-domain consisted of smaller cells to more accurately capture the high gradients of the main jet flow and its free shear layer (adaptive meshing was not available). The inner sub-domain was constructed as an inverted truncated cone to mimic the jet's radial spread as it travels downstream. The inner sub-domain encompasses most of the jet's flow throughout the entire grid domain. The jet enters this sub-domain through the lower face and exits through the top with entrainment coming in from the sides. The bottom boundary of the inner sub-domain is slightly larger than the jet exit diameter to facilitate a finer mesh (more accurate solution) around this transitional flow area.
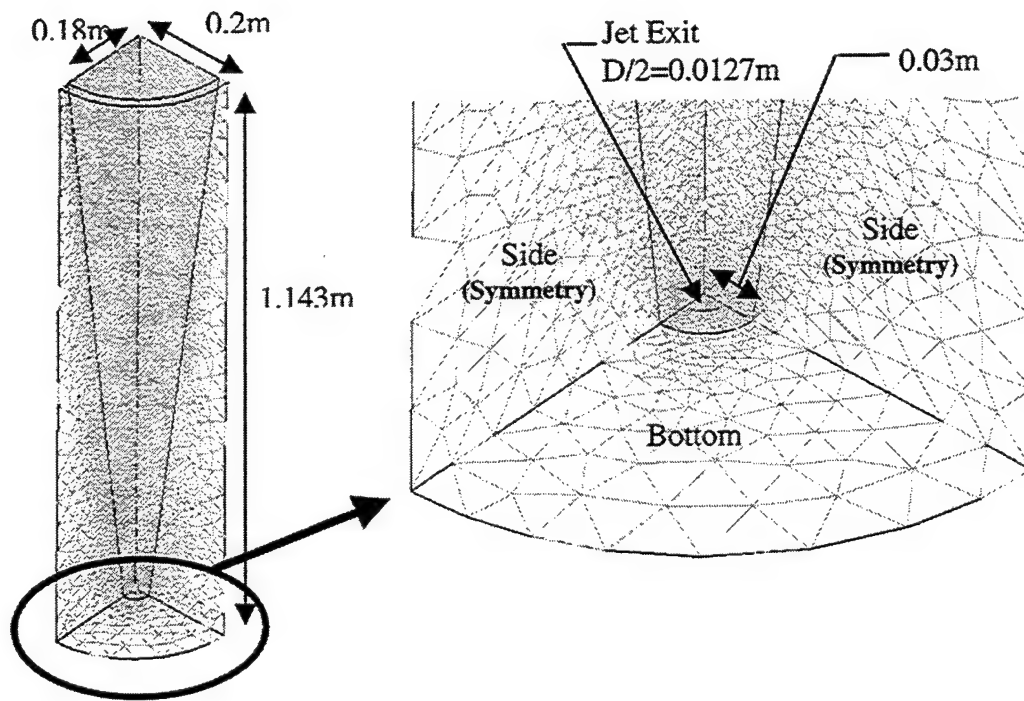
Figure 5.   Axisymmetrical Jet Grid

Before generating the internal tetrahedral volume grid, the inner sub-domain's boundary surface grids were automatically generated using the following dimensionless control parameters.

- Maximum cell size: 0.007

- Minimum cell size: 1.143×10^{-5}

- Curvature Criterion: 8

- Surface Transition Factor: 1.1

The Curvature Criterion defines the approximate maximum angle of curvature per cell that will be generated at edges that are curved. The Transition Factor limits the rate of cell growth (size change) when generating triangular surface cells from a curved edge to areas far from all curved edges.

After all surfaces of the inner sub-domain were gridded, a separate volume tool was used to invoke the tetrahedral volume grid generation algorithm. The tetrahedral volume grid generation algorithm used in CFD-GEOM is a variation of the advancing front grid generation technique. The size of the generated tetrahedrons change smoothly, based on the properties of the surface grids. One additional mechanism (besides those used in surface generation) was used to control the tetrahedral grid volume generation. The Volume Transition Factor, similar to the Surface Transition Factor, determined how far off a face that a field point would be generated for the formation of a new tetrahedron. For the inner sub-domain, the Volume Transition Factor was set at 1.1

In general, the outer sub-domain contained larger cells to model the airflow in the relatively slower moving surrounding environment. The outer boundaries of this domain were made vertical on the sides and horizontal on the top and bottom to simplify boundary conditions at these areas. The grid generation controls for this domain were set as follows.

- Maximum cell size: 0.05

- Minimum cell size: 1.143×10^{-5}

- Curvature Criterion: 30

- Surface Transition Factor: 1.2

- Volume Transition Factor: 1.2

The outer sub-domain grid was generated after the inner sub-domain so that the tetrahedral cells could progress smoothly from the small inner cells to the larger outer sub-domain cells at the grid boundaries.

Overall, the entire domain contained 317,273 tetrahedral cells with the following grid qualities as computed by the code. The CFDRC User Manual (2000) can be consulted for further definition of each criterion.

- Dihedral Angle: 3 cells were less than 5 degrees (default min.=5 degrees)

- Worst Centroid/Face Angle: 7.24 degrees (default min.=5 degrees)

- Sliver Quality: 5 cells were greater than 7 (default max.=7)

- Skew Quality: 52 cells were greater than 0.95 (default max.=0.95)

Only a small faction of the cells in non-critical areas violated the default limits and the gridded domain was determined to be satisfactory. Several other complex domain configurations were tried to further concentrate small cells in high gradient areas without greater grid quality

success. In addition, the higher domain complexity adversely effected the solution convergence. More controls are needed to properly manage the automatic grid generation process for unstructured cells and CFDRC plans to release future versions addressing this problem.

2. Solver Setup

a. *Overall*

Table 5 below provides a summary of all solver [CFD-GUI / CFD-ACE (U)] inputs. To simulate the heated jet, the flow, heat transfer and turbulence modules were activated. The relatively simple k-ε turbulence model was chosen to gain experience manipulating the code while maximizing solution convergence. As mentioned in Appendix B, the k-ε turbulence model constants can not be changed (within the code) for axisymmetrical flows as suggested by Launder/Spalding (1974). Therefore, without being able to vary C_μ and $C_{\varepsilon 1}$ (turbulence model closure constants) across the profile, the overall prediction accuracy for axisymmetrical jets was expected to be poor.

b. *Volume Conditions*

Air at ambient conditions was selected as the computational fluid. To simulate the heated jet ($\Delta T \cong 30K$), density calculations evaluated using the Ideal Gas Law while the viscosity was determined by Sutherland's Law [$\mu = AT^{3/2}/(B+T)$], where A and B are constants specified in Table 5. Since the simulation involved small differential temperatures, fluid conductivity (K) and specific heat (Cp) evaluations were determined by selecting the constant molecular Prandtl Number (Pr = 0.7) option and constant Cp = 1000 J/kg-K, respectively.

c. Boundary Conditions

The grid inlet boundary was modeled as 0.0254m (1-inch) diameter jet exit nozzle with a constant velocity (top hat) profile. Since the grid domain was modeled as a 1/4th section, the inlet boundary is shaped like a 1/4th "pie section" with a radius D/2 = 0.0127m. The ideal 'top hat' outlet jet velocity profile approximates the flow that most researches try to develop using large nozzle contractions. Although 'real' jets have small boundary layers which can drastically effect their development, an ideal top hat profile was used to simplify the CFD model. With a properly supplied sub-routine, a user can define any desirable inlet jet velocity profiles, however, the improvement in the final CFD solution was expected to be negligible when compared to the widely varying experimental jet data.

The constant jet nozzle exit velocity (U_e) {grid inlet} was initially set at 40m/s, in the axial direction (x), with a uniform temperature of 330 degrees, K. All inlet turbulence kinetic energies (k) needed for the Favre-Averaged Navier-Stokes (FANS) conservation equations (Equations 42 and 43) were calculated from Equation 37, in which the turbulence intensity (T_u) was assumed to be contemporary experimental values. A turbulence intensity of T_u = 0.5% was originally selected which resulted in $k = 0.06 \ \text{m}^2/\text{s}^2$.

$$k = \frac{3}{2}T_u^2 U_e^2 \qquad (37)$$

The inlet dissipation rate (ε) was input into the code by using the 'length scale option' as discussed in Appendix B. This method required that the inlet size dimension (L) be specified, then the turbulent length scale (0.3% of the size of the inlet size dimension) is subsequently calculated within the program. Since the grid inlet boundary is a "pie section", the size dimension was set at L = 0.0127m (inlet boundary radius).

The straight sides of the $1/4^{th}$ section grid domain were set as symmetric boundaries. The rest of the grid boundaries (top, curved front surface and rest of the bottom) were established as fixed (static) ambient pressure outlets. This setup, however, does allow flow to enter the grid domain through the side and bottom boundaries for entrainment. The outlet boundary parameters were set to characterize the flow as it entered the grid domain from the infinite surroundings.

d. *Initial Conditions*

The initial conditions are displayed in Table 5. The starting turbulent viscosity was artificially elevated (via k and L) to enhance solution convergence during the earliest solution iterations.

e. *Solver Control*

A 1st-order upwind spatial differencing scheme was chosen for all variables in the jet models to simplify convergence operations and minimize solution times (typically 2-3 days). The default CGS+Pre (conjugate-gradient-squared plus preconditioning) linear equation solver

was also chosen to resolve the algebraic equations for each dependent variable and the controlling parameters. The solver performed satisfactory without approaching its internal default maximum number of sweeps criterion (50 or 500 sweeps, depending on the variable). The under-relaxation parameters were also left at their default values (see Table 5), which seemed to work adequately.

Table 5.   Summary of Round Jet Solver Settings

Problem Type		
Modules		Flow Heat Transfer Turbulence
Global		Steady Time Dependence
Model Options		
Flow	Reference Pressure	10^5 (Pa)
Turbulence	K-Epsilon Model	$Pr_t = 0.7$
Volume Conditions		
Both Domains	Property Mode	Fluid
	Density Evaluation Method	Ideal Gas Law M.W. = 29 (default)
	Viscosity Evaluation Method	Sutherland's Law A = 1.4605E-6 B = 112 (default)
	Specific Heat Evaluation Method	Constant Cp = 1000 J/kg-K (default)
	Conductivity Evaluation Method	Mol. Prandtl Number Pr = 0.7
Boundary Conditions		
Inlet	Mode	Fix Vel. (Cartesian)
	U Velocity (u)	40 (m/s)
	V Velocity (v)	0 (m/s)
	W Velocity (w)	0 (m/s)
	Relative pressure (p)	0 (Pa)
	Temperature (T)	330 (K)
	Turbulent Kinetic Energy (k)	Constant: 0.06 (m^2/s^2)
	Dissipation Rate {Length Scale Method} (L)	0.0127 (m)
Outlets	Mode	Fixed Pressure
	Relative pressure (p)	0 (Pa)
	Temperature (T)	300 (K)
	Turbulent Kinetic Energy (k)	Constant: 0.00015 (m^2/s^2)
	Dissipation Rate {Length Scale Method} (L)	0.1 (m)
Initial Conditions		
Flow	Initial Source	Constant Values
	U Velocity (u)	10 (m/s)
	V Velocity (v)	0 (m/s)
	W Velocity (w)	0 (m/s)
	Relative pressure (p)	0 (Pa)
Heat	Temperature (T)	300 (K)
Turbulence	Turbulence Kinetic Energy (k)	1.0 (m^2/s^2)
	Dissipation Rate {Length Scale Method} (L)	0.01 (m)
Solver Control		
Spatial Differencing Scheme	Velocities	Upwind (default)
	Density	Upwind (default)
	Enthalpy	Upwind (default)
	Turbulence	Upwind (default)
Solver Selection	Velocity	CGS+Pre (default)
	P Correction	CGS+Pre (default)
	Enthalpy	CGS+Pre (default)
	Turbulence	CGS+Pre (default)
Under-Relaxation Parameters	Velocities	0.2 (default)
	P Correction	0.2 (default)
	Enthalpy	0.05 (default)
	Turbulence	0.2 (default)
	Pressure	1 (default)
	Density	1 (default)
	Viscosity	1 (default)
	Temperature	1 (default)

D.   HEATED PLANAR JET MODEL

1.   Grid Domain

Again, only 3-dimensional unstructured tetrahedral cells were used in the generation of the planar grid domain. A rectangular grid was used to model half (1/2) of the developing planar jet and its still surroundings. See Figure 6 below for typical grid dimensions and overall configuration. The total grid length was selected to be 40 jet exit heights (H). A grid width of approximate 11.5 jet exit heights and depth of 4 jet exit heights was established in order to capture the flow features without boundary interference. The overall grid domain was again divided into two separate sub-domains. The inner sub-domain consisted of smaller cells to more accurately capture the high gradients of the main jet flow and its free shear layer. The jet enters the inner sub-domain through the lower face and exits through the top with entrainment coming from the non-symmetrical far side. The bottom boundary of the inner sub-domain is slightly larger than the jet exit diameter to facilitate a finer mesh (more accurate solution) around this transitional flow area.
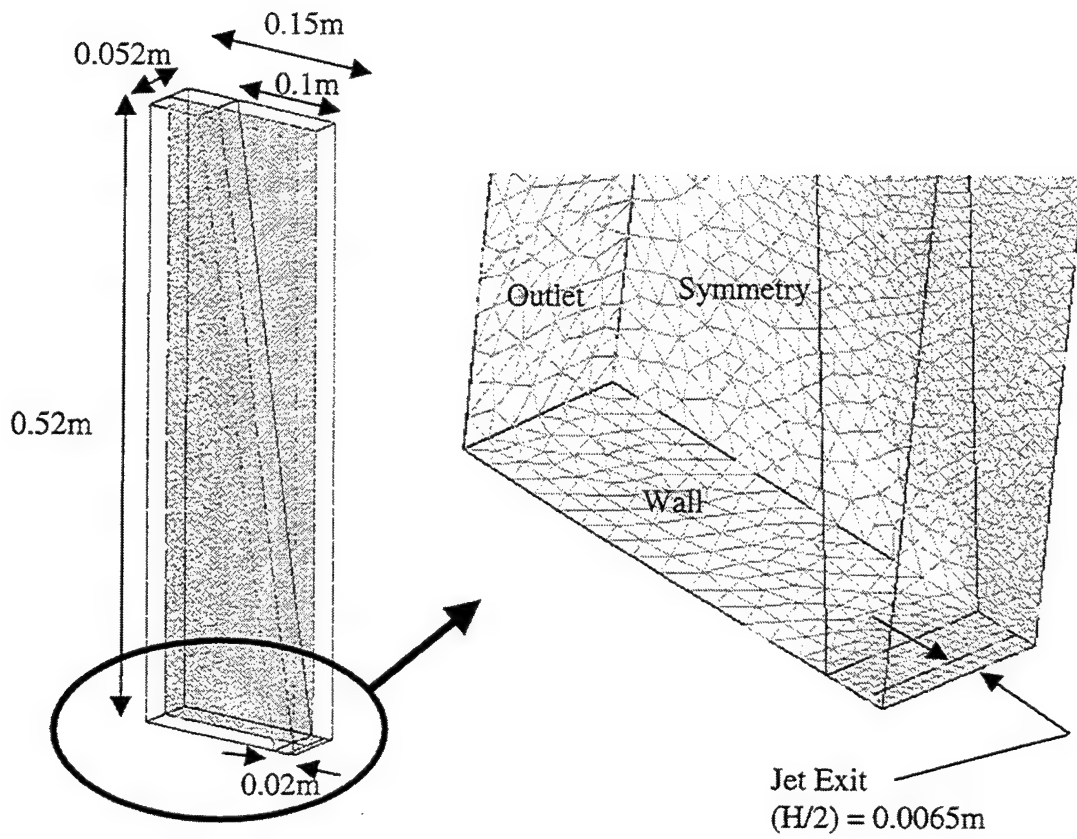
Figure 6.   Two-Dimensional Jet Grid

The inner sub-domain's boundary surface and volume grid was automatically generated using the following control parameters.

- Maximum cell size: 0.004

- Minimum cell size: 5.2×10^{-6}

- Surface Transition Factor: 1.1

- Volume Transition Factor: 1.1

The outer sub-domain grid generation controls were as follows.

- Maximum cell size: 0.01

- Minimum cell size: 5.2×10^{-6}

- Surface Transition Factor: 1.1

- Volume Transition Factor: 1.1

The outer sub-domain grid was generated after the inner sub-domain so that the tetrahedral cells could progress smoothly from the small inner cells to the larger outer sub-domain cells at the grid boundaries. The typical cell size was smaller than the axisymmetric jet model due to the smaller overall grid volume (limited to approximately 300,000 cells).

Overall, the entire domain contained 297,657 tetrahedral cells with the below grid qualities as computed by the code. All grid quality checks were within limits and the gridded domain was determined to be satisfactory.

- Worst Dihedral Angle: 6.54 degrees (default min.=5 degrees)

- Worst Centroid/Face Angle: 18.11 degrees (default min.=5 degrees)

- Sliver Quality: 1 cell at 7.01 (default max.=7)

- Worse Skew Quality: 0.93 (default max.=0.95)

2.   Solver Setup

a.   *Overall*

Table 6 below provides a summary all of the solver inputs, which are very similar to the round jet simulation.

b.   *Boundary Conditions*

The 2-dimensional jet exit nozzle (grid inlet boundary) was modeled with a height of 0.013m (1/2-inch) and a constant 'top hat' velocity profile. Since the grid domain was a 1/2 section, the inlet boundary has a half-height of D/2 = 0.0065m. Therefore, the inlet dissipation rate (ε), using the length scale option, was set at L = 0.0065m to match the grid inlet size (similar to the axisymmetrical jet model).

The bottom boundary was established as an adiabatic wall to emulate the configuration of most heated planar jet experiments. The rest of the grid boundaries were established as fixed ambient pressure outlets. The outlet boundary parameters were again set to characterize the surrounding flow if it entered the grid domain from the infinite surroundings.

c.   *Initial Conditions*

The initial conditions are displayed in Table 6. The starting turbulent viscosity was artificially elevated (via k and L) to enhance solution convergence during the earliest iterations.

46

d.   *Solver Control*

A 1st-order upwind spatial differencing scheme was chosen for all variables in the jet models to simplify convergence operations and minimize solution times (typically 3 days). The default CGS+Pre (conjugate-gradient-squared plus preconditioning) linear equation solver was also chosen to resolve the algebraic equations for each dependent variable and the controlling parameters.   The solver performed satisfactory without approaching its internal default maximum number of sweeps criterion (50 or 500 sweeps, depending on the variable). Again, the under-relaxation parameters were also left at their default values, which seemed to work adequately.

Table 6. Summary of Planar Jet Solver Settings

Problem Type		
Modules	Flow Heat Transfer Turbulence	
Global	Steady Time Dependence	
Model Options		
Flow	Reference Pressure	10^5 (Pa)
Turbulence	K-Epsilon Model	$Pr_t = 0.5$
Volume Conditions		
Both Domains	Property Mode	Fluid
	Density Evaluation Method	Ideal Gas Law M.W. = 29 (default)
	Viscosity Evaluation Method	Sutherland's Law A = 1.4605E-6 B = 112 (default)
	Specific Heat Evaluation Method	Constant Cp = 1000 J/kg-K (default)
	Conductivity Evaluation Method	Mol. Prandtl Number Pr = 0.7
Boundary Conditions		
Inlet	Mode	Fix Vel. (Cartesian)
	U Velocity (u)	35 (m/s)
	V Velocity (v)	0 (m/s)
	W Velocity (w)	0 (m/s)
	Relative pressure (p)	0 (Pa)
	Temperature (T)	330 (K)
	Turbulent Kinetic Energy (k)	Constant: 0.00735 (m^2/s^2)
	Dissipation Rate {Length Scale Method} (L)	0.0065 (m)
Outlets	Mode	Fixed Pressure
	Relative pressure (p)	0 (Pa)
	Temperature (T)	300 (K)
	Turbulent Kinetic Energy (k)	Constant: 0.00015 (m^2/s^2)
	Dissipation Rate {Length Scale Method} (L)	0.05 (m)
Initial Conditions		
Flow	Initial Source	Constant Values
	U Velocity (u)	10 (m/s)
	V Velocity (v)	0 (m/s)
	W Velocity (w)	0 (m/s)
	Relative pressure (p)	0 (Pa)
Heat	Temperature (T)	300 (K)
Turbulence	Turbulence Kinetic Energy (k)	1.0 (m^2/s^2)
	Dissipation Rate {Length Scale Method} (L)	0.01 (m)
Solver Control		
Spatial Differencing Scheme	Velocities	Upwind (default)
	Density	Upwind (default)
	Enthalpy	Upwind (default)
	Turbulence	Upwind (default)
Solver Selection	Velocity	CGS+Pre (default)
	P Correction	CGS+Pre (default)
	Enthalpy	CGS+Pre (default)
	Turbulence	CGS+Pre (default)
Under-Relaxation Parameters	Velocities	0.2 (default)
	P Correction	0.2 (default)
	Enthalpy	0.05 (default)
	Turbulence	0.2 (default)
	Pressure	1 (default)
	Density	1 (default)
	Viscosity	1 (default)
	Temperature	ault)

48

V.   COMPARISON OF CFD RESULTS TO EXPERIMENTS

CFD simulation velocity and temperature profiles at different axial distances for both jets are displayed in Figures 7-8 for the round jet and Figures 15-16 for the planar jet. By using the similarity equations (Equations 5 through 36), the non-dimensional plots (Figures 9-14 for round jet and Figures 17-22 for planar jet) were generated to investigate the self-similar ranges of each jet. As shown, the simulated round jet doesn't achieve self-similarity until approximately 30 diameters downstream of the jet exit (see Figures 9, 10, 13, and 14). The simulated planar jet, on the other hand, reached similarity within approximately 25 nozzle heights (see Figures 17, 18, 21, and 22).

The centerline decay and spreading rates, as well as the virtual origins, for planar and round jet simulations are listed in Table 7. Regression ranges were calculated in the similarity region between 30 and 40 jet diameters (or slot heights) for both jet types. Several values (half-radius/length or centerline) were analyzed by a Microsoft Excel spreadsheet regression program to determine the slope [spreading or centerline decay rate (K)] and imaginary X-intercept [virtual origin (C)] of each plot. See Appendix C for a typical sample of the Excel spreadsheet used for round jet calculations.

49
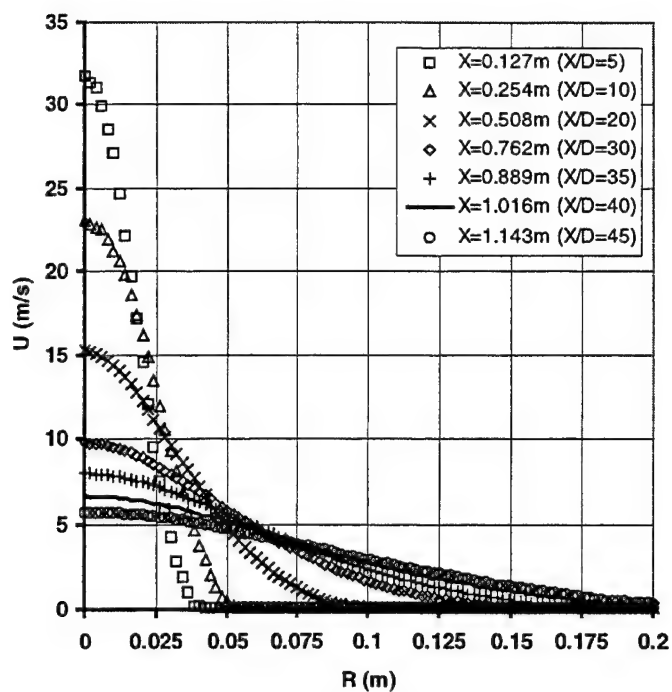
Figure 7.   Round Jet Velocity Profiles
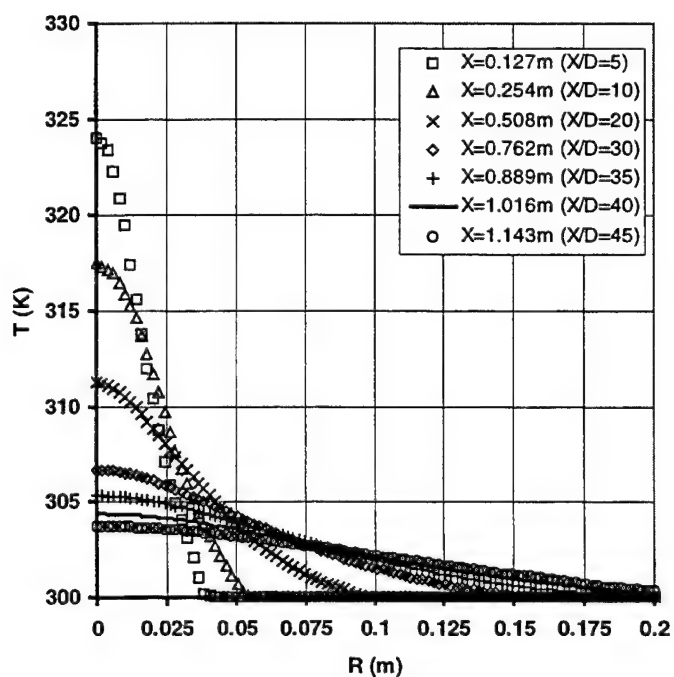
Figure 8.   Round Jet Temperature Profiles

50

Figure 9.   **Round Jet Centerline Velocity Decay**

Figure 10.   **Round Jet Centerline Temperature Decay**

51
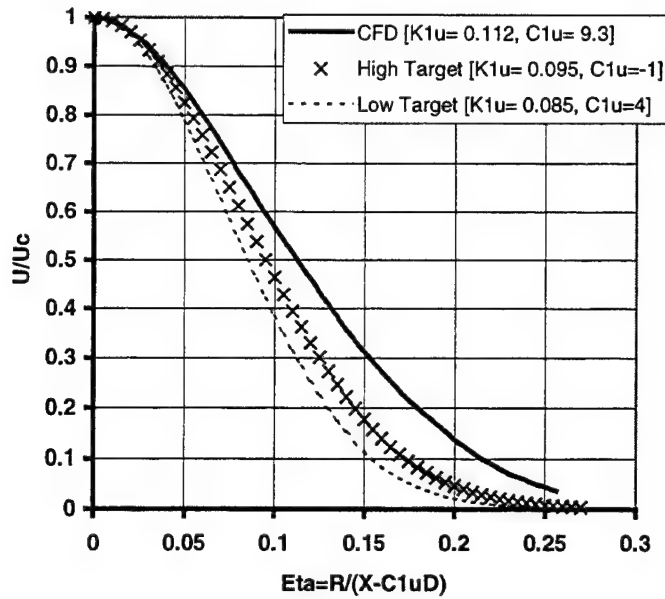
Figure 11.   Round Jet Velocity Profile in the Self-similar Region
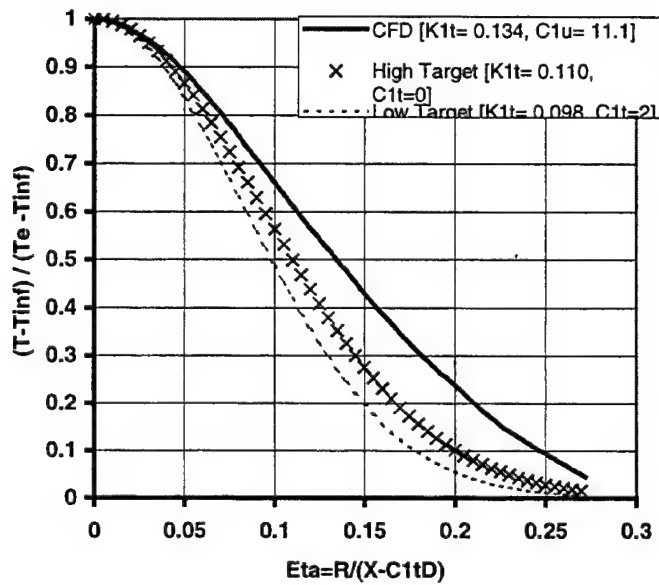
Figure 12.   Round Jet Temperature Profile in the Self-similar Region
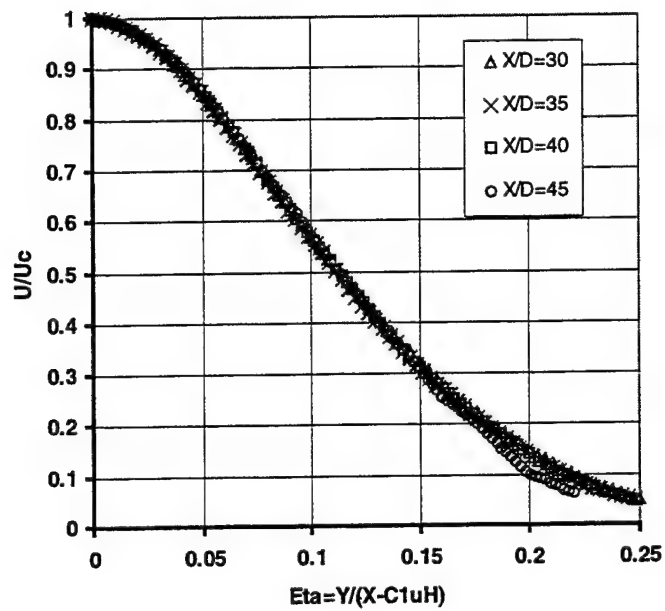
Figure 13.   Round Jet Velocity Similarity
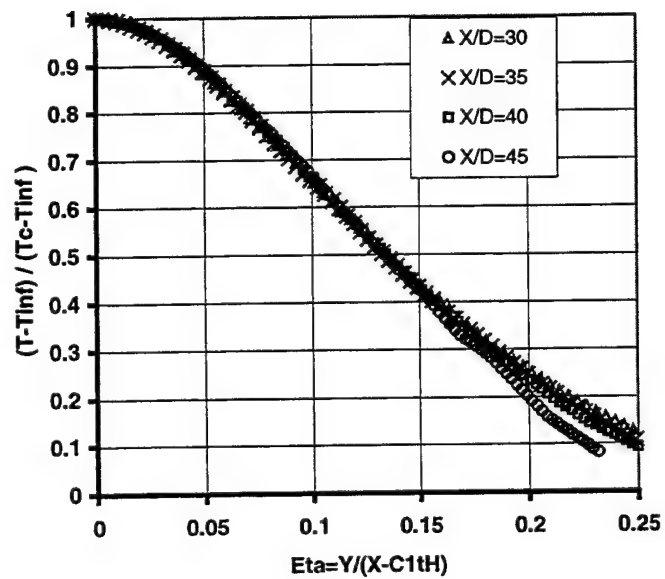
Figure 14.   Round Jet Temperature Similarity

53
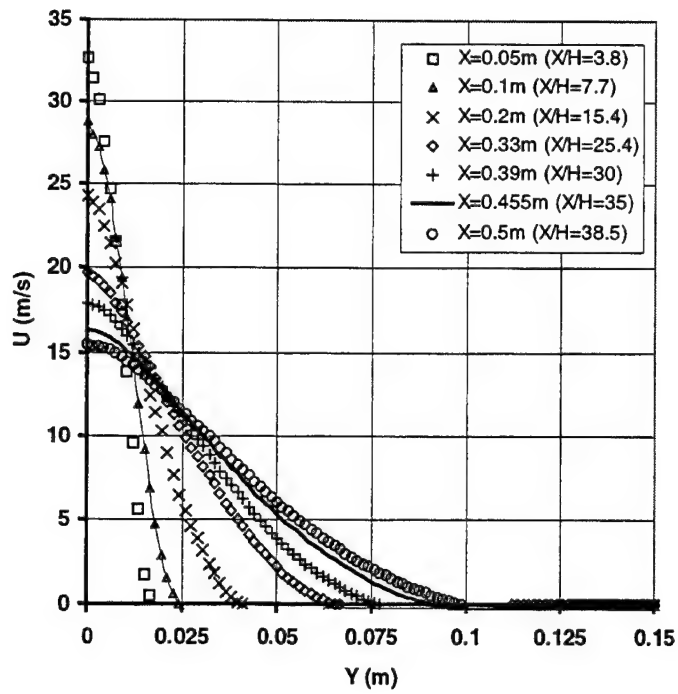
Figure 15.   Planar Jet Velocity Profiles
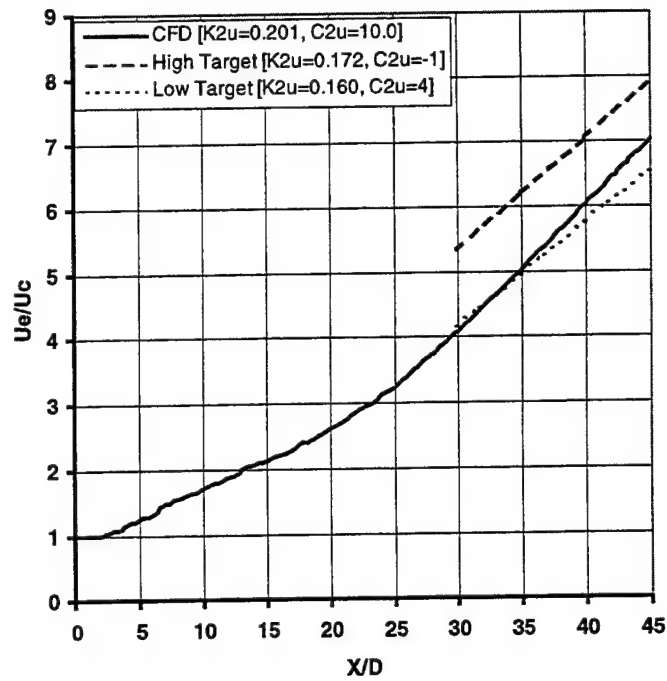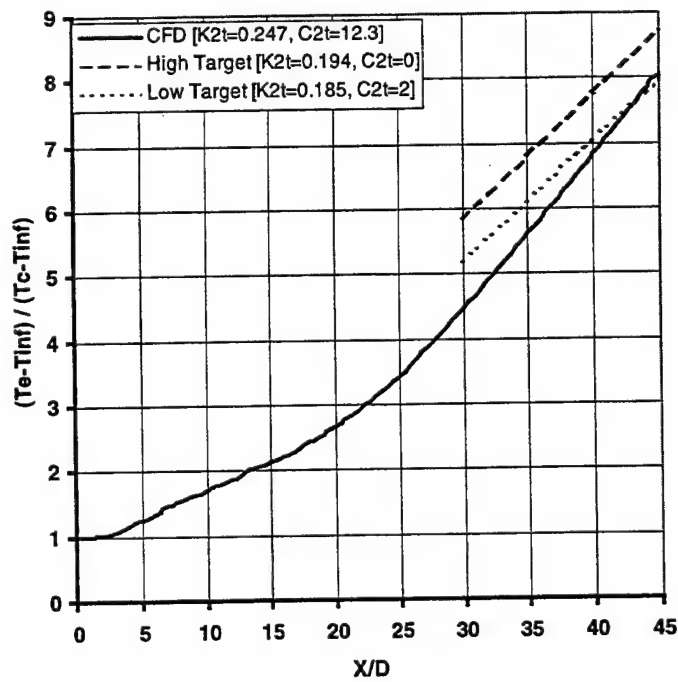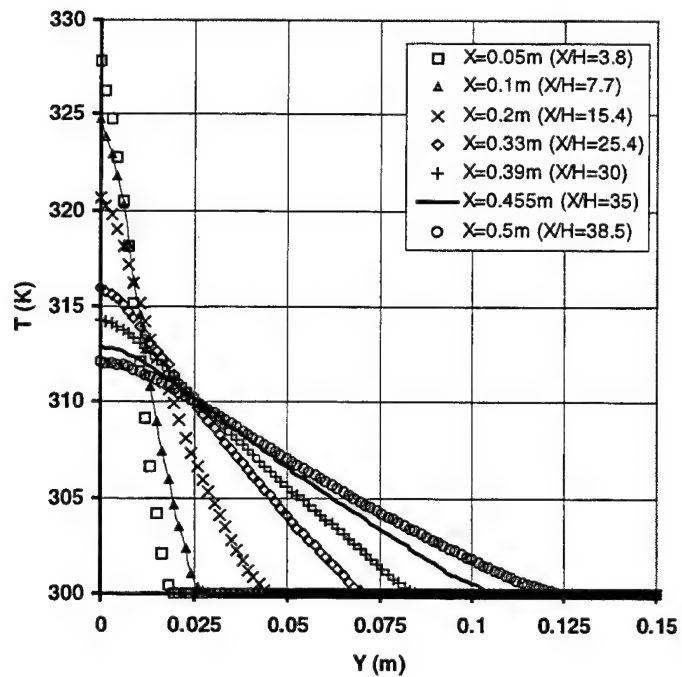

Figure 16.   Planar Jet Temperature Profiles

54

Figure 17.   Planar Jet Centerline Velocity Decay

Figure 18.   Planar Jet Centerline Temperature Decay

55

Figure 19. **Planar Jet Velocity Profile in the Self-similar Region**

Figure 20. **Planar Jet Temperature Profile in the Self-similar Region**

56

Figure 21.   Planar Jet Velocity Similarity

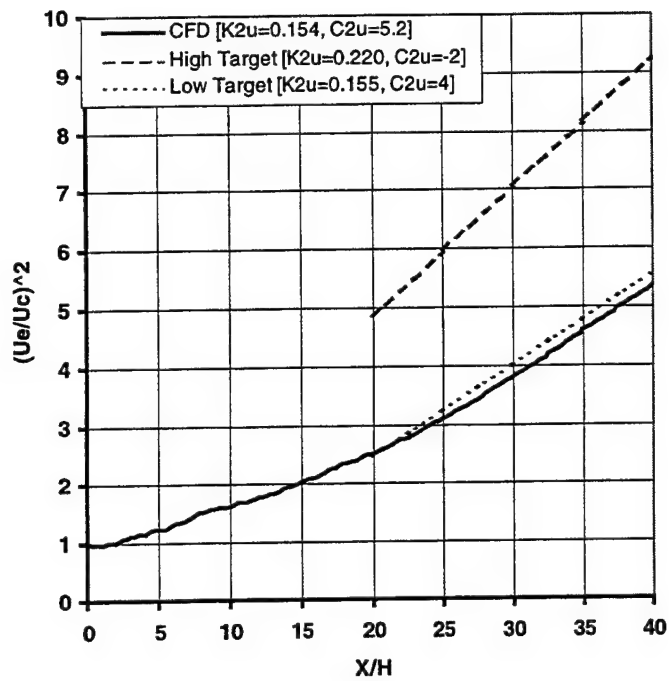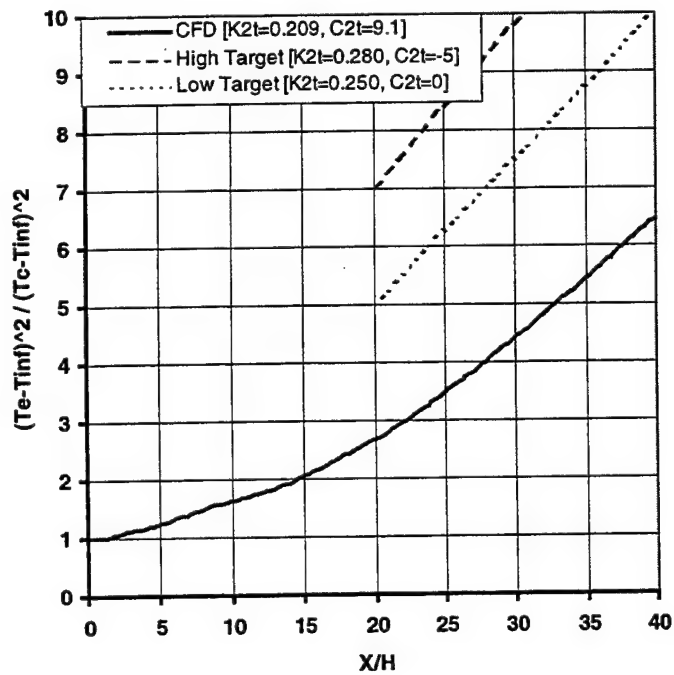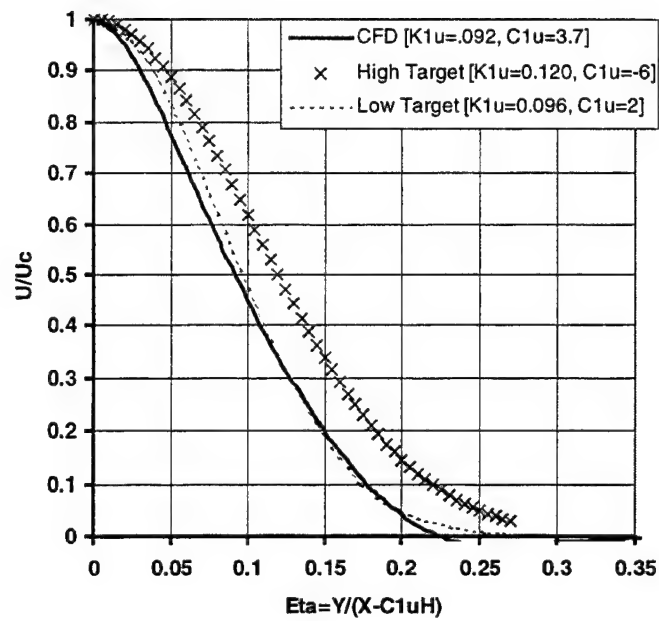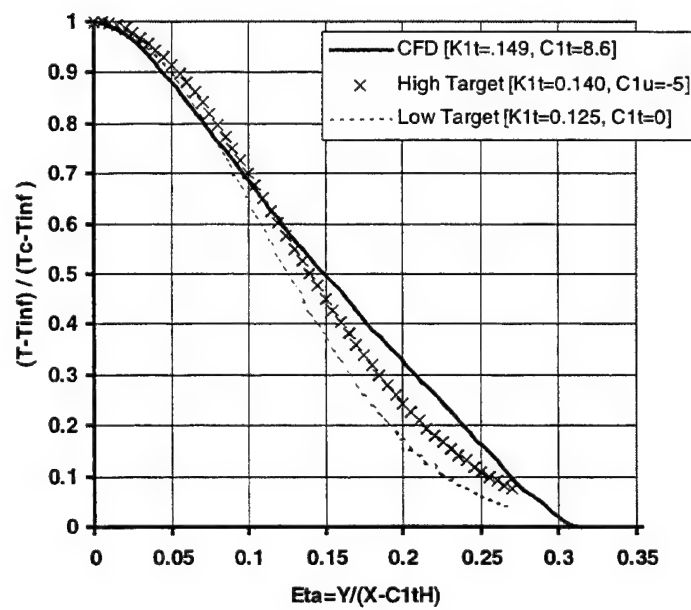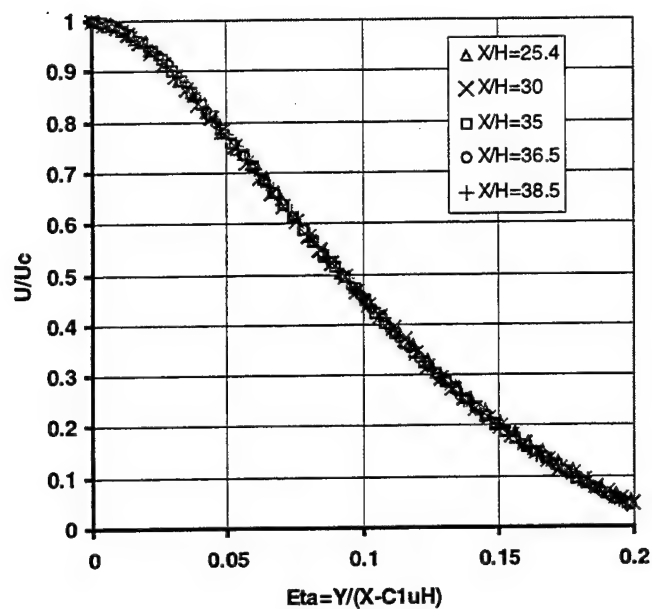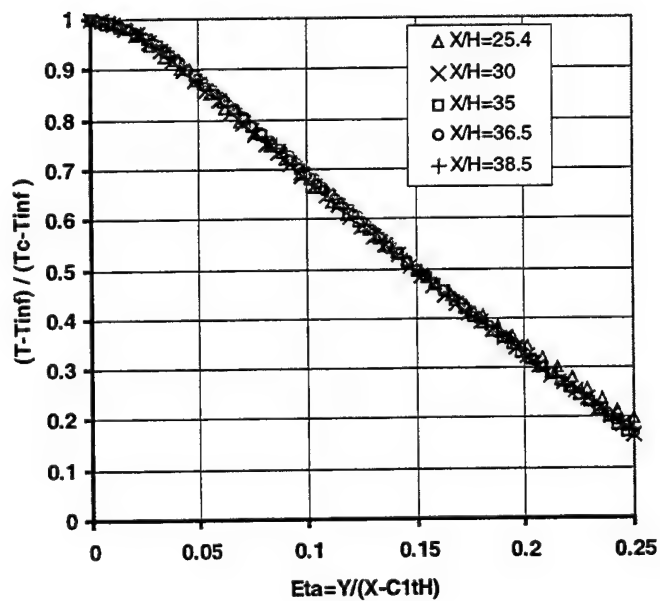**Figure 22.   Planar Jet Temperature Similarity**

57

Table 7.   CFD Simulation Predictions

Flow Type		Vel. Spread Rate $\{K_{1u}\}$	Geom. Virt. Orig. $\{C_{1u}\}$	C/L Vel. Decay $\{K_{2u}\}$	Kin. Virt. Orig. $\{C_{2u}\}$	Temp. Spread Rate $\{K_{1t}\}$	Spread Virt. Orig. $\{C_{1t}\}$	C/L Temp. Decay $\{K_{2t}\}$	Decay Virt. Orig. $\{C_{2t}\}$
Round Jet	CFD	0.112	9.3	0.201	10.0	0.134	11.1	0.247	12.3
	Target Values	0.085-0.095	-1.0 to 4.0	0.160-0.172	-1.0 to 4.0	0.098-0.110	0.0 to 2.0	0.185-0.194	0.0 to 2.0
	Eval.	+24%	+7.8D	+21%	+7.5D	+29%	+10.1D	+30%	+11.3D
Planar Jet	CFD	0.092	3.7	0.154	5.2	0.149	8.6	0.209	9.1
	Target Values	0.096-0.120	-6.0 to 2.0	0.155-0.220	-2.0 to 4.0	0.125-0.140	-5.0 to 0.0	0.250-0.280	-5.0 to 0.0
	Eval.	-17%	+5.7H	-22%	+6.2H	+12%	+11.1H	-27%	+11.6H

The CFD predictions can be compared to the target values listed in Table 7 and visualized in Figures 9 through 12 for the round jet and 17 though 20 for the planar jet. These non-dimensionalized CFD profile plots were generated at X/D=40 for the round jet (X/H=35 for the planar jet). The target value ranges, indicated on the figures for each jet, represent the reported variation of experimental data (target value range) in the self-similar region only. The 'High Target' curves indicate the upper bound on experimental data while the 'Low Target' curves represent the lower experimental data boundaries. As indicated, none of the CFD predictions fell within the targeted ranges. Evaluations were performed to quantify the difference between CFD results and the target value ranges. Each CFD value (K or C) was compared to the 'middle value' of the target value range and presented as the 'Eval' values in Table 7.

58

A.   HEATED AXISYMMETRICAL JET RESULTS

As expected, the k-ε turbulence model simulated the round jet poorly as discussed in Section IV.C.2 and Appendix B. The round jet results indicated that the code over-predicted the velocity-spreading rate by 24% and the temperature-spreading rate by 29% when compared to the middle of their respective target value range. In addition, the centerline velocity and temperature decay rates were also over-predicted by 21% and 30%, respectively. The geometric and kinematic virtual origins were over-predicted, as well, by approximately 7.5 diameters for the velocity profiles and 10.5 diameters for the temperature profiles. Although experimental virtual origin data display significant variation, typical values are usually reported close to the jet exit $[-1 < X/D < 4]$.

B.   HEATED TWO-DIMENSIONAL JET RESULTS

Planar jet simulation was generally closer to experimental data ranges, with an under-prediction of the velocity-spreading rate of approximately 17% with an over-predicted temperature-spreading rate of 12%. The centerline velocity and temperature decay rates were both under-predicted at 22% and 27%, respectively. Again, the geometric and kinematic virtual origins were over-predicted by approximately 7.5 slot heights for the velocity profiles and 10.5 slot heights for the temperature profiles.

C. DIMENSIONAL JET COMPARISONS

To evaluated the actual differences between the CFD results and experiments, the non-dimensional experimental parameters (K's and C's) were used to generate actual profiles [velocity (m/s) and temperature (K: degrees Kelvin)] using the similarity equations (Equations 5 through 36). By comparing the actual profiles, further insight was discovered about the accuracy of the CFD code.

The 'middle values' of the target value ranges (experimental data ranges) were chosen for comparison with the CFD profiles (see Table 8). These middle values were used to generate 'average experimental profiles' and were not based on any specific study, but did establish a foundation for evaluation.

Table 8.   Simulation Comparison Parameters

Flow Type		Vel. Spread Rate $\{K_{1u}\}$	Geom. Virt. Orig. $\{C_{1u}\}$	C/L Vel. Decay $\{K_{2u}\}$	Kin. Virt. Orig. $\{C_{2u}\}$	Temp. Spread Rate $\{K_{1t}\}$	Spread Virt. Orig. $\{C_{1t}\}$	C/L Temp. Decay $\{K_{2t}\}$	Decay Virt. Orig. $\{C_{2t}\}$
Round Jet	CFD	0.112	9.3	0.201	10.0	0.134	11.1	0.247	12.3
	Middle Target	**0.090**	**1.5**	**0.166**	**1.5**	**0.104**	**1.0**	**0.190**	**1.0**
Planar Jet	CFD	0.092	3.7	0.154	5.2	0.149	8.6	0.209	9.1
	Middle Target	**0.108**	**-2.0**	**0.188**	**1.0**	**0.133**	**-2.5**	**.265**	**-2.5**

The CFD jet simulation exit velocities [Ue=40m/s round jet (Ue=35m/s planar jet)], temperatures (Te=330K), and jet sizes [D=0.254m round jet (H=0.013 planar jet)] were used as inputs to the produce the average experimental profiles. This approach, of coarse, ignores the effects of velocity and temperature on the development of coherent structures within free jets. However, an overall comparison was still desired.

The CFD and average experimental profiles were evaluated at X/D = 40 for the round jet and are displayed in Figures 23 and 24. The higher CFD centerline values (Uc, Tc) are the result of lower Ue/Uc and ΔTe/ΔTc values at X/D = 40 as displayed in Figures 9 and 10. Even though, the CFD results displayed higher centerline decay rates (K_{2u}, K_{2t}), their excessively large virtual origins (C_{2u}, C_{2t}) produced higher centerline values (Uc, Tc) at X/D = 40.

The planar jet profiles were evaluated at X/H = 35 and are shown in Figures 25 and 26. Again, the CFD simulations display larger centerline values (Uc, Tc) due to excessive virtual origins (see Figures 17 and 18). Even though the planar jet simulation predicted spreading and centerline decay rates (K's) closer to experimental data than the round jet simulation, the differences in the actual profiles at X/H = 35 was generally worse for the planar jet due to its excessive virtual origins. At different distances from both jet exits, the actual results will vary due to the offsetting errors in the virtual origins and spreading/decay rates.

61
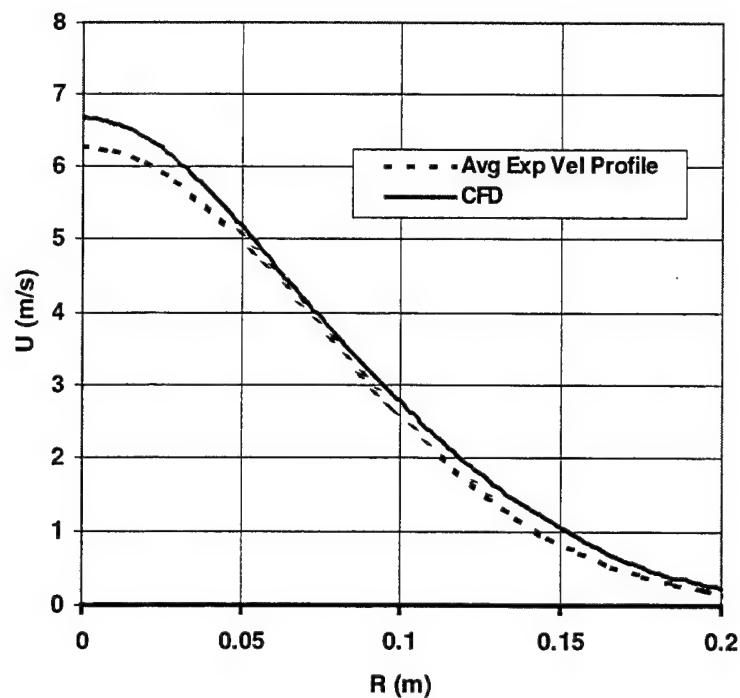
Figure 23.   Actual Round Jet Velocity Profiles at X=1.016m (X/D=40)
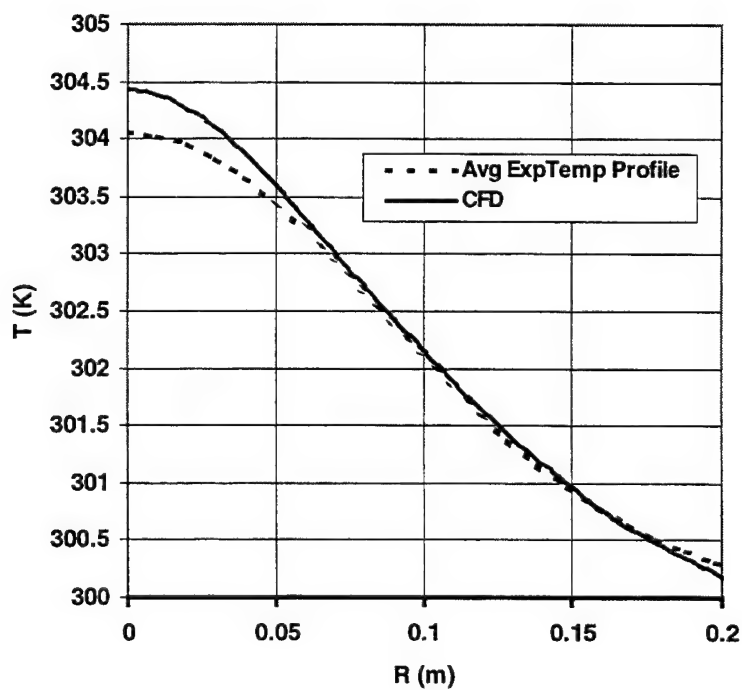
Figure 24.   Actual Round Jet Temperature Profiles at X=1.016m (X/D=40)
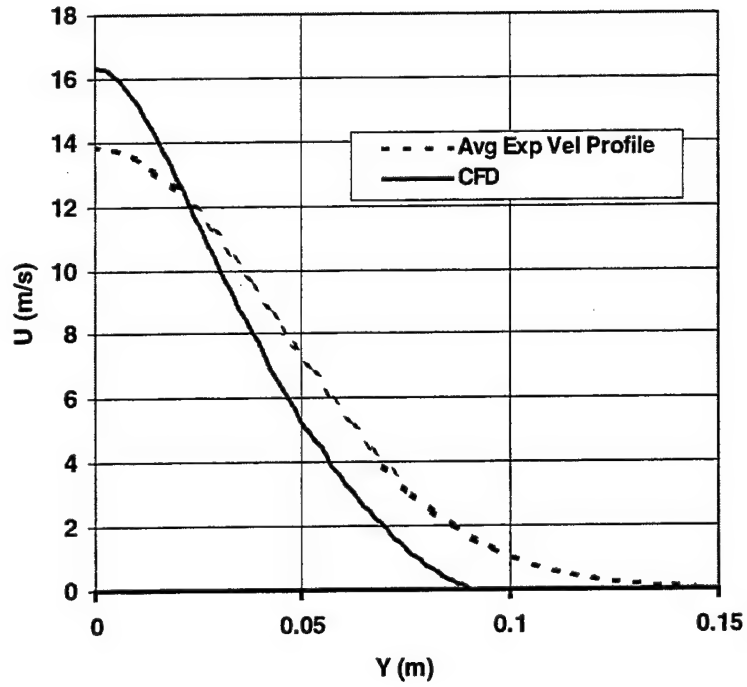
Figure 25. Actual Planar Jet Velocity Profiles at X=0.455m (X/H=35)
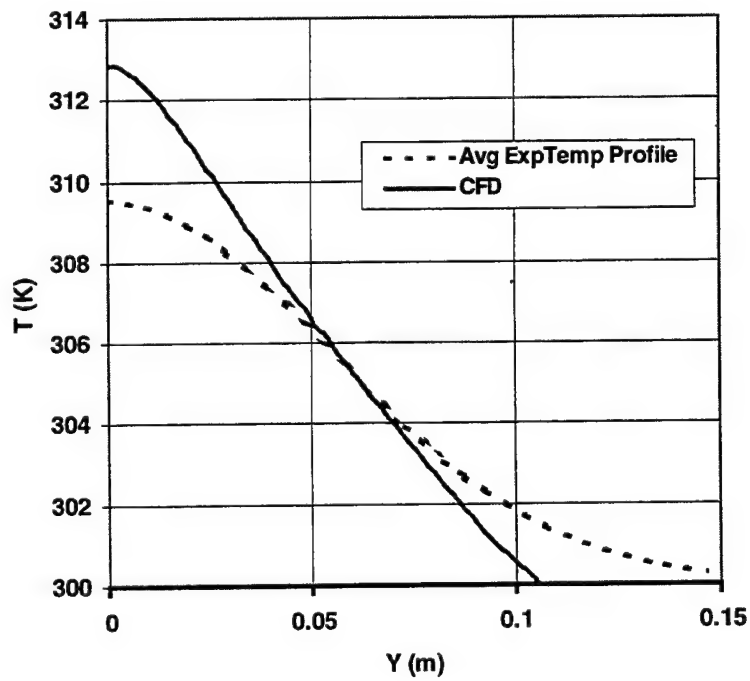
Figure 26. Actual Planar Jet Temperature Profiles at X=0.455m (X/H=35)

63

THIS PAGE INTENTIONALLY LEFT BLANK

VI. SENSITIVITY ANALYSIS

To evaluate the sensitivity of the CFD models and possibly produce more accurate results, various parameters were changed to observe their resultant effects. This baseline knowledge will be used in further research to help predict jet-type flows more accurately.

A. JET TURBULENCE INTENSITY

The jet turbulence intensity was varied from 0.002 to 0.01 on the round jet (nominal = 0.005) and from 0.001 to 0.01 on the planar jet (nominal = 0.002). Table 9 and Figures 27 to 34 in Appendix D (Section A) display the results. The round jets virtual origins (C's) decrease slightly with increasing jet turbulence intensity while the multiplication constants (K's) remain relatively constant. The planar jet displays similar characteristics, but deviated in different directions. The smaller differences may be due to slight variations in the regression evaluation and not a result of jet turbulence intensity changes. Overall, the effects were minimal (<5%) within the given turbulence range.

B. TURBULENT PRANDTL NUMBER

The turbulent Prandtl Number (Pr_t) had one of the largest effects (~15%) on the jet predictions. The effects of changing the Pr_t by ±0.2 are shown in Table 10 and Figures 35 to 42 in Appendix D (Section B). For both jets, the Pr_t had no effect on the velocity characteristics as expected, but markedly changed the temperature features. When the Pr_t was lowered, the CFD code correctly produced wider temperature profiles (increased spreading) and larger centerline

temperatures decay rates as more emphasis was artificially placed on the heat transport mechanism relative to the momentum transport mechanism.

In general, the Pr_t can be adjusted to produce the desired temperature characteristics in relation to the velocity profiles. For both jet simulations, the recommended free jet Pr_t's (0.5-Planar, 0.7-Round) produced temperature profiles that were approximately same magnitude greater than the velocities profiles as reported by experimental data. However, for the round jet especially, the predicted velocity profiles were excessively wide, therefore the resultant temperature profiles were also too broad.

C.   JET LENGTH SCALE

Varying the characteristic length (L) artificially changed the jet turbulent length scale (ℓ) as described in Appendix B. The characteristic length was varied from 0.001m to 0.1m for both jets to investigate the resultant effect. Table 11 and Figures 43 to 50 in Appendix D (Section C) display the results. As shown, changes in the results were negligible (<1%) and the original length scales used in each simulation were determined to be adequate.

D.   JET VELOCITY

The jet velocity was varied from 20 to 60 m/s on the round jet (nominal = 40m/s) and between 15 and 55 m/s on the planar jet (nominal = 35m/s). These ranges were limited to typical experimental values in order to identify any trends at these lower velocities. The results are

66

shown in Table 12 and Figures 51 through 58 in Appendix D (Section D). The change in velocity did not appreciably effect (<1%) either jet prediction. Since no boundary layers alterations were simulated at the jet nozzle (top hat velocity profile), the velocity variations did not change the solution results.

E.   JET TEMPERATURE

The jet exit temperatures for both models were elevated to 500K degrees (200K above ambient surroundings) to show the effects of a larger temperature difference. By limiting differential temperatures to less than 200K, errors associated with using the "constant specific heat capacity" option within the simulation were minimized. As mentioned before, the "constant specific heat capacity" option greatly reduced solution convergence problems and is consistent with low working differential temperatures.

The results are displayed in Table 13 and Figures 59 to 66 in Appendix D (Section E). As indicated the temperature difference effects on the velocity and temperature profiles (and spreading rate) are negligible (<1%) within the simulated temperature range. However, the velocity and temperature centerline decay rates (K_{2u}, K_{2t}) increased markedly (~5%). The centerline decay characteristics are consistent with experimental data as described in Chapter III, Section C.2, however the simulated spreading rates (K_{1u}, K_{1t}) do not exhibit the coherent structure effect, as expected.

F.   GRID REFINEMENT

The individual cell sizes for the round jet model was reduced by two-thirds (three-fourths for planar jet) to investigate grid dependence of the solution. Since the computational ability was limited, overall grid length was reduced (by half) to keep the total number of cells less than 300,000. All other aspects of the models were kept the same. Figures 67 to 74 in Appendix D (Section F) illustrate the results. The plots are shown differently due to the inability of the shorter refined model to reach similarity. Therefore, the similarity equations could not be used to evaluate the jet characteristics and the predictions had to be displayed as shown.

The differences between the nominal and refined models were found to be small (<5%), therefore grid resolution was deemed satisfactory for both jets. Several additional grid configurations were attempted without successful solution convergence. However, future grid refinement in the jet shear layer and other high gradient areas may be able to produce more significant changes in the solution results. Time constraints limited further research in this area.

VII.   SUMMARY AND RECOMMENDATIONS

A critical review of free-jet experimental data was summarized and compared to CFD simulations. The CFDRC flow code, using the k-ε turbulence model, predicted round axisymmetric jets poorly while marginally estimating the two-dimensional planar jet flow. By not being able to vary some of the turbulence model constants, the code over predicted the velocity spreading and centerline decay of the round jet by approximately 25 percent. Accuracy of the planar jet simulations was generally better within an approximately 15 overall percent deviation, however larger centerline temperature decay errors existed.

Sensitivity analysis on both jet simulations indicated that changes in jet exit velocity (Ue), turbulence intensity (Tu), and turbulent length scale (L) had little or no effect on the solution results. The jet exit temperature (Te) and turbulent Prandtl Number (Pr_t), conversely, produced significant changes in the results. The recommended free-jet Prandtl Numbers (Chapter III, Section E.2) resulted in correct temperature profiles (spreading rates) when compared to the velocity profiles. The change in jet exit temperature also created correct centerline decay variations, but failed to produce appropriate spreading rate changes as reported in experiments.

Even though all attempts to increase the accuracy of the simulations failed, the sensitivity analysis and insights reported in this study should be extremely useful to follow-on researchers utilizing CFDRC's CFD-ACE+ code. Recommendations for further work include evaluating the alternative RNG k-ε turbulence model contained within the program. This turbulence model is

an updated variation of the k-ε model that uses a renormalization group approach to systematically remove the smallest scales of motion. The RNG k-ε turbulence model was tried several times without obtaining proper solution convergence, most probably due to grid size/refinement limitations (<300,000 cells). Time constraints prevented further in-depth troubleshooting attempts

More realistic jet exit profiles should also be simulated and compared to experimental data. By using Fortran input subroutines within the code, the user can import realistic jet velocity and temperature exit profiles. Since jet nozzle boundary layers have a significant effect on real jet behavior, their effects and sensitivity on the simulated results should also be investigated. In addition, turbulence quantities (k,ε) of the initial conditions should be varied to investigate their possible effects.

APPENDIX A. THE CFDRC PROGRAM

The CFD Research Corporation (CFDRC) provides a variety of tools for the simulation and analysis of fluid flow and associated physics for an assortment of industrial applications. CFDRC has specifically developed their software so that the average engineering professional can easily manipulate several multi-disciplinary engineering project simulations.

Typical numerical simulations involve three distinct process steps:

1) The volume of interest (or solution space) must be divided into discrete control volumes or cells.

2) One must then define the boundary conditions, initial conditions, and the required equations to be solved at each cell. In addition, the numerical technique used to solve the required equations must also be defined.

3) Finally, after the solution has been calculated, the information needed must be extracted from the large volume of data generated in the solution process.

CFDRC provides software modules and packages to address each of these steps for a total overall solution. This program, entitled CFD-ACE+ (Version 6.2), uses three separate, yet interactive codes to impart an "all in one" seamless commercial code flow solver. CFD-GEOM provides interactive geometry modeling and grid generation capabilities. Similar to computer aided design (CAD), geometry modeling is the process of creating a computer model of the geometry that makes up a problem domain. CFD-GEOM offers a NURBS-based geometry

71

engine with a variety of geometric construction tools. It also has the ability to import and export IGES data from most major industry CAD programs. Grid generation is the process of discretizing the problem domain with individual cells over which the flow equations are integrated. CFD-GEOM provides for the production of two classes of cells: structured and unstructured.

CFD-ACE (U) is an unstructured, polyhedral cell flow solver. It is also integrated with a wide variety of physics modules making it the core of a multi-disciplinary analysis environment. Inputs are specified for CFD-ACE (U) using CFD-GUI, an advanced graphical user interface that allows complete specification of the multi-physics problem.

CFD-ACE (U) employs a cell-centered control volume solution approach. This approach implies that the discrete equations are formulated by evaluating and integrating the fluxes across the faces that surround each control volume. In addition, CFD-ACE (U) uses a pressure-based methodology in which pressure becomes one of the dependent variables evaluated at each cell.

The CFD-ACE (U) unstructured flow solver can simulate a wide variety of flow regimes and phenomenon as listed below.

- Internal or External Flow
- Laminar or Turbulent Flow: (involves the solution of one or more additional equations)
- Incompressible or Compressible Flow

- Heat Transfer

- Mixing and Reaction: Flows involving multiple gases that mix

    and react can be modeled.

- Steady- state or Transient

- Several others [see CFDRC User Manuals (2000)]

CFD-ACE (U) also offers a variety of differencing schemes (1st-order upwind to high-speed 3rd-order) to compute the variables within the domain. The type of differencing scheme determines how the cell face values are calculated from adjacent cells. These schemes can be independently selected for each variable to be solved; however, for this investigation a 1st-order upwind scheme was chosen for all variables in the jet models to simplify convergence operations.

CFD-ACE (U) employs an iterative solution technique in which the assembled equations for each dependent variable are solved sequentially and repeatedly, with the goal of improving the overall solution with each iteration. This solution convergence reduces the variable value changes within each control volume until acceptably small values are obtained and the final overall solution is determined. The nonlinear coupled nature of the Navier-Stokes (and other relevant equations) makes it necessary to restrain or under-relax the iteration-to-iteration changes of each variable in order to obtain a stable convergence of the solution procedure. Under-relaxation constrains the amount that each variable can change from one iteration to the next. The dependent variables (u, v, w, and k) are modified by using an Inertial Factor. However, a

linear under-relaxation technique is applied to the auxiliary variables (p, T, μ, ρ). The code allows the user to change these under-relaxation values within the program to ensure stable solution convergence.

CFD-ACE (U) generates a wide variety of graphical and printed outputs. This output includes graphics files with information at each cell for use in CFD-VIEW and the printed output, which allows the user to monitor several variables at a fixed location in the problem domain. Integrated quantities such as mass flow-rates, heat transfer rates, and pressure forces can be written to the text output file. In addition, the change in the solution from iteration to iteration, or the residual, can be graphically monitored to assess convergence.

One of the larger challenges in computational modeling is the management of the large volume of data generated with each simulation. These data must be reduced to extract useful information, which can be applied to practical problems. To aid in the data reduction process, the CFD-ACE+ suite includes a 3-D graphical post-processor called CFD-VIEW.

CFD-VIEW contains a variety of tools to visualize and extract data from complex 3-D data sets. Various types of visual surfaces can be generated such as constant computational plane surfaces, cutting plane surfaces, iso-value surfaces, and unstructured surfaces. On each surface, contour levels of any of the variables in the data set can be displayed as value-colored lines, flooded contour levels, and continuously shaded value-colored surfaces. Vector fields can also be displayed on these planes using arrows that indicate magnitude and direction.

Other miscellaneous features of CFD-VIEW include a point probe that allows one to extract data from any point in the flow field, a line probe used to make X-Y plots, and a streamline tracer to create particle traces using any vector field in the model. CFD-VIEW also contains an expression calculator that allows one to perform many of the tasks necessary to reduce a computational data set into usable information. The calculator has a variety of built-in functions that enable cell-wise mathematical operations and derivative mathematical options that depend on more than one cell. Results of calculations can be visualized in the same way as any other data.

Overall, the three interactive codes of CFD-ACE+ {CFD-GEOM, CFD-GUI / CFD-ACE (U), and CFD-VIEW} work in harmony to step the user through the numerical simulation process. The reader is referred to the CFDRC User Manuals (2000) for more comprehensive information.

THIS PAGE INTENTIONALLY LEFT BLANK

APPENDIX B. CFD-ACE (U) STANDARD k-ε TURBULENCE MODEL

The non-linearity of the Navier-Stokes equations, coupled with the complexity of the boundary conditions, makes it impossible to obtain analytical solutions for all but a limited number of flows of engineering interest. Hence one is forced to resort to approximate or numerical methods. Even though a wide variety of numerical techniques can be applied to solve the Navier-Stokes equations for laminar flows, Direct Numerical Simulation (DNS) of turbulent flows is feasible only at very low Reynolds numbers. Turbulent flows are inherently unsteady and they contain a wide range of time and length scales, and resolution of these scales requires very short time steps and fine grids. The CPU and memory requirements are too large for most present day computers.

As most engineering applications only require time-mean quantities, the Navier- Stokes equations are usually averaged over time or ensemble of statistically equivalent flows to yield averaged equations. In the averaging process, a flow quantity is decomposed into mean and fluctuating parts. Reynolds (or time) averaging and Favre (or density) averaging are two of the more popular techniques generally used.

For turbulent flows, CFD-ACE (U) exclusively utilizes the Favre-Averaged Navier-Stokes (FANS) equations to solve for momentum and energy. Although the FANS equations contain less information than the full NS equations, they do contain additional unknown Reynolds stresses. These correlations between the fluctuating components arise in the averaging process, and are additionally modeled to achieve closure of the FANS equations. All the

turbulence models available in CFD-ACE (U) employ the generalized Boussinesq eddy viscosity concept in which the Reynolds stresses are treated as a linear function of the mean strain rate. The Generalized Transport Equation given below indicates the common form for all of the FANS equations.

$$\frac{\partial}{\partial t}(\rho\phi) + \frac{\partial}{\partial x_j}(\rho u_j\phi) = \frac{\partial}{\partial x_j}\Gamma_{eff}\frac{\partial\phi}{\partial x_j} + S_\phi \qquad (38)$$

{Transient} {Convection} {Diffusion} {Source}

The symbol ϕ may represent any of the velocity components, enthalpy, or other scalar flow variables. In the preceding equation, Γ_{eff} is the effective diffusivity and is modeled as:

$$\Gamma_{eff} = \frac{\mu}{Pr} + \frac{\mu_t}{Pr_t} \qquad (39)$$

S_ϕ is a generalized source term, which represents the mechanisms for the generation and destruction of ϕ. In addition, any terms that cannot be conveniently expressed as convection or diffusion (*e. g.*, the pressure gradient term in the momentum equations) can, in general, be lumped into the source term (S_ϕ).

The standard k-ε model, employed by CFD-ACE (U), is based on Launder / Spalding (1974). The two-equation model, in a FANS generalized form, governs the transport of turbulent kinetic energy (k) and its dissipation rate (ε). The square root of k is taken to be the velocity scale, while the length scale (ℓ) is modeled as:

$$\ell = \frac{C_\mu k^{3/2}}{\varepsilon} \qquad (40)$$

The expression for eddy kinematic viscosity is:

$$v_t = \frac{\mu_t}{\rho} = \frac{C_\mu k^2}{\varepsilon}$$

(41)

Therefore, the modeled equations for k and ε are:

$$\frac{\partial}{\partial t}(\rho k) + \frac{\partial}{\partial x_j}(\rho u_j k) = \rho P - \rho\varepsilon + \frac{\partial}{\partial x_j}\left[\left(\mu + \frac{\mu_t}{\sigma_k}\right)\frac{\partial k}{\partial x_j}\right]$$

(42)

$$\frac{\partial}{\partial t}(\rho\varepsilon) + \frac{\partial}{\partial x_j}(\rho u_j \varepsilon) = C_{\varepsilon 1}\frac{\rho P \varepsilon}{k} - C_{\varepsilon 2}\frac{\rho\varepsilon^2}{k} + \frac{\partial}{\partial x_j}\left[\left(\mu + \frac{\mu_t}{\sigma_\varepsilon}\right)\frac{\partial\varepsilon}{\partial x_j}\right]$$

(43)

with the production (P) defined as:

$$P = v_t\left(\frac{\partial u_i}{\partial x_j} + \frac{\partial u_j}{\partial x_i} - \frac{2}{3}\frac{\partial u_m}{\partial x_m}\delta_{ij}\right)\frac{\partial u_i}{\partial x_j} - \frac{2}{3}k\frac{\partial u_m}{\partial x_m}$$

(44)

The five constants used in the k-ε model are listed below. All of them are internal to the code and can not be changed for axisymmetrical flows as suggested by Launder/Spalding

$$C_\mu = 0.09$$

$$C_{\varepsilon 1} = 1.44$$

$$C_{\varepsilon 2} = 1.92$$

$$\sigma_k = 1.0$$

$$\sigma_\varepsilon = 1.3$$

(1974). Therefore, without being able to vary C_μ and $C_{\varepsilon 1}$ across the jet profile, the overall prediction accuracy for axisymmetrical jets will be poor.

The standard k-ε model is a high Reynolds Number model and is not intended to be used in the near-wall regions where viscous effects dominate the effects of turbulence. Instead, "wall functions" are used in cells adjacent to walls. The k and ε transport equations are not numerically integrated in these cells. Instead, semi-empirical expressions are used to relate k, ε, and the friction velocity $(\breve{u})$. These expressions are obtained from analysis of the momentum and turbulence equations for a flat plate boundary layer, assuming a logarithmic velocity profile.

$$k = \frac{\breve{u}^2}{\sqrt{C_\mu}} \tag{45}$$

$$\varepsilon = \frac{C_\mu^{3/4} k^{3/2}}{\kappa y} \tag{46}$$

The friction velocity $(\breve{u})$ is defined as:

$$\breve{u} = \sqrt{\frac{\tau_w}{\rho}} \tag{47}$$

where τ_w is the shear stress at the wall and is obtained by assuming the velocity profile between the wall and the next-to-wall grid points obeys the following "law of the wall":

For $y^+ < 11.5$ $\qquad u^+ = y^+$ $\qquad\qquad\qquad\qquad$ (48)

For $y^+ > 11.5$ $\qquad u^+ = \dfrac{1}{\kappa}\ln(Ey^+)$ $\qquad\qquad\qquad$ (49)

with the dimensionless distances y^+ and u^+ defined as:

$$y^+ = \frac{\rho y \breve{u}}{\mu} \qquad (50)$$

$$u^+ = \frac{u}{\breve{u}} \qquad (51)$$

The wall shear stress (τ_w) is calculated iteratively from the known values of y and u in the first cell. The constants appearing in Equations 46 and 49 are experimentally determined to be $E = 9.0$ and $\kappa = 0.4$ (von-Karman constant). Because the semi-empirical relations for k and ε in the first cell assume a logarithmic velocity profile, the turbulence wall functions are strictly valid only if the center of the cell nearest the wall is inside the logarithmic boundary layer ($30 < y^+ < 150$ suggested range). The wall shear stress, evaluated using Equations 48 and 49, is used to calculate the boundary condition for the velocity components parallel to the wall.

For specifying turbulence characteristics at inlet and outlet boundaries, three quantities can be utilized; turbulent kinetic energy (k), dissipation rate (ε), and length scale (ℓ). The code requires that only two of the three quantities be specified. It is usually more convenient, to provide a length scale instead of a dissipation rate value. For example, the length scale is usually the inlet diameter or height. In this case, the program will internally calculate the boundary value of ε from the given values of k and ℓ as shown in Equation 52, where the constant, C_μ still has the value 0.09.

$$\varepsilon = \frac{C_\mu k^{3/2}}{0.03L} \tag{52}$$

This formula assumes that the characteristic length scale for the turbulent eddies is approximately 0.3% of the size of the inlet dimension [L = D (or H) in our case]. The eddy-viscosity (μ_t) at the boundary is then internally calculated using the given k and the calculated (or given) ε as:

$$\mu_t = \frac{C_\mu \rho k^2}{\varepsilon} \tag{53}$$

After applying the Favre averaging procedure, the total enthalpy energy equation becomes:

$$\frac{\partial}{\partial t}(\rho h_o) + \frac{\partial}{\partial x_j}(\rho u_j h_o) = \frac{\partial}{\partial x_j}\left(K\frac{\partial T}{\partial x_j}\right) + \frac{\partial p}{\partial t} + \frac{\partial}{\partial x_i}(\tau_{ij} u_j) \tag{54}$$

where the total (stagnation) enthalpy is defined as:

$$h_o = i + \frac{p}{\rho} + \frac{1}{2}\left(u^2 + v^2 + w^2\right) \tag{55}$$

Similar to the momentum equation analysis, the viscous stress tensor (τ_{ij}) for Newtonian fluids can be related to the velocity gradients by the following equation.

$$\tau_{ij} = \mu\left(\frac{\partial u_i}{\partial x_j} + \frac{\partial u_j}{\partial x_i}\right) - \frac{2}{3}\mu\left(\frac{\partial u_m}{\partial x_m}\right)\delta_{ij} \tag{56}$$

where δ_{ij} is the Kroneker delta function: $\qquad \delta_{ij} = \begin{cases} 0 & \text{for } i \neq j \\ 1 & \text{for } i = j \end{cases}$

THIS PAGE INTENTIONALLY LEFT BLANK

Profile (Spreading) Calculations

CFD Spreading Data

X/D	R_1/2r	R_1/2i	R_1/2rD	R_1/2iD
40	0.087025	0.09183	3.429232283	3.865472441
35	0.072506	0.0805643	2.854566929	3.171822835
30	0.05894	0.0644259	2.320472441	2.538462756

REGRESSION SUMMARY OUTPUT FOR R_1/2i/D vs X/D (30<X/D<40)

Regression Statistics

Multiple R	0.999776922
R Square	0.999553894
Adjusted R Sq	0.99107787
Standard Error	0.016562967
Observations	3

ANOVA

	df	SS	MS	F	Signfic F
Regression	1	0.614674194	0.614674194	2240.617233	0.013447195
Residual	1	0.000274333	0.000274333		
Total	2	0.614948527			

	Coef's	Std Error	t Stat	P-value	Lower 95%
Intercept	-1.012568696	0.082538422	-12.26784895	0.0517887	-2.061314497
X Variable 1	0.110876984	0.0023402436	47.33515853	0.013447195	0.081113605

K1u	C1u
0.110876984	9.132445628

REGRESSION SUMMARY OUTPUT for R_1/2i/D vs X/D (30<X/D<40)

Regression Statistics

Multiple R	0.999679661
R Square	0.999359425
Adjusted R Sq	0.998718851
Standard Error	0.023792517
Observations	3

ANOVA

	df	SS	MS	F	Signfic F
Regression	1	0.883146662	0.883146662	1560.098563	0.016114296
Residual	1	0.000566084	0.000566084		
Total	2	0.883712745			

	Coef's	Std Error	t Stat	P-value	Lower 95%
Intercept	-1.460319554	0.118565382	-12.31657609	0.051574918	-2.966829123
X Variable 1	0.132901969	0.00336477	39.49808303	0.016114296	0.090148694

K1t	C1t
0.132901969	10.98794625

X	1.016
Dia	0.0254

CFD OUTPUT / PLOT DATA

R	U	T	Ea-u	U/Uc	Ea-t	dT/dTc
0	6.86301	304.4269	0		0	1
0.002020202	6.670361	304.4207	0.00257667	0.998107141	0.002741484	0.998599471
0.004040404	6.659651	304.3457	0.005153341	0.99066467	0.005482929	0.997470013
0.006060606	6.647218	304.4097	0.007730012	0.994944181	0.00931493	0.996114663
0.008080808	6.616752	304.3933	0.010306581	0.990085457	0.010366885	0.992410039
0.01010101	6.58298	304.3769	0.012883352	0.985536883	0.013707321	0.989705415
0.01212121	6.56349	304.3597	0.015460019	0.981047166	0.016448783	0.985045969
0.01414141	6.519808	304.3407	0.018036687	0.975579421	0.019190245	0.980528135
...	...	...	...	...	...	...
0.1494949	1.070193	300.9775	0.190673544	0.160136801	0.202868292	0.220809144
0.1515152	1.017661	300.9352	0.193250339	0.152275823	0.205603989	0.211253925
0.1535354	0.962434	300.89	0.195827008	0.144912033	0.20836135	0.20104362
0.1555556	0.9070294	300.8445	0.198403675	0.135721668	0.211063942	0.190765547
0.1575758	0.8545669	300.8011	0.200980343	0.127871539	0.213834274	0.180361647
0.159596	0.8157841	300.7677	0.20355701	0.122063353	0.216575735	0.173417084
0.1616162	0.7757773	300.7333	0.206133678	0.116082003	0.219317197	0.166646389
0.1636364	0.7299552	300.6931	0.208710346	0.110090827	0.222058658	0.156565542
0.1656566	0.6963856	300.6552	0.211287014	0.102706041	0.22480012	0.148004247
0.1676768	0.6453919	300.6188	0.213863682	0.099572024	0.227541581	0.139781789
0.169697	0.6163389	300.5927	0.216440349	0.092224732	0.230283043	0.133886015
0.1717172	0.5863876	300.5661	0.219017017	0.087743025	0.233024605	0.127876296
0.1737374	0.5497217	300.5364	0.221593685	0.082256691	0.235765966	0.121166312
0.1757576	0.5130562	300.5087	0.224170353	0.076770216	0.238507428	0.114453328
0.1777778	0.4763904	300.477	0.22674021	0.071128797	0.241248889	0.107750344
0.179798	0.44761	300.4495	0.229323688	0.066917295	0.243990351	0.101538323
0.1818182	0.4250531	300.4239	0.231900356	0.063600035	0.246731812	0.095755495
0.1838384	0.4024965	300.3982	0.234477024	0.06002692	0.249947314	0.089950078
0.1858586	0.3799396	300.3725	0.237053692	0.05685156	0.252214736	0.084144661
0.1878788	0.357383	300.3469	0.239630359	0.053476345	0.254956197	0.078361833
0.189899	0.3356434	300.3207	0.242207027	0.05022338	0.257697669	0.072443471
0.1919192	0.3149324	300.2941	0.244783695	0.047124326	0.2604391	0.066643751
0.1939394	0.2942213	300.2675	0.247360363	0.04402526	0.263180582	0.060426032
0.1959596	0.2735102	300.2408	0.249937031	0.040926193	0.265922043	0.054394723
0.1979798	0.2527991	300.2142	0.252513698	0.037827126	0.268663505	0.048386004
0.2	0.2320881	300.1876	0.255090366	0.034728074	0.271404967	0.042377284

Centerline Decay Calculations

Jet Diameter	
D (m)=	0.0254

REGRESSION SUMMARY OUTPUT for Ue/Uc vs X/D (X/D>35)

Regression Statistics

Multiple R	0.999916979
R Square	0.999833964
Adjusted R Sq	0.999826058
Standard Error	0.008171861
Observations	23

ANOVA

	df	SS	MS	F	Significe F
Regression	1	8.444775385	8.444775385	126457.9641	3.53025E-41
Residual	21	0.001402365	6.67793E-05		
Total	22	8.446177751			

	Coeff's	Std Error	t Stat	P-value	Lower 95%
Intercept	-2.013931725	0.022669582	-88.83850272	1.53726E-28	-2.0610757
X Variable 1	0.200967727	0.000565136	355.6092857	3.53025E-41	0.19979246

K2u	C2u
0.200967727	10.02116986

REGRESSION SUMMARY OUTPUT for dTe/dTc vs X/D (X/D>35)

Regression Statistics

Multiple R	0.999897749
R Square	0.999795508
Adjusted R Sq	0.99978577
Standard Error	0.011148643
Observations	23

ANOVA

	df	SS	MS	F	Significe F
Regression	1	12.7613985	12.7613985	102672.5364	3.14632E-40
Residual	21	0.002610137	0.00012429		
Total	22	12.76400863			

	Coeff's	Std Error	t Stat	P-value	Lower 95%
Intercept	-3.043807626	0.030927481	-98.41757104	1.79884E-29	-3.108124754
X Variable 1	0.247048035	0.000771	320.4255552	3.14632E-40	0.245444653

Kt	C2t
0.247048035	12.32071134

CFD OUTPUT / PLOT DATA

X	Uc	Tc	X/D	Ue/Uc	dTe/dTc
0	39.99972	330	0		
0.01154545	40.04134	329.9984	0.45454726	0.999960574	1.000053336
0.02309091	40.07048	329.9904	0.90909049	0.99823411	1.000320102
0.03463636	39.9202	329.8821	1.36363622	1.001987707	1.003945508
0.04618182	39.53506	329.599	1.81818189	1.011241545	1.01352721
0.05772727	39.04815	329.2261	2.27272165	1.024369144	1.026479756
0.06927273	37.94578	328.4631	2.727272835	1.054128285	1.053996227
0.08081818	37.05332	327.8035	3.18181811	1.079517841	1.079000845
.	.	.	.	.	.
.	.	.	.	.	.
.	.	.	.	.	.
0.8428182	8.537625	305.7753	33.1818189	4.685110906	5.194535349
0.8543636	8.398851	305.6621	33.6363622	4.762522874	5.298387524
0.8659091	8.243897	305.5517	34.09090945	4.852040243	5.403750203
0.8774546	8.093073	305.4422	34.54545669	4.942463759	5.512476572
0.889	7.958456	305.3417	35	5.02605337	5.616185603
0.9005455	7.822799	305.2403	35.45454724	5.113223641	5.72486308
0.9120909	7.681531	305.1428	35.90909055	5.207288813	5.833398149
0.9236364	7.563874	305.0524	36.3636378	5.289256371	5.937772148
0.9351818	7.435015	304.96	36.8181811	5.378911137	6.048387097
0.9467273	7.313878	304.8752	37.27272835	5.469016574	6.153593699
0.9582728	7.184611	304.782	37.72727659	5.567416246	6.273526721
0.9698182	7.077387	304.7012	38.1818189	5.65176365	6.381349443
0.9813637	6.963366	304.6189	38.6363614	5.744308141	6.495062935
0.9929091	6.851489	304.5395	39.09090945	5.838109614	6.608657341
1.004454	6.744654	304.4669	39.54543307	5.930581465	6.716067071
1.016	6.635124	304.3889	40	6.028481156	6.835426733
1.027545	6.53774	304.3195	40.46452756	6.118279405	6.945248293
1.039091	6.441493	304.2482	40.90909449	6.209697038	7.061814416
1.050636	6.342113	304.1803	41.36362205	6.307002099	7.176518432
1.062182	6.246802	304.1132	41.81818898	6.403231606	7.293591364
1.073727	6.164253	304.0547	42.27271654	6.488980903	7.398821121
1.085273	6.077325	303.9919	42.72728346	6.58179709	7.615218317
1.096818	5.95516	303.9301	43.18181102	6.672002082	7.633393552
1.108364	5.913419	303.8712	43.63637795	6.764228961	7.749635028
1.119909	5.84544	303.8139	44.09090551	6.842892922	7.865963974
1.131455	5.772453	303.7627	44.54547244	6.929414683	7.972998113
1.143	5.707756	303.7317	45	7.007965995	8.039231449

APPENDIX D. SENSITIVITY ANALYSIS FIGURES AND TABLES

A. JET TURBULENCE INTENSITY

Table 9.　　CFD Simulation Predictions with Varying Jet Turbulence Intensity

Jet Turb. Intensity $\{Tu\}$	Vel. Spread Rate $\{K_{1u}\}$	Geom. Virt. Orig. $\{C_{1u}\}$	C/L Vel. Decay $\{K_{2u}\}$	Kin. Virt. Orig. $\{C_{2u}\}$	Temp. Spread Rate $\{K_{1t}\}$	Spread Virt. Orig. $\{C_{1t}\}$	C/L Temp. Decay $\{K_{2t}\}$	Decay Virt. Orig. $\{C_{2t}\}$
AXISYMMETRICAL ROUND JET								
Target Values	0.085-0.095	-1.0 to 4.0	0.160-0.172	-1.0 to 4.0	0.098-0.110	0.0 to 2.0	0.185-0.194	0.0 to 2.0
0.002	0.111	9.4	0.200	10.2	0.134	11.3	0.246	12.5
(0.005)$_{nom}$	0.112	9.3	0.201	10.0	0.134	11.1	0.247	12.3
0.01	0.115	8.8	0.203	9.2	0.137	10.4	0.249	11.4
TW0-DIMENSIONAL PLANAR JET								
Target Values	0.096-0.120	-6.0 to 2.0	0.155-0.220	-2.0 to 4.0	0.125-0.140	-5.0 to 0.0	0.250-0.280	-5.0 to 0.0
0.001	0.091	3.6	0.152	5.1	0.145	8.4	0.207	9.1
(0.002)$_{nom}$	0.092	3.7	0.154	5.2	0.149	8.6	0.209	9.1
0.01	0.092	3.3	0.154	4.8	0.149	8.4	0.208	8.5
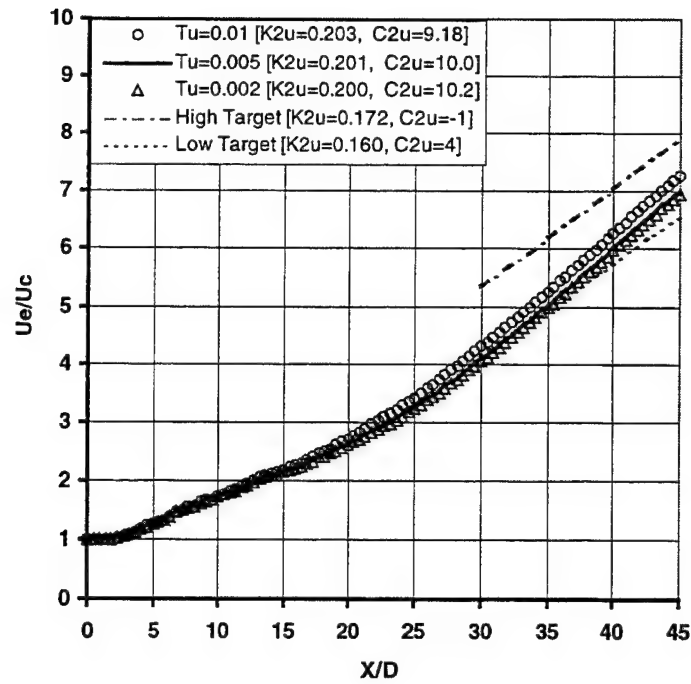
Figure 27. Round Jet Centerline Vel. Decay with Varying Jet Turb. Intensity
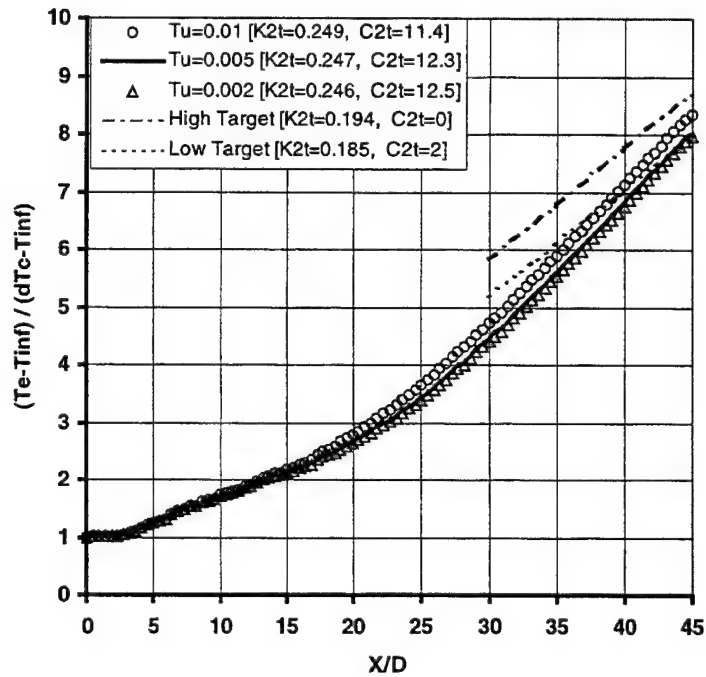
Figure 28. Round Jet Centerline Temp. Decay with Varying Jet Turb. Intensity
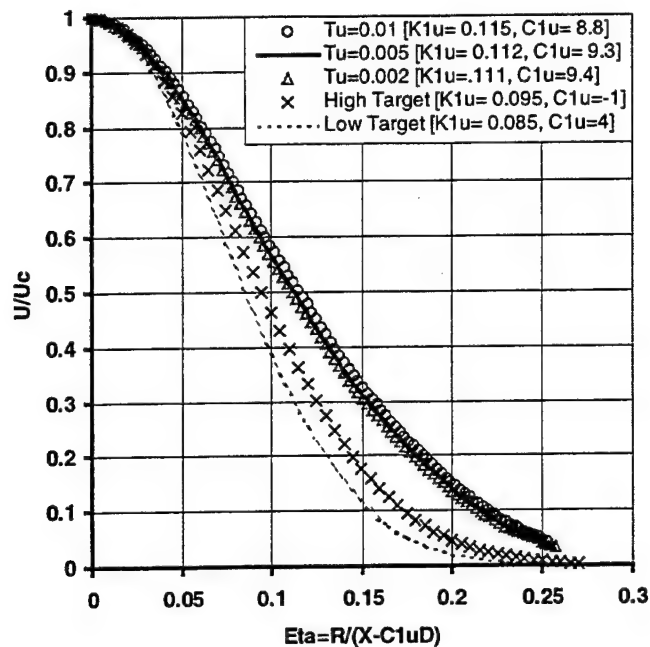
Figure 29.   Round Jet Velocity Profile with Varying Jet Turbulence Intensity
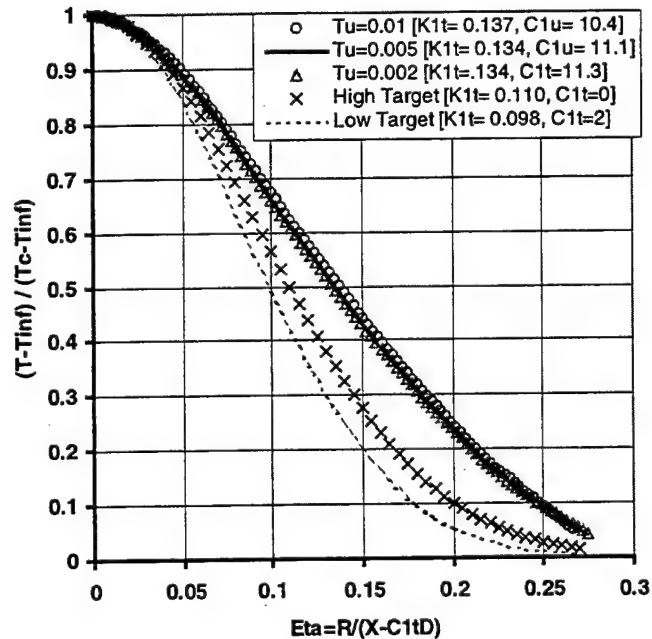
Figure 30.   Round Jet Temp. Profile with Varying Jet Turbulence Intensity

89
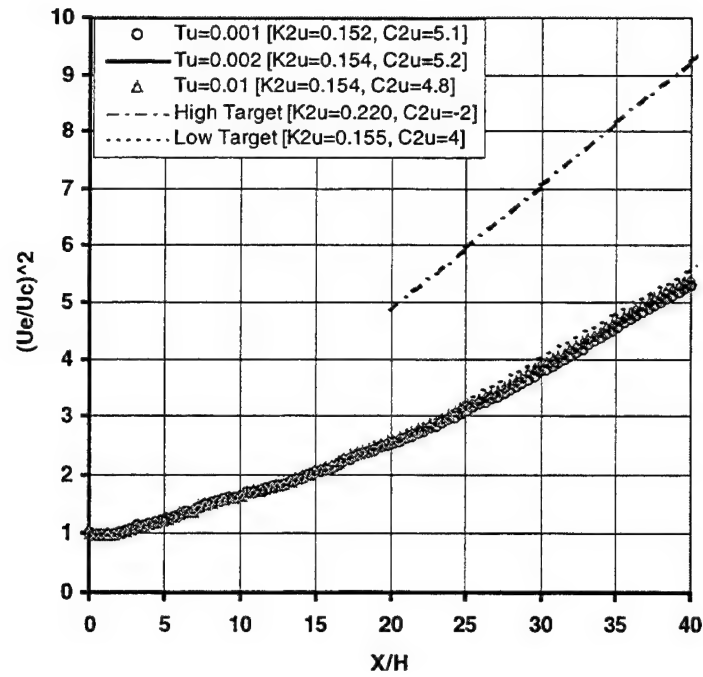
Figure 31. Planar Jet Centerline Vel. Decay with Varying Jet Turb. Intensity
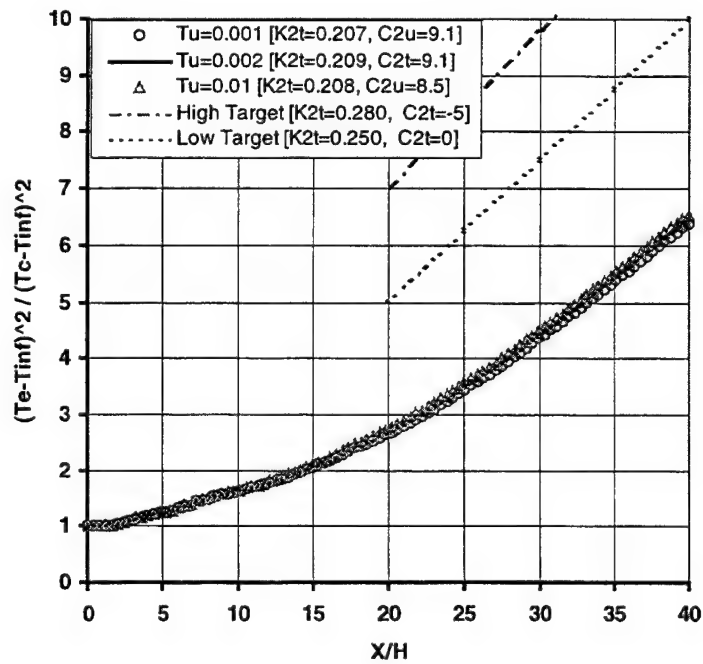
Figure 32. Planar Jet Centerline Temp. Decay with Varying Jet Turb. Intensity

90
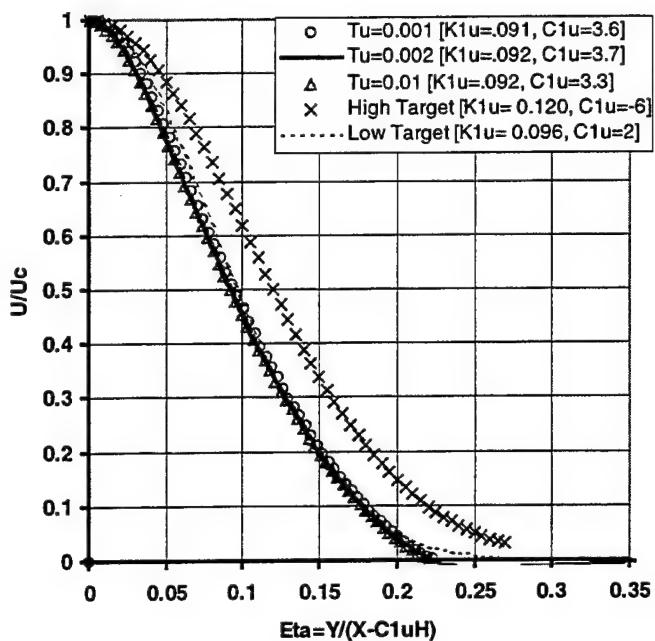
Figure 33.   Planar Jet Velocity Profile with Varying Jet Turbulence Intensity
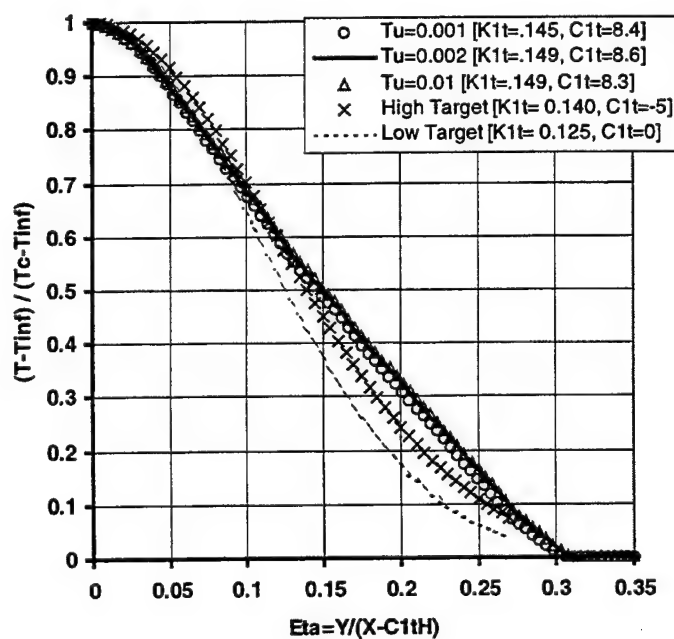
Figure 34.   Planar Jet Temp. Profile with Varying Jet Turbulence Intensity

91

B. TURBULENT PRANDTL NUMBER

Table 10.   CFD Simulation Predictions with Varying Prandtl Number

Jet Turb. Pr_t $\{Pr_t\}$	Vel. Spread Rate $\{K_{1u}\}$	Geom. Virt. Orig. $\{C_{1u}\}$	C/L Vel. Decay $\{K_{2u}\}$	Kin. Virt. Orig. $\{C_{2u}\}$	Temp. Spread Rate $\{K_{1t}\}$	Spread Virt. Orig. $\{C_{1t}\}$	C/L Temp. Decay $\{K_{2t}\}$	Decay Virt. Orig. $\{C_{2t}\}$
AXISYMMETRICAL ROUND JET								
Target Values	0.096-0.120	-1.0 to 4.0	0.155-0.220	-1.0 to 4.0	0.125-0.140	0.0 to 2.0	0.250-0.280	0.0 to 2.0
0.5	0.112	9.3	0.201	10.0	0.159	11.4	0.286	12.7
(0.7)$_{nom}$	0.112	9.3	0.201	10.0	0.134	11.1	0.247	12.3
0.9	0.111	9.2	0.199	10.0	0.112	9.4	0.214	11.5
TW0-DIMENSIONAL PLANAR JET								
Target Values	0.096-0.120	-6.0 to 2.0	0.155-0.220	-2.0 to 4.0	0.125-0.140	-5.0 to 0.0	0.250-0.280	-5.0 to 0.0
0.3	0.091	3.6	0.152	5.1	0.173	5.6	0.240	8.4
(0.5)$_{nom}$	0.092	3.7	0.154	5.2	0.149	8.6	0.209	9.1
0.7	0.091	3.6	0.152	5.1	0.118	7.2	0.177	8.1

92
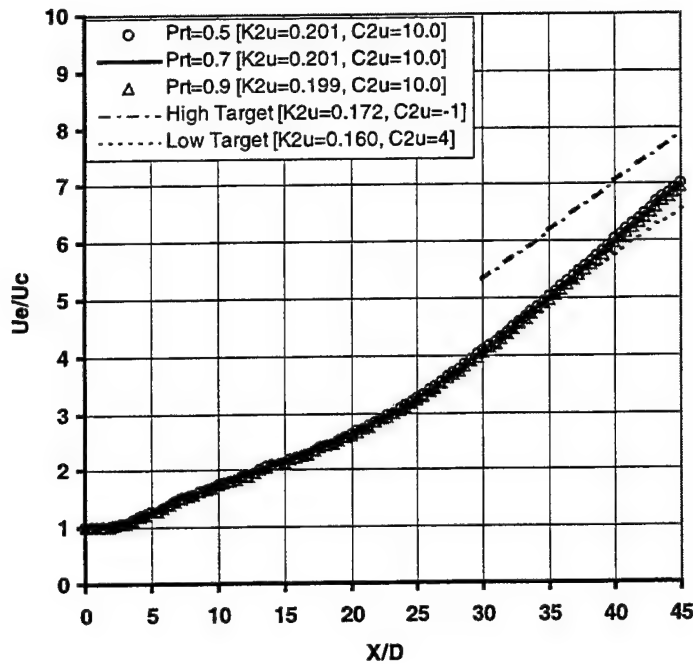
Figure 35. Round Jet Centerline Vel. Decay with Varying Prandtl Number
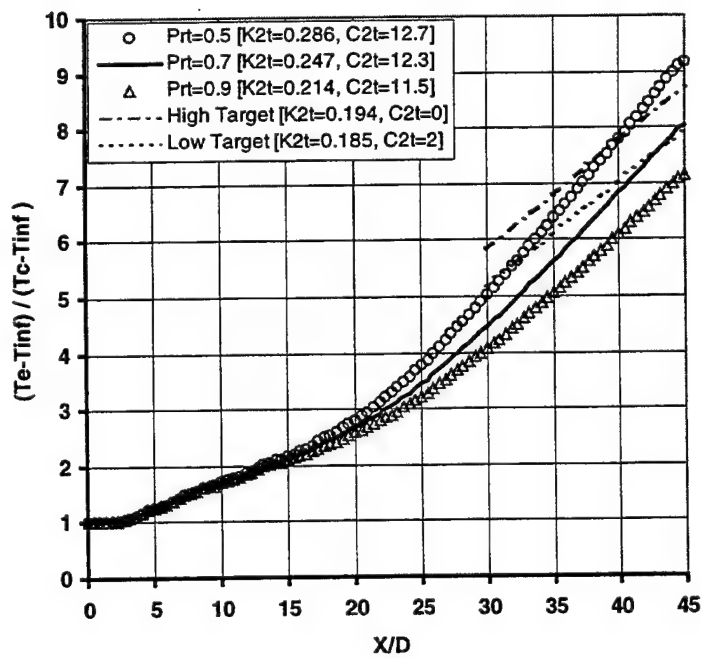
Figure 36. Round Jet Centerline Temp. Decay with Varying Prandtl Number

93
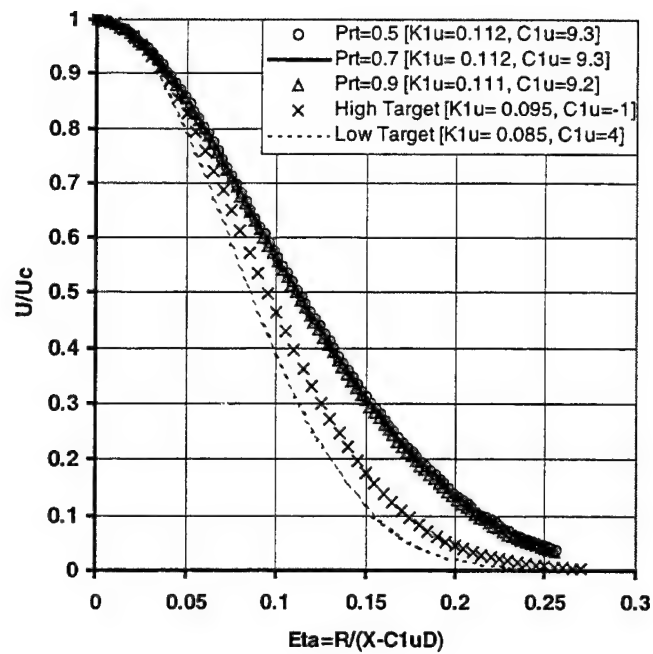
Figure 37.   Round Jet Velocity Profile with Varying Prandtl Number
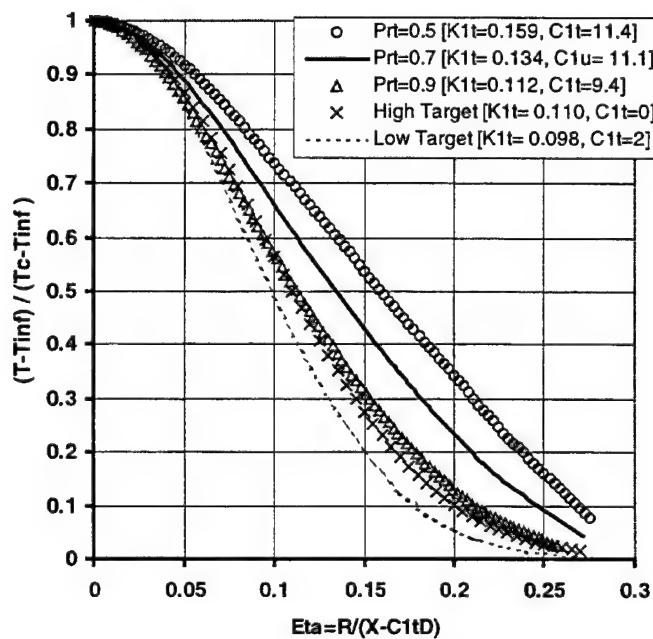
Figure 38.   Round Jet Temp. Profile with Varying Prandtl Number

94
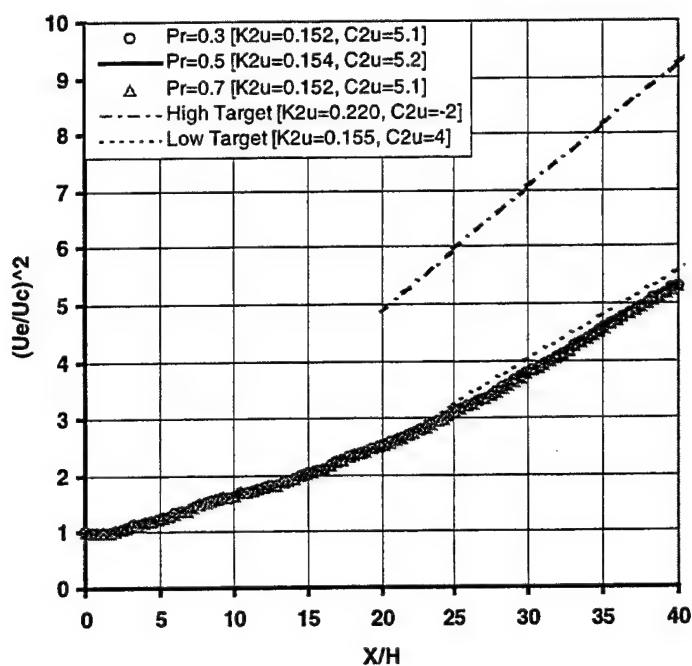
Figure 39. **Planar Jet Centerline Vel. Decay with Varying Prandtl Number**
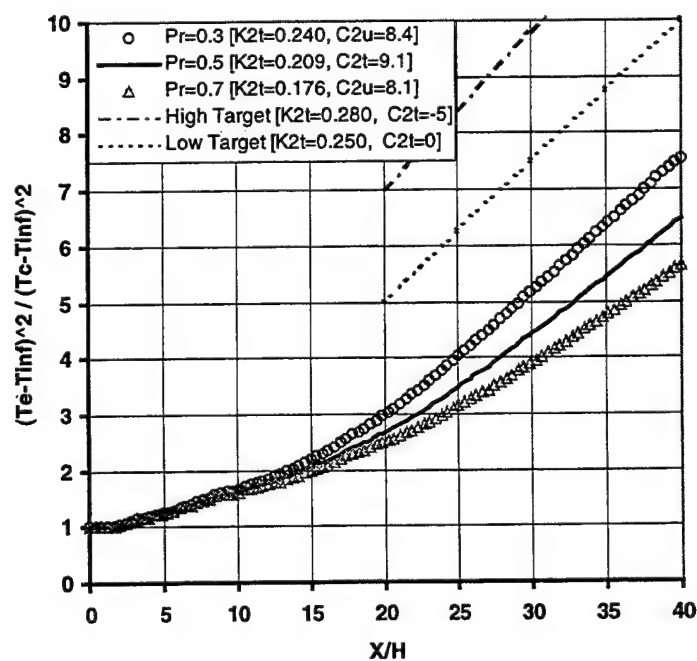
Figure 40. **Planar Jet Centerline Temp. Decay with Varying Prandtl Number**
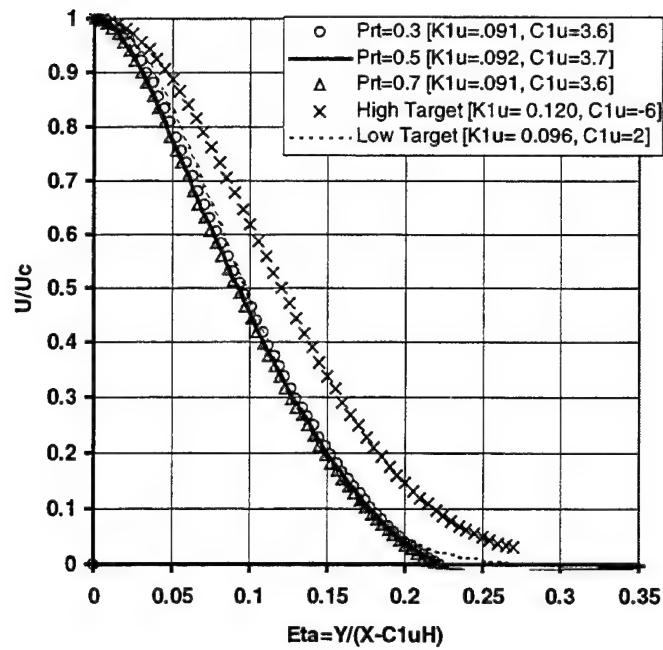
Figure 41.   Planar Jet Velocity Profile with Varying Prandtl Number
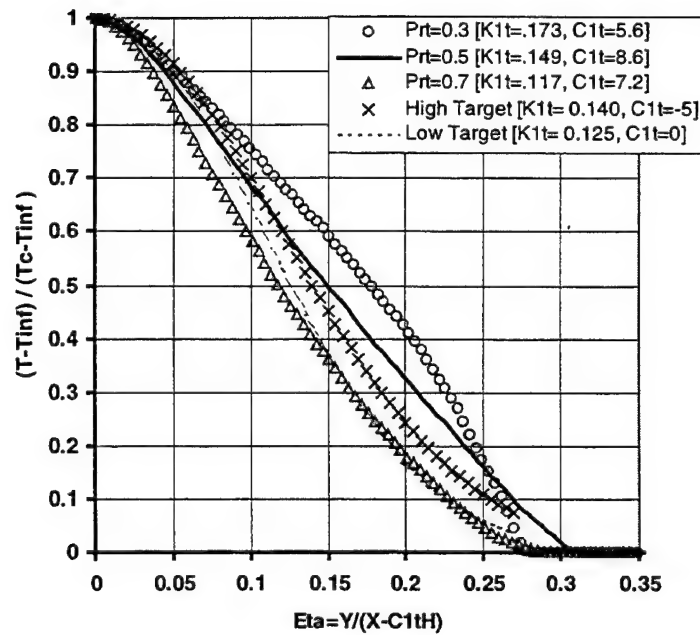
Figure 42.   Planar Jet Temp. Profile with Varying Prandtl Number

96

C. JET LENGTH SCALE

Table 11.   CFD Simulation Predictions with Varying Jet Length Scale

Jet Length Scale {L}	Vel. Spread Rate {K_{1u}}	Geom. Virt. Orig. {C_{1u}}	C/L Vel. Decay {K_{2u}}	Kin. Virt. Orig. {C_{2u}}	Temp. Spread Rate {K_{1t}}	Spread Virt. Orig. {C_{1t}}	C/L Temp. Decay {K_{2t}}	Decay Virt. Orig. {C_{2t}}
AXISYMMETRICAL ROUND JET								
Target Values	0.085-0.095	-1.0 to 4.0	0.160-0.172	-1.0 to 4.0	0.098-0.110	0.0 to 2.0	0.185-0.194	0.0 to 2.0
0.1	0.111	9.1	0.199	10.0	0.133	11.0	0.245	12.3
(.0127)_{nom}	0.112	9.3	0.201	10.0	0.134	11.1	0.247	12.3
0.001	0.110	9.2	0.199	10.1	0.132	11.1	0.244	12.5
TW0-DIMENSIONAL PLANAR JET								
Target Values	0.096-0.120	-6.0 to 2.0	0.155-0.220	-2.0 to 4.0	0.125-0.140	-5.0 to 0.0	0.250-0.280	-5.0 to 0.0
0.1	0.091	3.6	0.152	5.1	0.146	8.4	0.207	9.0
(.0065)_{nom}	0.092	3.7	0.154	5.2	0.149	8.6	0.209	9.1
0.001	0.091	3.6	0.152	5.1	0.145	8.4	0.207	9.1
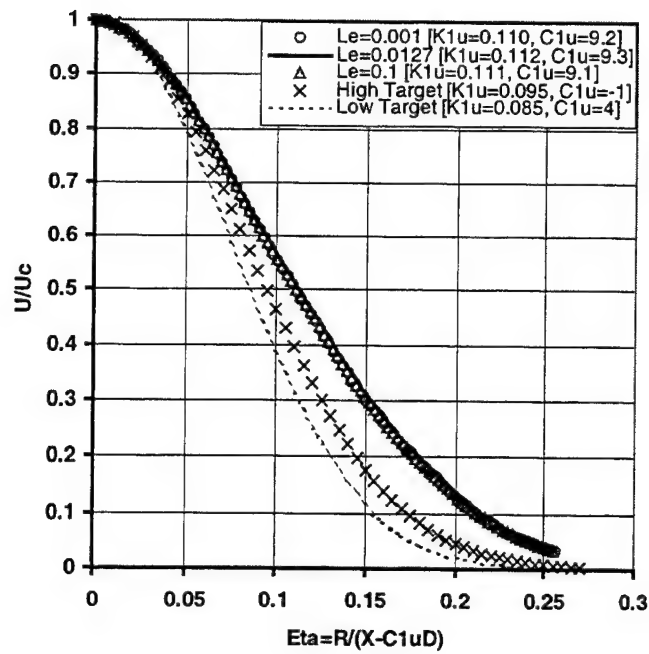
Figure 43.　　　**Round Jet Centerline Vel. Decay with Varying Jet Length Scale**
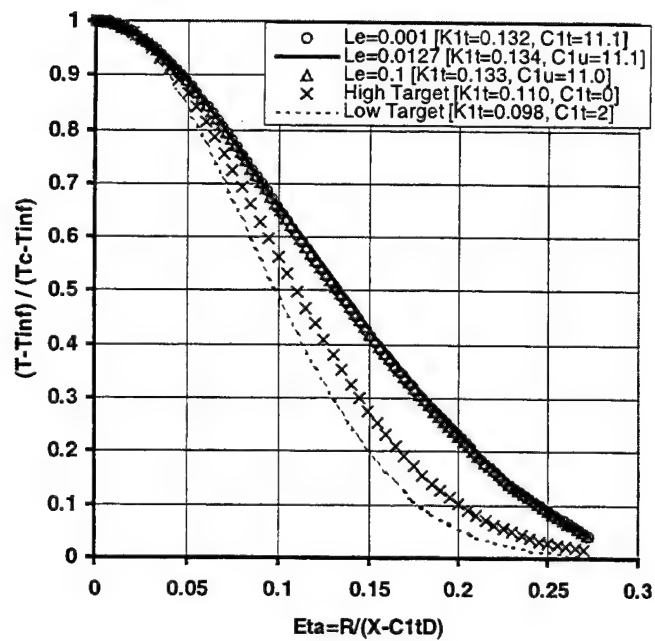

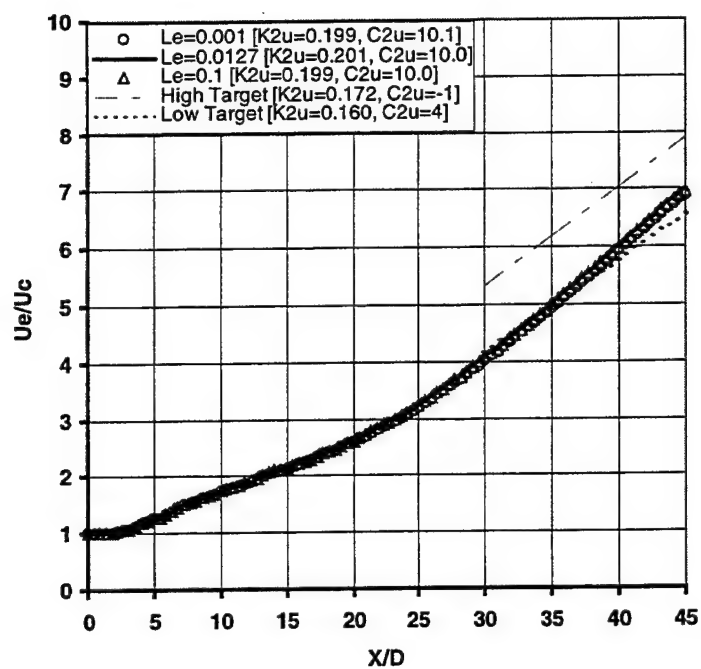**Figure 44.**　　　**Round Jet Centerline Temp. Decay with Varying Jet Length Scale**

Figure 45. Round Jet Velocity Profile with Varying Jet Length Scale
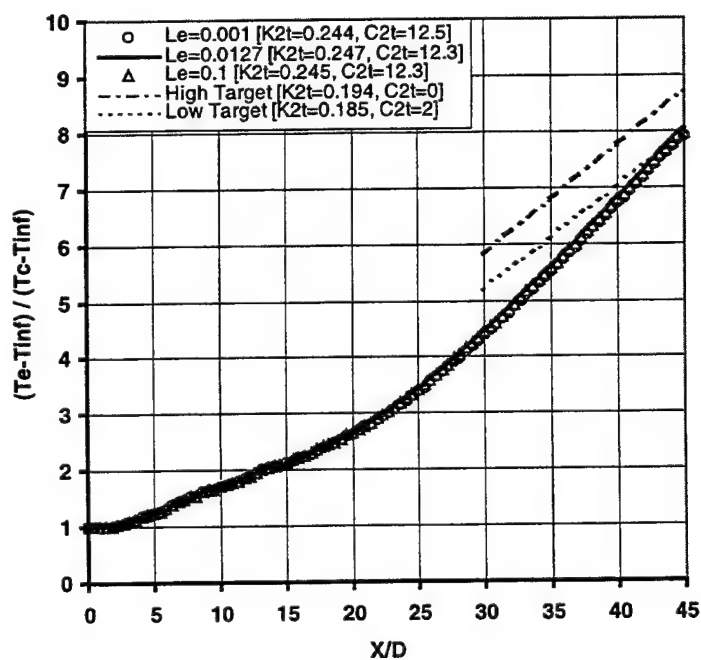

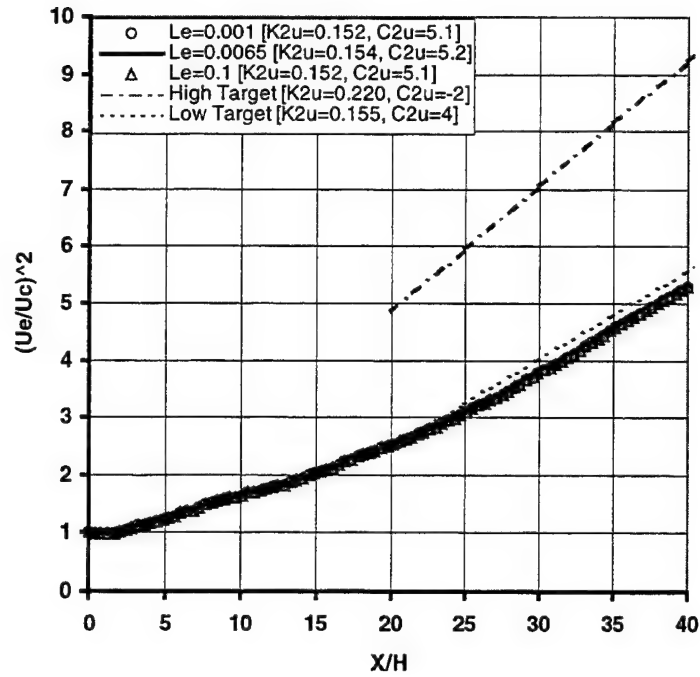**Figure 46.** Round Jet Temp. Profile with Varying Jet Length Scale

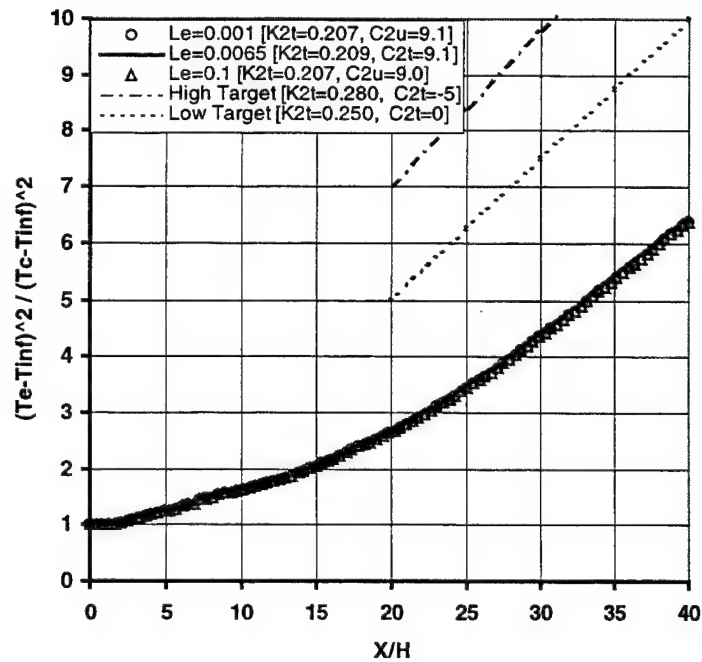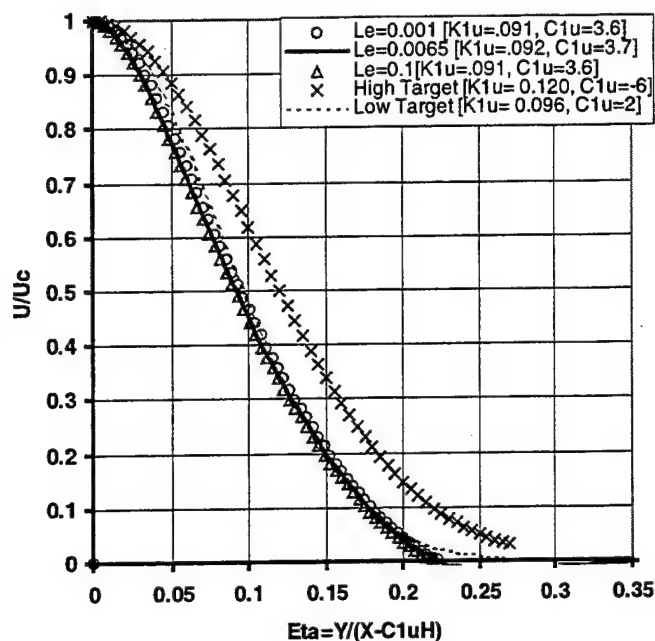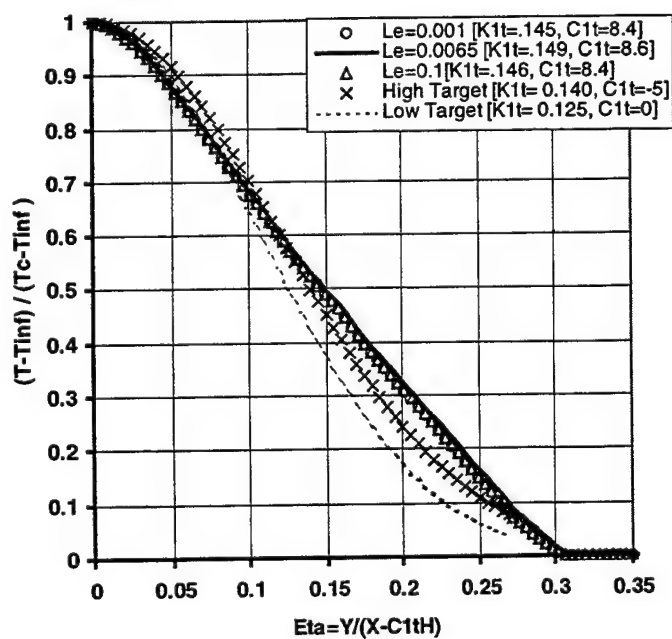**Figure 47.** Planar Jet Centerline Vel. Decay with Varying Jet Length Scale

Figure 48. Planar Jet Centerline Temp. Decay with Varying Jet Length Scale

100

Figure 49. Planar Jet Velocity Profile with Varying Jet Length Scale

Figure 50. Planar Jet Temp. Profile with Varying Jet Length Scale

101

D.   JET VELOCITY

Table 12.   CFD Simulation Predictions with Varying Jet Velocity

| Jet Exit Vel $\{Ue\}$	Vel. Spread Rate $\{K_{1u}\}$	Geom. Virt. Orig. $\{C_{1u}\}$	C/L Vel. Decay $\{K_{2u}\}$	Kin. Virt. Orig. $\{C_{2u}\}$	Temp. Spread Rate $\{K_{1t}\}$	Spread Virt. Orig. $\{C_{1t}\}$	C/L Temp. Decay $\{K_{2t}\}$	Decay Virt. Orig. $\{C_{2t}\}$
AXISYMMETRICAL ROUND JET								
Target Values	0.085- 0.095	-1.0 to 4.0	0.160- 0.172	-1.0 to 4.0	0.098- 0.110	0.0 to 2.0	0.185- 0.194	0.0 to 2.0
20	0.111	9.1	0.194	9.5	0.130	10.8	0.250	12.4
$(40)_{nom}$	0.112	9.3	0.201	10.0	0.134	11.1	0.247	12.3
60	0.113	9.4	0.203	10.2	0.136	11.1	0.240	12.2
TW0-DIMENSIONAL PLANAR JET								
Target Values	0.096- 0.120	-6.0 to 2.0	0.155- 0.220	-2.0 to 4.0	0.125- 0.140	-5.0 to 0.0	0.250- 0.280	-5.0 to 0.0
15	0.091	3.5	0.153	5.1	0.146	8.3	0.212	9.1
$(35)_{nom}$	0.092	3.7	0.154	5.2	0.149	8.6	0.209	9.1
55	0.091	3.6	0.152	5.1	0.146	8.4	0.198	8.8
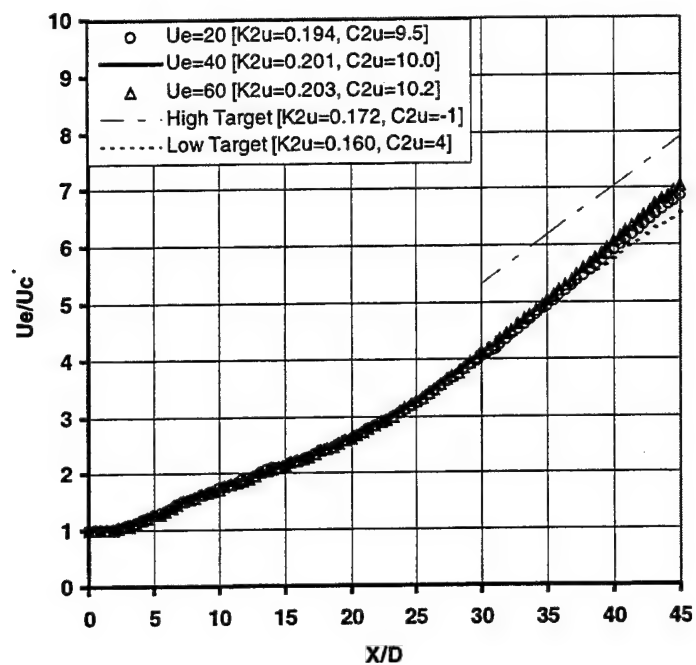
Figure 51. Round Jet Centerline Vel. Decay with Varying Jet Velocity
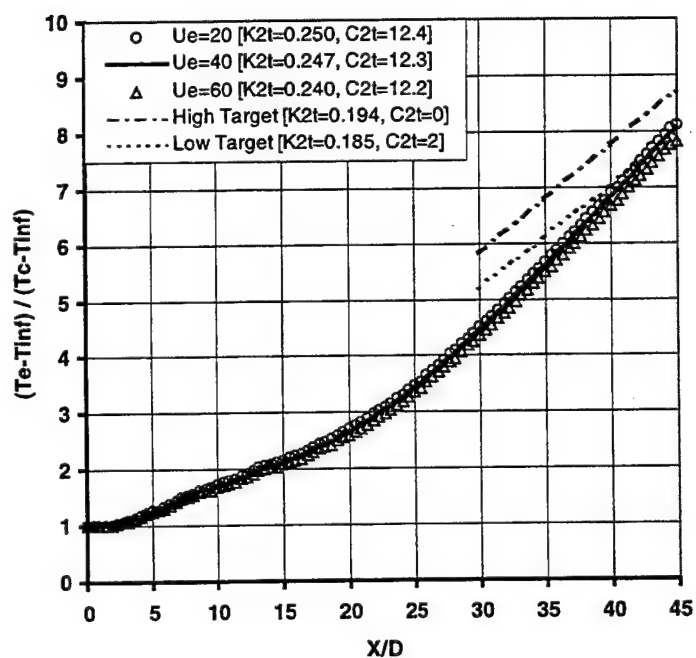

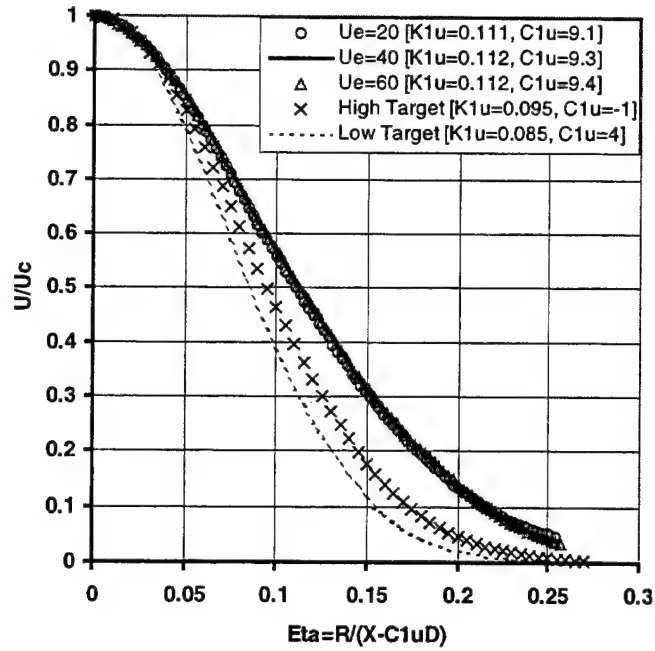**Figure 52.** Round Jet Centerline Temp. Decay with Varying Jet Velocity

Figure 53.   Round Jet Velocity Profile with Varying Jet Velocity
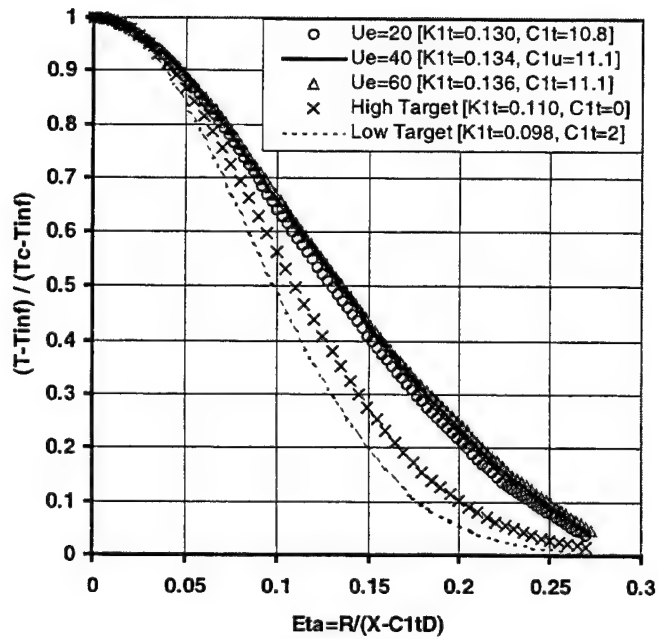

Figure 54.   Round Jet Temp. Profile with Varying Jet Velocity
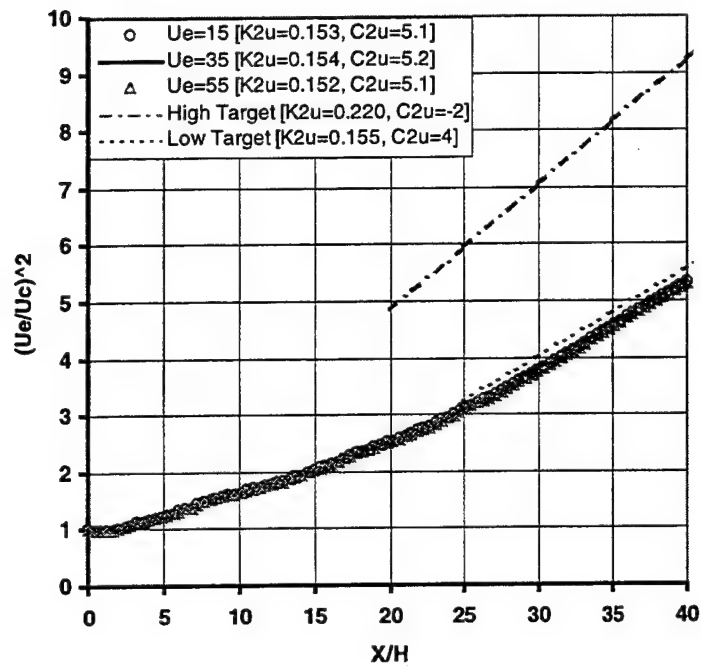
104

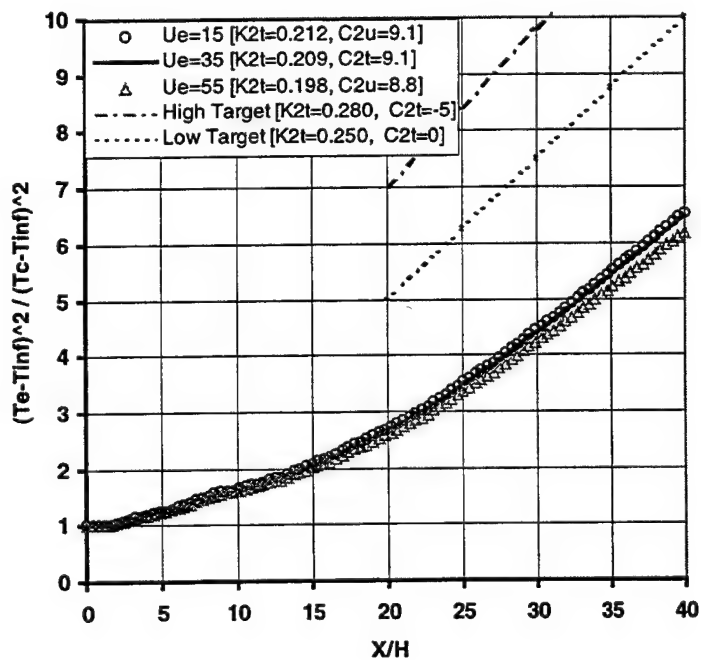**Figure 55.** Planar Jet Centerline Vel. Decay with Varying Jet Velocity

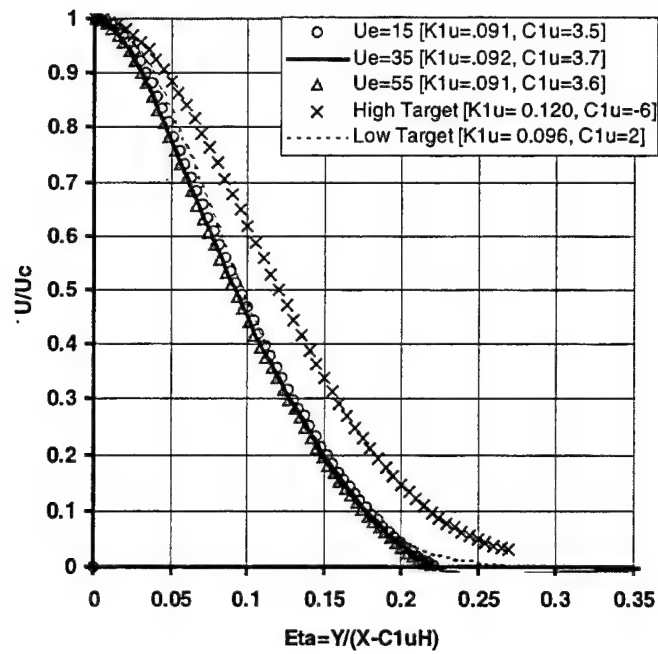**Figure 56.** Planar Jet Centerline Temp. Decay with Varying Jet Velocity

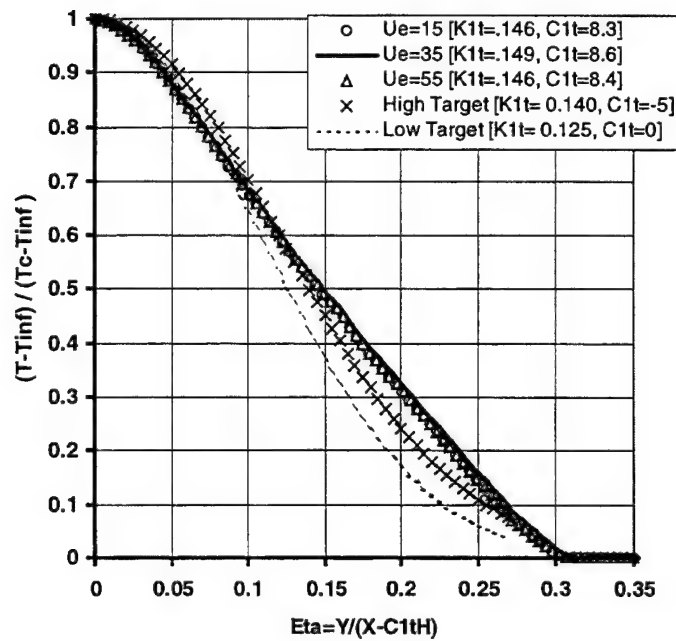**Figure 57.** **Planar Jet Velocity Profile with Varying Jet Velocity**

Figure 58. **Planar Jet Temp. Profile with Varying Jet Velocity**

106

E. JET TEMPERATURE

Table 13. CFD Simulation Predictions with Jet Temperature

Jet Exit Temp {Te}	Vel. Spread Rate {K₁ᵤ}	Geom. Virt. Orig. {C₁ᵤ}	C/L Vel. Decay {K₂ᵤ}	Kin. Virt. Orig. {C₂ᵤ}	Temp. Spread Rate {K₁ₜ}	Spread Virt. Orig. {C₁ₜ}	C/L Temp. Decay {K₂ₜ}	Decay Virt. Orig. {C₂ₜ}
Jet Exit Temp $\{T_e\}$	Vel. Spread Rate $\{K_{1u}\}$	Geom. Virt. Orig. $\{C_{1u}\}$	C/L Vel. Decay $\{K_{2u}\}$	Kin. Virt. Orig. $\{C_{2u}\}$	Temp. Spread Rate $\{K_{1t}\}$	Spread Virt. Orig. $\{C_{1t}\}$	C/L Temp. Decay $\{K_{2t}\}$	Decay Virt. Orig. $\{C_{2t}\}$
AXISYMMETRICAL ROUND JET								
Target Values	0.085-0.095	-1.0 to 4.0	0.160-0.172	-1.0 to 4.0	0.098-0.110	0.0 to 2.0	0.185-0.194	0.0 to 2.0
$(330)_{nom}$	0.112	9.3	0.201	10.0	0.134	11.1	0.247	12.3
500	0.112	9.2	0.244	10.4	0.133	10.8	0.309	12.6
TW0-DIMENSIONAL PLANAR JET								
Target Values	0.096-0.120	-6.0 to 2.0	0.155-0.220	-2.0 to 4.0	0.125-0.140	-5.0 to 0.0	0.250-0.280	-5.0 to 0.0
$(330)_{nom}$	0.092	3.7	0.154	5.2	0.149	8.6	0.209	9.1
500	0.093	4.2	0.148	8.4	0.133	10.	0.301	10.5
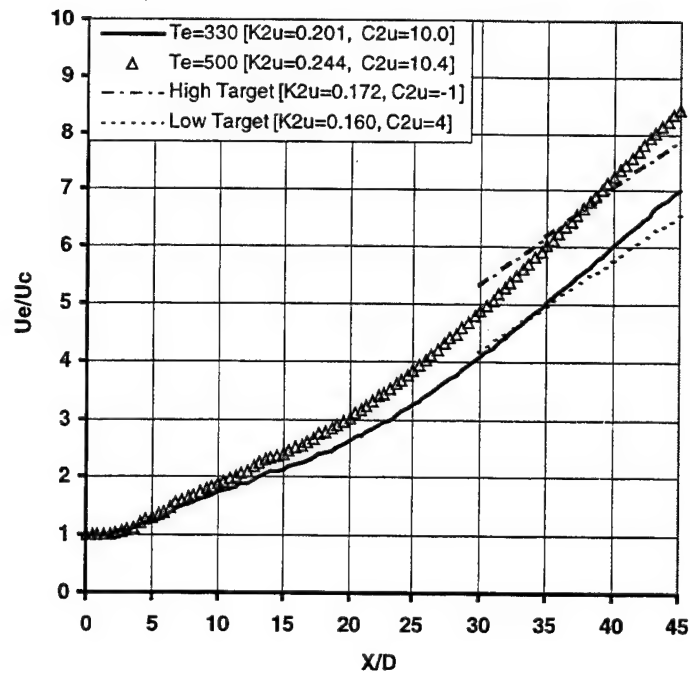
Figure 59.   **Round Jet Centerline Vel. Decay with Varying Temperature**
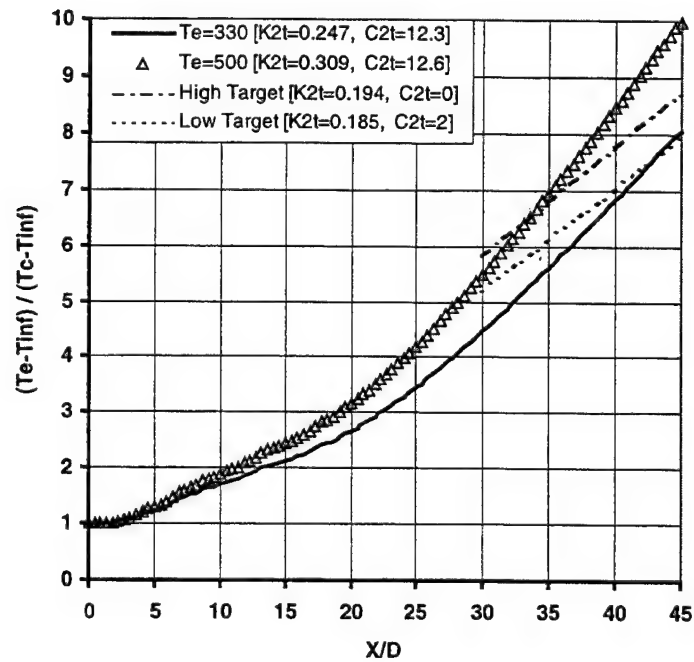
Figure 60.   **Round Jet Centerline Temp. Decay with Varying Temperature**

108
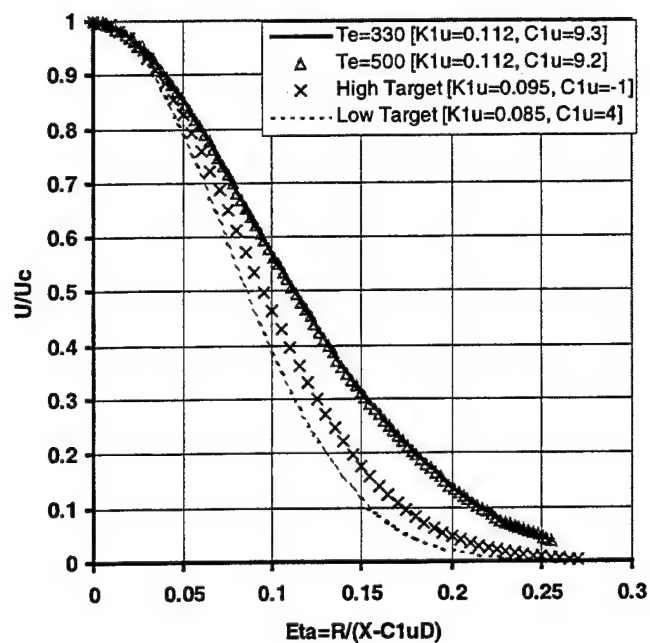
Figure 61. Round Jet Velocity Profile with Varying Temperature
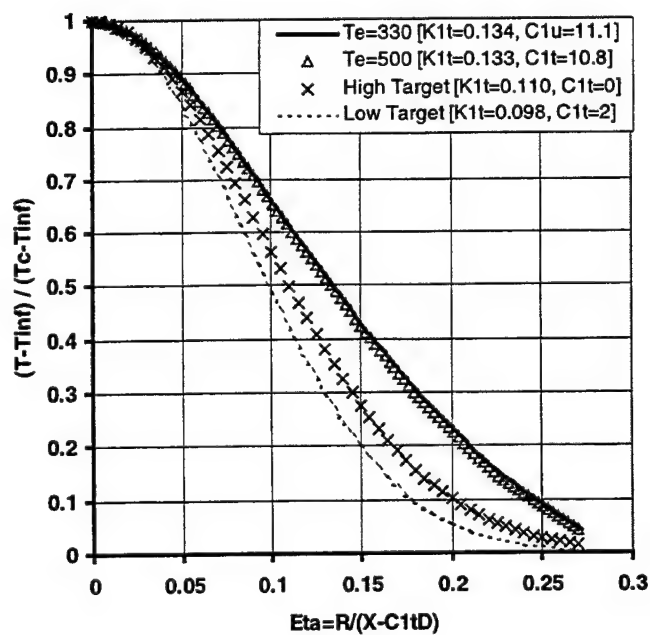
Figure 62. Round Jet Temp. Profile with Varying Temperature

109
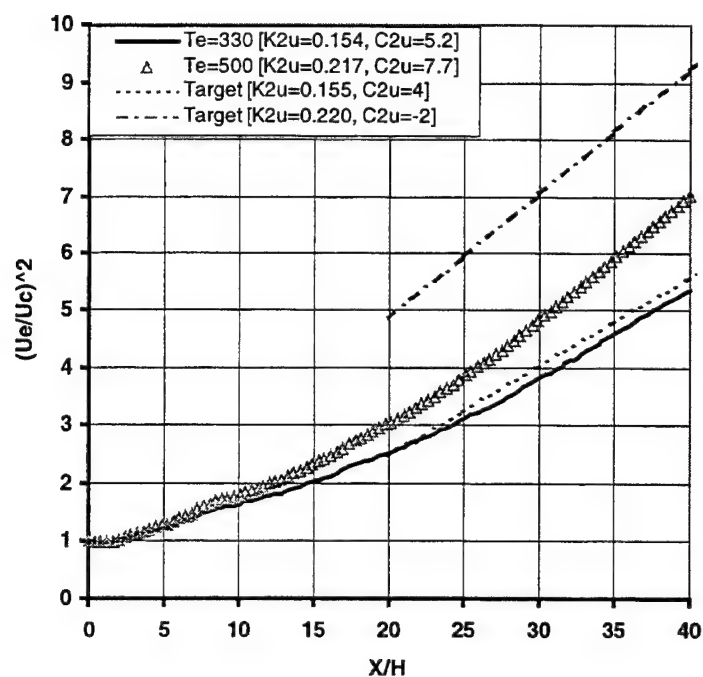
Figure 63.   Planar Jet Centerline Vel. Decay with Varying Temperature
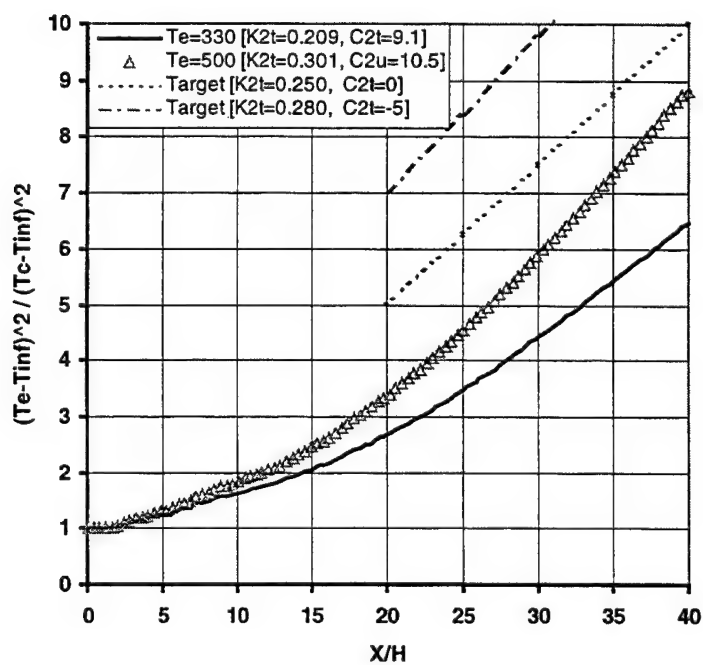
Figure 64.   Planar Jet Centerline Temp. Decay with Varying Temperature

110
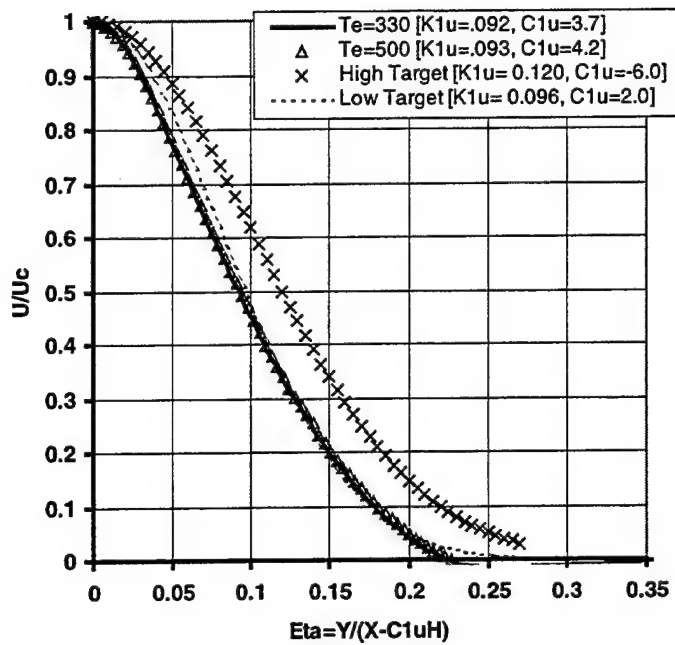
Figure 65. **Planar Jet Velocity Profile with Varying Temperature**
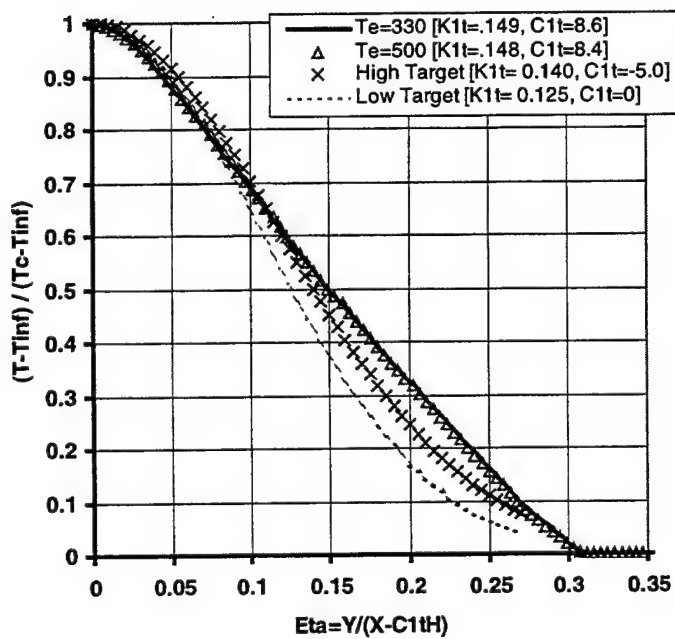
Figure 66. **Planar Jet Temp. Profile with Varying Temperature**

111
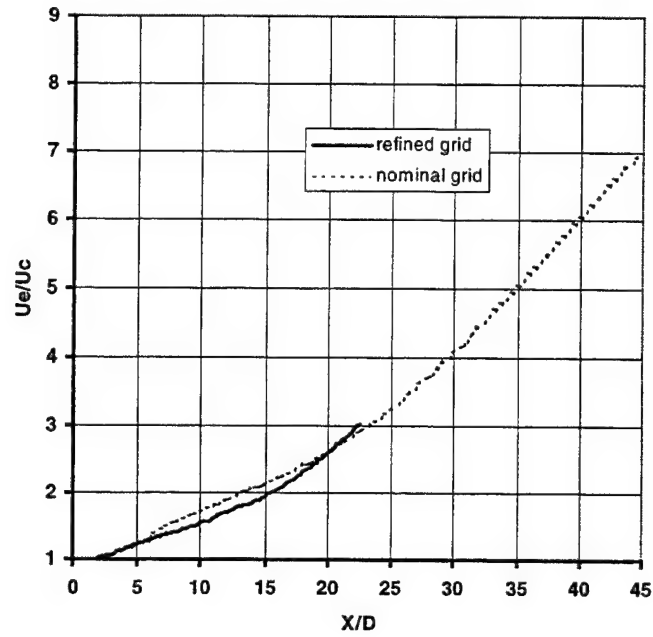
F.   GRID REFINEMENT

Figure 67.   Round Jet Centerline Vel. Decay with Grid Refinement
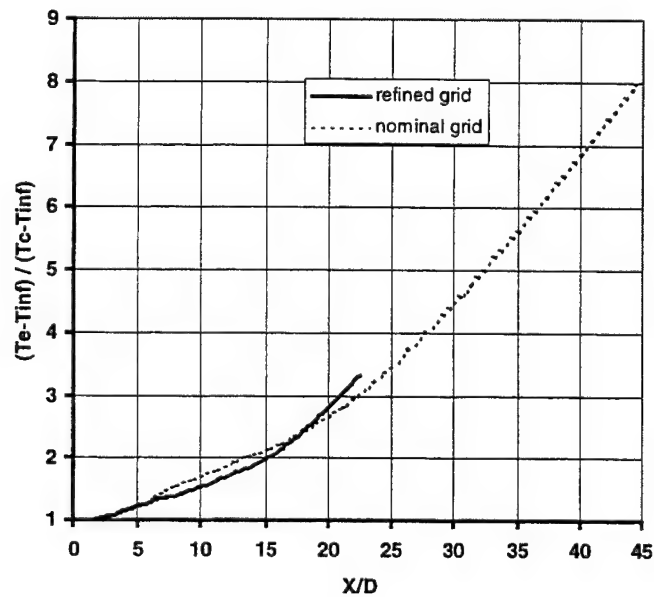
Figure 68.   Round Jet Centerline Temp. Decay with Grid Refinement

112
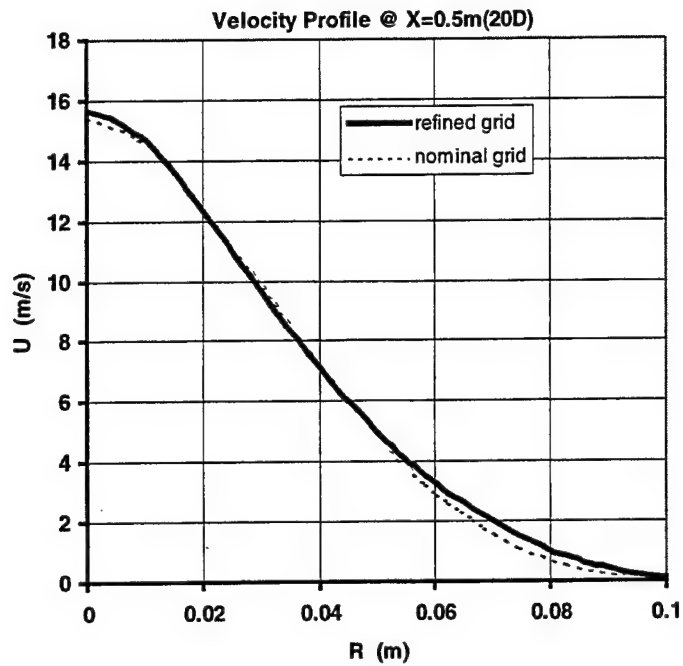
Figure 69.   **Round Jet Velocity Profile with Grid Refinement**
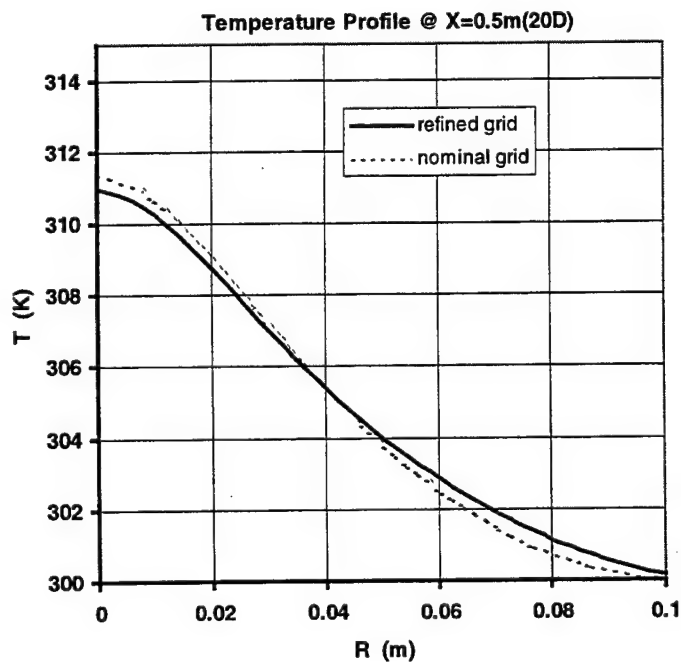
Figure 70.   **Round Jet Temp. Profile with Grid Refinement**

113
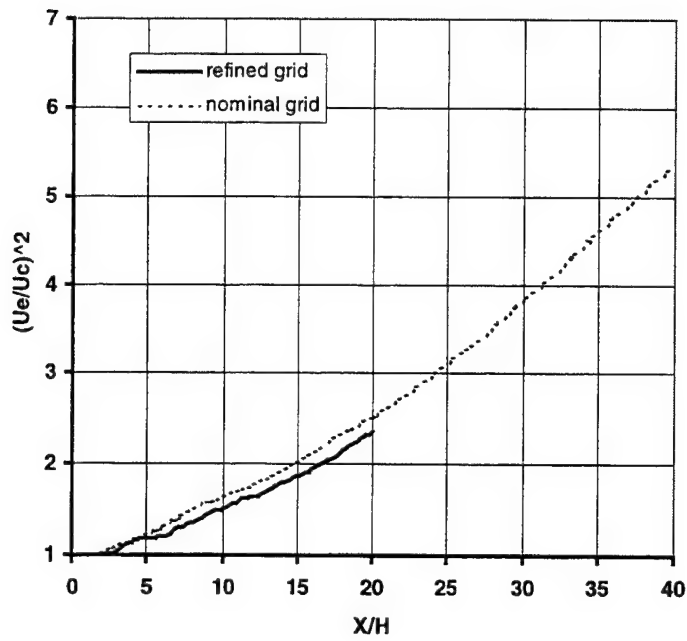
Figure 71.   Planar Jet Centerline Vel. Decay with Grid Refinement
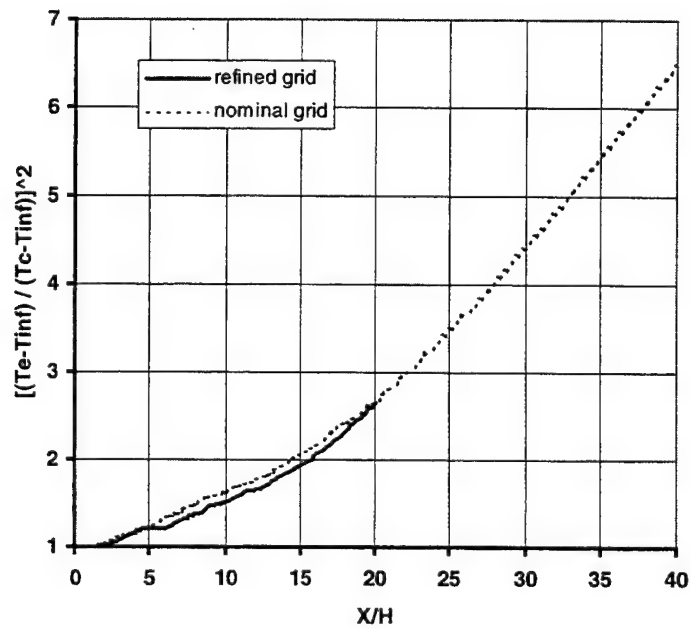
Figure 72.   Planar Jet Centerline Temp. Decay with Grid Refinement

114
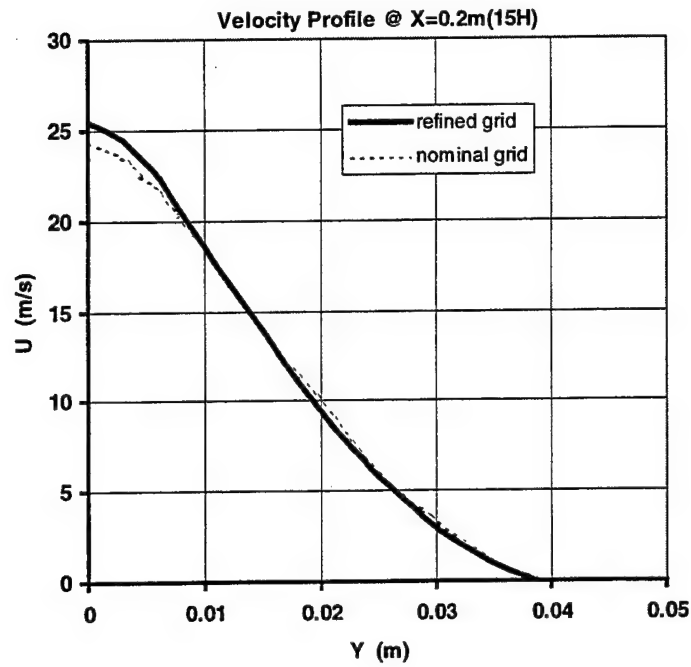
Figure 73. Planar Jet Velocity Profile with Grid Refinement
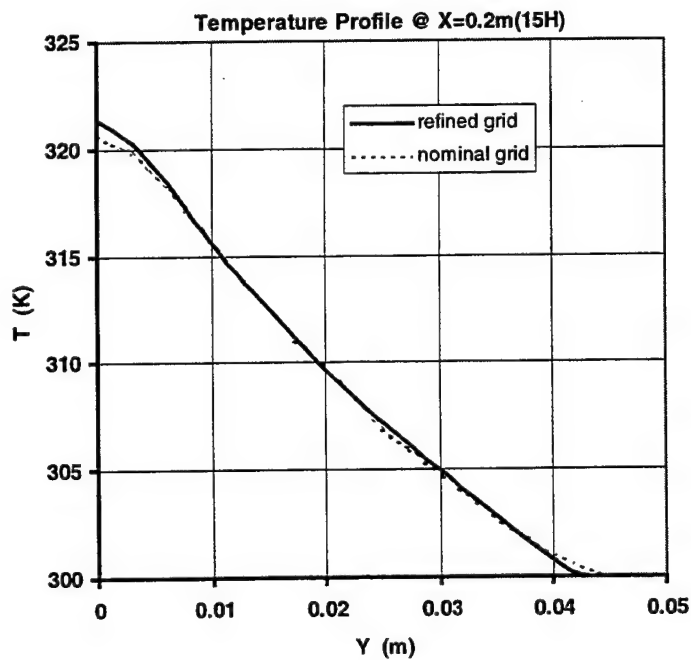
Figure 74. Planar Jet Temp. Profile with Grid Refinement

THIS PAGE INTENTIONALLY LEFT BLANK

LIST OF REFERENCES

Abramovich, G., The Theory of Turbulent Jets, The MIT Press, Massachusetts, 1963.

CFD Research Corporation, CFDRC User Manuals, Jan. 2000.

Chen, J., Rodi, W., "Vertical Turbulent Buoyant Jets: A Review of Experimental Data", HMT (book), V4, 1980.

Corrsin, S., Kistler, A., "Free-Stream Boundaries of Turbulent Flows", NACA Report 1244, 1954.

Crow, S., Champagne, F., "Orderly structure in jet turbulence", J. Fluid Mech., V48, 1971.

Davies, A., Keffer, J., Baines, W., "Spread of a Heated Plane Turbulent Jet", Phys. Fluids, V18(7), 1975.

Drobniak, S., Elsner, J., El-Kassem, E., "The relationship between coherent structures and heat transfer processes in the initial region of a round jet", Exp. Fluids, V24, 1998.

Flora, J., Goldschmidt, V., "Virtual Origins of a Free Plane Turbulent Jet", AIAA Journ., V7(12), 1969.

George, W., "The self-preservation of turbulent flows and its relationship to initial conditions and coherent structures", Advances in Turbulence, Hemisphere, 1989.

Goldschmidt, V., Bradshaw, P., "Effects of Nozzle Exit Turbulence on the Spreading Rate of Plane Free Jets", ASME Report 81-FE-22, 1981.

Grandmaison, E., Rathgeber, D., Becker, H., "Some Characteristics of Concentration Fluctuations in Free Turbulent Jets", Canadian J. Chem. Eng., V60, 1982.

Gutmark, E., Wygnanski, I., "The Planar Turbulent Jet", J. Fluid Mech., V73, 1976.

Gutmark, E., Ho, C., "Preferred Modes and the Spreading Rates of Jets", Phys. Fluids, V26(10), 1983.

Harsha, P., Launder, B., Free Turbulent Shear Flows, NASA SP-321, 1973.

Hinze, J., Turbulence, McGraw-Hill Pub., 1975.

Hinze, J., van der Hegge Zijnen, B., "Transfer of Heat & Matter in the Turbulent Mixing Zone of an Axially Symmetrical Jet", Appl. Sci. Res., Vol. A1, 1949.

Hussain, A., Clark, A., "Upstream Influence on the Near Field of a Plane Turbulent Jet", Phys. Fluids, V20(9), 1977.

Hussain, A., "Coherent Structures- reality and myth", Phys. Fluids, V26(10), 1983.

Hussein, H., Capp, S., George, W., "Velocity Measurements in a High Reynolds-number, momentum-conserving, axisymmetric, turbulent jet", J. Fluid Mech., V258, 1994.

Jenkins, P., Goldschmidt, V., "Mean Temperature and Velocity in a Plane Turbulent Jet", J. Fluids Eng., Dec, 1973.

Kleis, S., Foss, J., "The Effect of Exit conditions on the Development of an Axisymmetric Turbulent Free Jet", NASA NGR 23-004-068, 1974.

Kotsovinos, N., "A note on the spreading rate and virtual origin of a plane turbulent jet", J. Fluid Mech., V77, 1976.

Kyle, D., Sreenivasan, K., "The Instability & Breakdown of a Round Variable-density Jet", J. Fluid Mech., V249, 1993.

Launder,B., Spalding,D. "The numerical computation of turbulent flows", Comput. Methods Appl. Mech. Eng., Vol. 3, 1974.

List, E., ed. by Rodi, W., Turbulent Buoyant Jets and Plumes, HMT-6, Pergamon Press, 1982.

Malmstrom, T., Kirkpatrick, A., Christensen, B., Knappmiller, K., "Centerline velocity decay measurements in low-velocity axisymmetric jets", J. Fluid Mech., V246, 1997.

Miller, D., Comings, E., "Static Pressure Distribution in the Free Turbulent Jet", J. Fluid Mech., V3, 1957.

Monkewitz, P., Bechert, D., Barsikow, B., Lehmann, B., "Self-Excited Oscillations & Mixing in a Heated Round Jet", J. Fluid Mech., V213, 1990.

Moum,J., Kawall, J., Keffer, J., "Coherent Structures within the Plane Turbulent Jet", Phys. Fluids, V26(10), 1983.

Pai, S., Fluid Dynamics of Jets, D. Van Nostrand Company Inc., Canada, 1954.

Panchapakesan, N., Lumley, J., "Turbulence Measurements in axisymmetric jets of air and helium. Part 1. Air Jet", J. Fluid Mech., V246, 1993.

Papadopoulos, G., Pitts, W., "Generic Centerline Velocity Decay Curve for Initially Turbulent Axisymmetric Jets", J. Fluids Eng. – ASME, Mar 1999.

Reynolds, A., "The Variation of Turbulent Prandtl and Schmidt Numbers in Wakes and Jets", Int, J. Heat Mass Transfer., V19, 1976.

Rodi, W., ed. by Launder, B., Studies in Convection, Academic Press, 1975.

Russ, S., Strykowski, P., "Turbulent Structure & Entrainment in Heated Jets: The Effect of Initial Conditions", Phys. Fluids A, V5(12), 1993.

Sautet, J., Stepowski, D., "Dynamic Behavior of Variable-density Turbulent Jets in Their Near Development Fields.", Phys. Fluids, V7(11), 1995.

Schetz, J., Injection and Mixing in Turbulent Flow, AIAA Publ., 1980.

Schetz, J., Fuhs, A., Fundamentals of Fluid Mechanics, Wiley-Interscience Publ., 1996.

Schlichting, H., Boundary-Layer Theory, McGraw-Hill Inc., New York, NY, 1979.

Thomas, F., Prakash, K., "An Experimental Investigation of the Natural Transition of an Untuned Planar Jet", Phys. Fluids, Vol. A3(1), 1991.

Townsend, A., The Structure of Turbulent Shear Flow, Cambridge Univ. Press, 1976.

Wygnanski, I., Fiedler, H., "Some Measurements in the Self-Preserving Jet", J. Fluid Mech, V38, 1969.

van der Hegge Zijenen, B., "Measurements of the Velocity Distribution in a Plane Turbulent Jet of Air", Appl. Sci. Res., V7(A), 1957.

THIS PAGE INTENTIONALLY LEFT BLANK

INITIAL DISTRIBUTION LIST

1. Defense Technical Information Center 2
   8725 John J. Kingman Road, Ste 0944
   Ft Belvoir, Virginia 22060-6218

2. Dudley Knox Library 2
   Naval Postgraduate School
   411 Dyer Rd.
   Monterey, CA 93943-5101

3. Professor Knox T. Millsaps Jr., Code ME/MI 2
   Department of Mechanical Engineering
   Naval Postgraduate School
   Monterey, CA 93943-5100

4. Professor Garth V. Hobson, Code AA 2
   Department of Aeronautics and Astronautics
   Naval Postgraduate School
   Monterey, CA 93943-5100

5. Professor Arthur Shavit 1
   Technion – MW Dept
   Haifa, 32000 ISRAEL

6. Engineering & Technology Curricular Office, Code 34 1
   Naval Postgraduate School
   Monterey, Ca 93943-5101

7. Mr. Ray Ratcliffe, Code 7230 1
   NSWC, Carderock Division
   9500 MacArthur Blvd
   West Bethesda, MD 20817-5700

8. Mr. Paul Chatterton 1
   Naval Sea Systems Command
   NAVSEA (03T)
   2531 Jefferson Davis Highway
   Arlington, VA 22242-5160

9. LT Mike Mehls, USN 1
   18900 Pasnow Ave
   Euclid, Oh 44119

10. LT Mike DeWulf, USN 1
    5265 Albright Drive
    Virginia Beach, VA 23464